DYNAMIC ANALYSIS OF BEAM WITH BREATHING CRACK USING FINITE ELEMENT METHOD

A THESIS SUBMITTED TO
THE GRADUATE SCHOOL OF NATURAL AND APPLIED SCIENCES
OF
MIDDLE EAST TECHNICAL UNIVERSITY

BY

BERKAY ÖZKAN

IN PARTIAL FULFILLMENT OF THE REQUIREMENTS
FOR
THE DEGREE OF MASTER OF SCIENCE
IN
THE DEPARTMENT OF MECHANICAL ENGINEERING

JULY 2017

NONLINEAR DYNAMIC ANALYSIS OF BEAMS WITH BREATHING CRACK USING FINITE ELEMENT METHOD

Submitted by **BERKAY ÖZKAN** in partial fulfillment of the requirements for the degree of **Master of Science in Mechanical Engineering Department, Middle East Technical University** by,

Prof. Dr. Gülbin Dural Ünver _____
Dean, Graduate School of **Natural and Applied Science**

Prof. Dr. R. Tuna Balkan _____
Head of Department, **Mechanical Engineering**

Prof. Dr. Fevzi Suat Kadıoğlu _____
Supervisor, **Mechanical Engineering Dept., METU**

Examining Committee Members:

Prof. Dr. Haluk Darendeliler _____
Mechanical Engineering Dept., METU

Prof. Dr. Fevzi Suat Kadıoğlu _____
Mechanical Engineering Dept., METU

Assoc. Prof. Dr. Ender Ciğeroğlu _____
Mechanical Engineering Dept., METU

Assist. Prof. Dr. Gökhan Özgen _____
Mechanical Engineering Dept., METU

Assist. Prof. Dr. M. Bülent Özer _____
Mechanical Engineering Dept., TOBB ETÜ

Date: 05.07.2017

I hereby declare that all information in this document has been obtained and presented in accordance with academic rules and ethical conduct. I also declare that, as required by these rules and conduct, I have fully cited and referenced all material and results that are not original to this wok.

Name, Last name: Berkay ÖZKAN

Signature : _____

ABSTRACT

DYNAMIC ANALYSIS OF BEAMS WITH BREATHING CRACK USING FINITE ELEMENT METHOD

Özkan, Berkay
MSc, Department of Mechanical Engineering
Supervisor: Prof. Dr. Fevzi Suat Kadıoğlu

July 2017, 102 pages

Nonlinear dynamic characteristics of a beam with a breathing crack are investigated using finite element method. This thesis has two main objectives: (1) to obtain a foresight for the vibration based crack detection by using finite element method (2) to investigate the effects of crack location, crack depth, excitation frequency, excitation amplitude and boundary conditions on the indications of crack presence. Two dimensional finite element approach is used to model a square cross sectional beam subjected to dynamic loading. Frictionless contact is introduced to avoid any penetration between the crack faces. Time histories and Fourier spectra are obtained for nodal acceleration at specified sensor locations on the beam. On the basis of the results of this research, the capability of finite element method on the crack detection is evidenced by the generation of sub- and higher-harmonics in the Fourier spectra. Both time and frequency domain responses deviate considerably from vibration response of an intact beam. The depth and position of the crack change the amplitude of the harmonics, which can be interpreted as an indicator on the severity of the damage. Furthermore, exciting the beam with frequency of first natural mode of the beam, makes the harmonics more detectable on the frequency domain.

Keywords: Nonlinear vibration, Breathing crack, Finite element method, Crack detection, Lateral vibration of beams

ÖZ

AÇILIP KAPANAN ÇATLAKLI KİRİŞLERİN SONLU ELEMAN YÖNTEMİ KULLANILARAK DİNAMİK ANALİZİ

Özkan, Berkay

Yüksek Lisans, Makina Mühendisliği Bölümü

Tez Yöneticisi: Prof. Dr. Fevzi Suat Kadıoğlu

Temmuz 2017, 102 sayfa

Açılıp kapanan çatlaklı kirişlerin doğrusal olmayan dinamik karakterleri sonlu eleman yöntemi ile analiz edilebilir. Bu tezin iki temel amacı vardır: (1) sonlu eleman analiz yöneteninin, titreyen yapılarda çatlak tespit edebilme kabiliyetini belirlemek (2) çatlak pozisyonunun, çatlak derinliğinin, tahrik etme frekansının, tahrik etme pozisyonunun, tahrik genliğinin ve sınır şartlarının çatlaktan kaynaklanan belirtiler üzerindeki etkisini belirlemek. Dinamik yükleme altındaki kare kesit alanına sahip kiriş, iki boyutlu sonlu eleman yaklaşımı kullanılarak modellenmiştir. Çatlak yüzeylerinin iç içe geçmesinin engellenmesi amacıyla, sürtünmesiz kontak modeli kullanılmıştır. Algılayıcı konumlarından, ivme ve yer değiştirme verisi, zaman düzleminde toplanmıştır. Elde edilen sonuçlara dayanarak, sonlu eleman analiz yönteminin, çatlak tespiti konusundaki yetkinliği, düşük ve yüksek harmoniklerin varlığı ile kanıtlanmıştır. Toplanan titreşim verisinde, çatlaklı kirişlerden alınan verilerin, çatlaksız kirişten alınandan oldukça farklılaştığı gözlemlenmiştir. Çatlak derinliği ve pozisyonunun, titreşim verisi üzerindeki etkisi kullanılarak, hasar miktarı hakkında yorum yapılabilmektedir. Çatlaklı kirişleri birinci eğilme frekansında tahrik etmenin, frekans düzleminden hasar tespitini daha kolay hale getirdiği gözlemlenmiştir.

Anahtar Sözcükler: Doğrusal olmayan titreşim, açılan kapanan çatlak, sonlu eleman yöntemi, çatlak tespiti, kirişlerin enine titreşimi

To My Family

ACKNOWLEDGMENTS

The author wishes to express his deepest gratitude to his supervisor Prof. Dr. Suat Kadıoğlu for his guidance, advice, criticism, encouragements and insight throughout the research.

The advice and comments of Dr. Ender Ciğeroğlu and Dr. Gökhan Özgen are also gratefully acknowledged.

I would like to thank to fatigue and damage tolerance lead Mr. Eyüp Evren Taşkınoğlu in Turkish Aerospace Industries for his great technical and moral support in this thesis.

The author also like to thank his family and close friends Yezdan Medet Korkmaz, Recep Hilmi Kanlıoğlu and Yasin Karasu for their support and patience during the thesis study. He also appreciates his colleagues Erhan Ferhatoğlu, Fatih Özbakış in Turkish Aerospace Industries for their valuable technical comments.

This study has been done under the TUBITAK project of 214M065 called as "Experimental investigation on vibration of cracked beams"

TABLE OF CONTENTS

LIST OF TABLES

LIST OF FIGURES

LIST OF ABBREVIATIONS

A	Cross sectional area
b	Thickness
C	Compliance of the crack
CWT	Continuous wavelet transforms
dc	Non-dimensional crack depth
E	Young modulus
F	Force
FFT	Fast Fourier Transform
FEM	Finite Element Method
h	Depth of the beam
HUMS	Health usage monitoring system
K	Stiffness matrix
L	Free length of the beam
Lf	Non-dimensional force location
Lc	Non-dimensional crack location
SHM	Structural health monitoring
t	Time
VHM	Vibration health monitoring
wc	Non-dimensional excitation frequency

CHAPTER 1

INTRODUCTION

Structural health monitoring has attracted the attention of researchers for the last few decades. The online monitoring of the structures is important especially in aerospace industry. The HUMS systems, for instance, are integrated to some helicopters in order to monitor safety of the rotorcraft. Reliable methods for detecting a failure in the structure are under investigation in the literature. One of the methods for analyzing the vibration response of the damaged structure under harmonic load.

Early studies conducted on the subject of damage detection in a simple structures like beams and shells focused on the modal characteristics. The change in the natural frequencies of the structure was taken into account in order to detect the presence of the cracks in these structures. Later, researchers were interested with the forced vibration characteristics of the damaged beams. These studies were based on linear approaches due to the fact that the interaction of the crack surfaces were not introduced in the model. Recent studies on this subject turned to nonlinear approaches for the investigation of the damage in the structure. More realistic representations of the nonlinear behavior of the structure caused by the interaction of the crack faces were studied in the recent publications by analytical, experimental and numerical methods.

The main objective of this study is to point out the effectivity of numerical methods on the detection of crack induced nonlinear effects such as generation of sub/super harmonics in the frequency response of the structure under forced vibration. Further, the effect of the crack location, crack depth, excitation frequency, excitation amplitude, excitation location and boundary conditions on the characteristics of harmonics are investigated. The analysis is conducted on a beam cantilevered from one side or both sides. A commercial finite element software is used in the modelling of the beam. Moreover, the time domain response is post processed to obtain clear frequency content.

1.1. Literature Review

The crack models which are used in the literature with the aim of detection, localization and identification of cracks can be classified into two major categories: (1) open crack models and (2) breathing or opening and closing crack models. In other words, the cracks are classified as linear where the crack closure effects are neglected or nonlinear where the crack face penetration is not allowed during vibration. Preliminary studies were concentrated on former one because of the technological limitations and the lack of theoretical approaches on the relevant subjects. Particularly, the number of numerical studies on the vibrations of cracked beams have increased in the last decades due to reduction in the computation times and advances in the modelling techniques of complex structures, i.e. geometries including contacts, cracks etc., by using easily available software packages. This literature review especially focuses on the numerical studies on the dynamic responses of cracked beams.

The studies on the open crack models were limited to the examination of modal characteristics of the beam. Namely, these damage detection approaches were based on the deviations in the natural frequencies and modes shapes resulting from changes in the system damping, mass and stiffness matrices. The most commonly encountered techniques used in the literature to represent open cracks were slots, grooves and linear elastic elements. Cawley and Ray (1988) conducted several experiments on the

cracked and slotted beams with different depth and profile to estimate the natural frequency changes due to cracks of depth equal to those of the slots. Authors concluded that there are differences between the slotted and cracked specimens. Particularly, the specimens having small cracks and slots show considerable difference in the natural frequency shift due to the limitations of the cutter used to open slots.

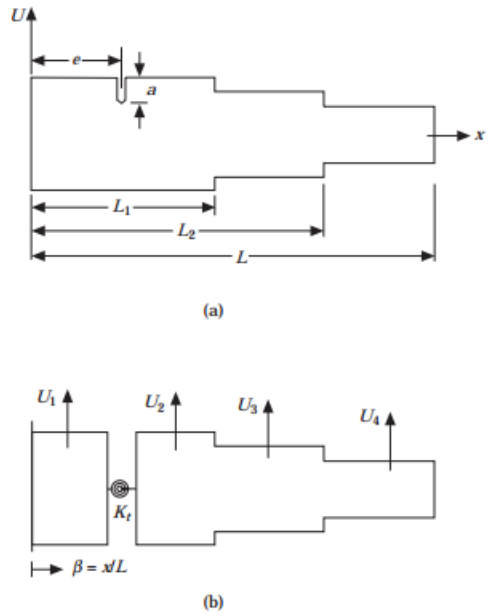

Figure 1: (a) Stepped cantilevered beam. (b) The rotational spring representation of the crack by (Nandwana and Maiti, 1997).

Researchers chose the linear elastic elements to represent cracks by assuming that the effect of cracks is local according to Saint Venant's principle. In other words, the effect of a crack reduces asymptotically with the distance. Tsai and Wang (1996) modeled a crack on a shaft as a joint of a local spring with a constant stiffness value that was derived from LEFM with the assumption of small deformations, homogeneous material and open crack. Authors attempted to estimate the crack depth by using the fundamental frequency shift from the one obtained from baseline intact shaft. In another study, the crack was modelled with constant stiffness rotational spring by Nandwana and Maiti (1997). The crack was located on a stepped beam as shown in Figure 1. A two-dimensional finite element model was also constructed with eigth-noded isoparametric elements in this study as presented in Figure 2.

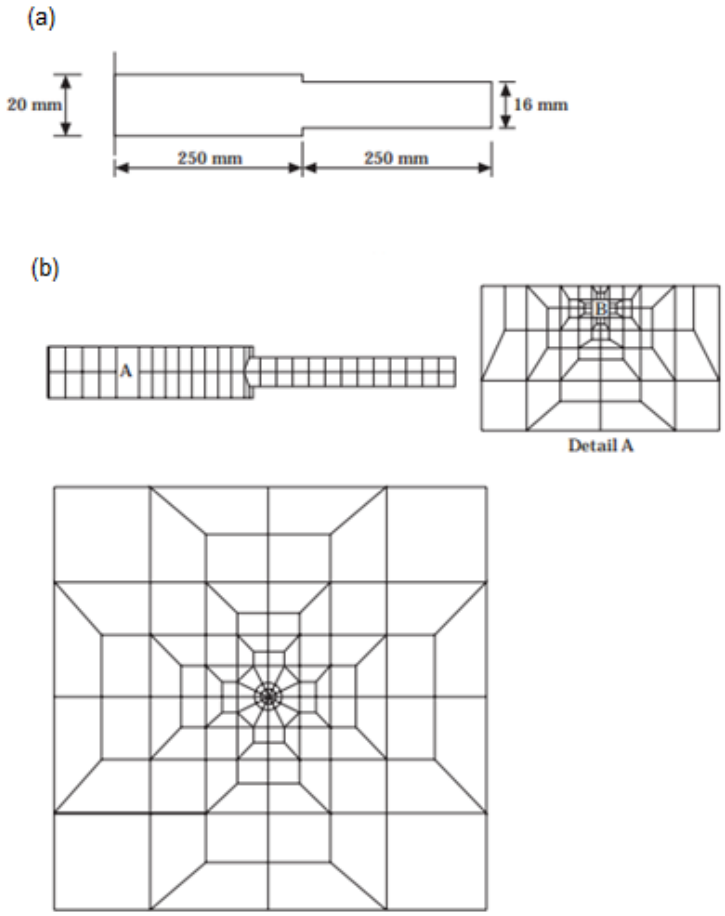

Figure 2: (a) Stepped beam geometry (b) Two dimensional finite element discretization by (Nandwana and Maiti, 1997)

Crack tip was meshed with smaller quad elements than the rest of the beam was modelled with. The beam behaved linearly since no contact definition was available on the crack faces. The authors claimed that the method predicted the location of crack with less than 3% error and crack size with the error less than 5%. Lele and Maiti (2002) published an article on this subject using rotational spring approach on short beams. The rotational spring method used in this paper was the same with other studies in the literature. A constant stiffness rotational spring was inserted to the cracked section. Their finite element model came up with better modelling of cracked region as shown on Figure 3.

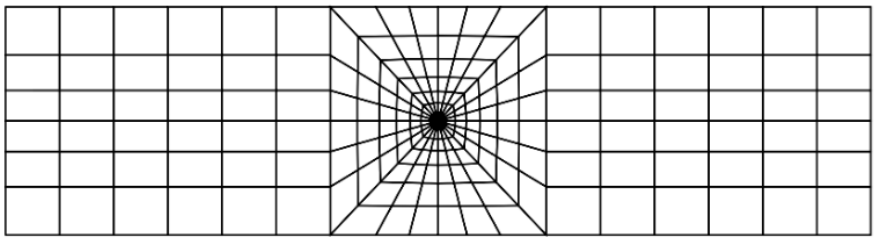

Figure 3: Finite element discretization of a cracked beam (Lele and Maiti, 2002).

The authors of this paper reported that the error of their analytical model reached up to 10% depending on the crack size and the considered natural frequency. Loya, et al (2006) modeled the crack by using linear and rotational springs together. The authors separated the beam into two parts from the cracked face and connected them with massless linear and rotational springs to represent the shear and bending stiffness of the beam. The model is demonstrated in Figure 4. Timoshenko beam theory was used to formulate the governing dynamic equations of the cracked beam with the corresponding compatibility equations. The authors compared direct and perturbative solutions using this model and showed good correlation between them. The vibration of a beam containing several cracks was studies by Aydın (2008). A Rotational spring was located instead of the crack in this study. The stiffness of the spring was taken as constant. The author examined the natural frequencies and mode shapes under different boundary conditions such as pinned-pinned, clamped-pinned, clamped-free, clamped-clamped and spring-spring. The effect of axial load was also investigated in this study. It was concluded that the fundamental frequency dropped about %50 due to a crack having a depth of 50% of the cross section. The solutions with different depth ratios and axial loads were also presented in this study.

Some of the previous studies introduced the effect of the crack by reducing the section modulus. These studies can be divided into two groups which use different approaches to introduce local reduction of modulus or local flexibility. First group of studies consider the construction of weaker stiffness matrix for the cracked section. Simply, it requires the computation of compliance matrix for the cracked section.

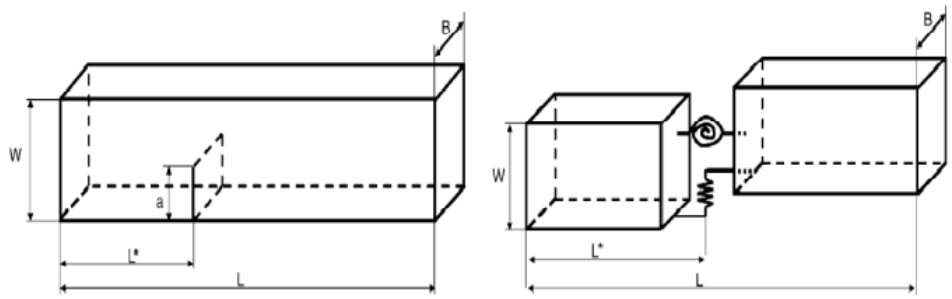

Figure 4: The combined rotational and linear spring representation of an edge crack by (Loya, Rubio and Saez, 2006).

Tlaisi, et al. (2011) conducted a research on the cracked circular shafts supported on bearings. Both numerical and experimental results were obtained in the article. The authors represented the actual crack with the shorter beam elements on the finite element model of the shaft, which reduces the modulus at the specified region. The representative model is illustrated on Figure 5. Two types of crack models were studied. The authors concluded that the crack represented by short elements as in the case of Figure 5a showed better agreement with the test results. Zheng and Kessissoglou (2004) added the flexibility of the crack to overall structure rather than a cracked section. In other words, the elements of overall stiffness matrix was multiplied by an additional dimensionless flexibility coefficient. The authors claimed that the results showed better accuracy in natural frequencies than those obtained by local stiffness matrix approach.

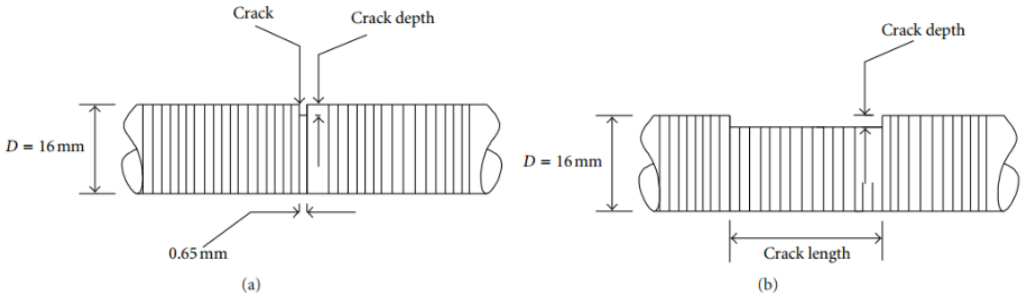

Figure 5: Diagram of: (a) one element representing crack effect and (b) a wider element representing the crack effect by (Tlaisi, Swamidas, Haddara and Akınturk, 2012).

The second group of studies considered the construction of element stiffness matrix for cracked finite element which was then assembled with intact system stiffness matrix, rather than calculating section compliance matrix. With element stiffness matrix, computational time became shorter and uncertainties in the stiffness or compliance calculation were avoided as stated by Saavedra and Cuitino (2001) in their article. Hjelmstad and Shin (1996) used this technique comprehensively. Instead of dealing with the system stiffness matrix, the authors of this article, were dealt with the element constitutive properties. In other words, the change in element constitutive properties can be considered as damage indications. The authors argued that this approach is attractive since it preserves structure topology and essential features of the flow of forces. Also, it was stated that element-based analysis came up with direct indications of damage. Two-dimensional plane stress element model and Euler beam element model were constructed in this article. The parametric constitutive properties were selected as Young's modulus E for plane stress elements and flexural stiffness EI for Bernoulli-Euler beam elements. Namely, these properties of the elements in the vicinity of the crack location were adjusted by the authors. Chondros (1998) developed a cracked beam model in which the crack flexibility was distributed throughout the beam. The authors also compared this model with the one which has local flexibility. The results showed good agreement with the local flexibility models and test results.

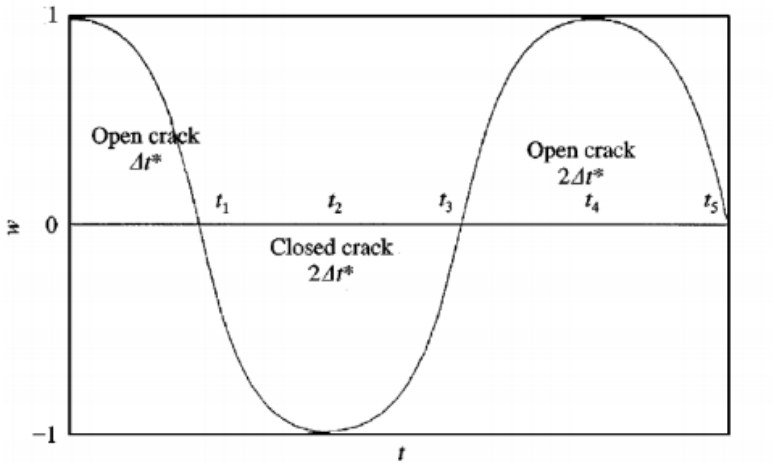

Figure 6: Stiffness section diagram of a bilinear system having breathing crack by (Chondros, Dimarogonas and Yao, 2001)

The studies related to breathing (opening and closing) crack models suggested that when the accuracy is the concern, the nonlinear effects due to crack face interaction cannot be disregarded. It is obvious that the global stiffness matrix depends on the state of the crack whether it is open, closed or both (partial contact of crack faces). Gudmundson (1982) emphasized the importance of crack closure by conducting experiments on transverse vibration of cracked beams. The author concluded that depending on the size and location, the crack may be closed, open or partially open. It was concluded that the techniques relying on the natural frequencies of the structure may fail to detect the crack if the crack stays closed due to crack closure effects. Clark et al. (1987) conducted several experiments on specimens under four point bending load to figure out the effect of crack closure on the crack detection methods. Thus, researchers gave more importance to the dynamic behavior of the cracked beams by considering the breathing behavior of the crack. In the breathing crack models, there are two distinct approaches. There are continuous models and bilinear models. The first group of studies defined the stiffness of the beam with a piecewise continuous function changing between two crack phases, i.e. open or close, whereas other group of studies defined it continuously. Chondros, Dimarogonas and Yao (2001) examined a one dimensional beam with breathing crack. In Figure 6, the transverse vibration of a cracked beam is presented. The modelled beam showed bilinear behavior since the transition from open to closed crack occurs exactly at the undeformed position. It can be observed that t1, t2 and t3 are the instants when the beam is in undeformed position. The authors indicate that the frequency drop due to crack was lower in breathing crack models than open crack models. It is also worth to note that under sufficient preload, the fatigue cracks can be considered as breathing cracks. Otherwise, the crack remains closed due to crack closure effects.

In bilinear models, crack phase changes instantaneously. Namely, the crack either closes or opens. This behavior is given by a piecewise function of stiffness or load on the cracked section in the literature. In the studies which used the stiffness matrix as a function, the common approach was that the additional flexibility of the cracked section is found by using linear elastic fracture mechanics and assembled with the intact beam stiffness matrix when the crack is open. In addition, the open and closed

crack modes were determined by a parameter such as curvature of the beam under deformation or relative displacements of crack faces. This parameter was used as a center point of piecewise continuous stiffness function. The governing equations of motion for this approach can be represented by Equation 1 using the general equation of motion for a damped system.

$$\boldsymbol{M\ddot{x} + C\dot{x} + K'x = F}sin(wt) \tag{1}$$

And,

$$\boldsymbol{K'} = \begin{cases} \boldsymbol{K_{intact}}, & crack\ close \\ \boldsymbol{K_{crack}}, & crack\ open \end{cases} \tag{2}$$

$$\boldsymbol{K_{crack} = K_{intact} + K}_{flexibility} \tag{3}$$

Where, M stands for mass matrix of the beam, C is the system damping matrix. It was assumed that mass and damping matrices of the system do not change with the crack. K' is the system stiffness matrix. It is a piecewise continuous function, which interchanges between intact and cracked system stiffness matrices. The stiffness matrix of cracked system was found mostly by introducing the flexibility matrix to the intact beam stiffness matrix. Flexibility of the system due to crack can be calculated by LEFM. The calculation of flexibility matrix is formulated in Equation 4 to 6. The strain release rate is given in Equation 4 in a general form.

$$\mathrm{J} = \frac{\partial \mathrm{U(F,A)}}{\partial \mathrm{A}} \tag{4}$$

In this equation, "U" is the strain energy in the system and "F" and "A" are the external force on the system and the area effected by the external force. The partial derivative of the system strain energy by the area gives the strain release rate of the system. The strain release rate is also defined by Griffith-Irwin theory for linear elastic fracture mechanics with the stress intensity factors at a crack tip under three different modes.

The Equation 5 defines the strain release rate in the Griffith-Irwin theory.

$$J = \frac{(1-\upsilon^2)}{E} {K_I}^2 + \frac{(1-\upsilon^2)}{E} {K_{II}}^2 + \frac{(1+\upsilon)}{E} {K_{III}}^2 \tag{5}$$

The strain intensity factors under different modes are required to calculate the strain release rate from Equation. By relating the Equation 4 and 5, the following equation is reached.

$$\frac{(1-\upsilon^2)}{E}{K_I}^2+\frac{(1-\upsilon^2)}{E}{K_{II}}^2+\frac{(1+\upsilon)}{E}{K_{III}}^2=\frac{\partial \mathrm{U(F,A)}}{\partial \mathrm{A}} \tag{6}$$

The strain energy in the system can also be defined by Castigliano's theorm follows,

$$u=\frac{\delta U(F,A)}{\delta F} \tag{7}$$

By substituting Equation 6 to 7,

$$u=\frac{\delta}{\delta F}\int_0^a(\frac{(1-\upsilon^2)}{E}{K_I}^2+\frac{(1-\upsilon^2)}{E}{K_{II}}^2+\frac{(1+\upsilon)}{E}{K_{III}}^2)\,\partial \mathrm{A} \tag{8}$$

The flexibility compliance matrix coefficients can be found by,

$$C=\frac{\partial u}{\partial F} \tag{8}$$

Finally,

$$C=\frac{\partial^2}{\partial F\partial F}\int_0^a(\frac{(1-\upsilon^2)}{E}{K_I}^2+\frac{(1-\upsilon^2)}{E}{K_{II}}^2+\frac{(1+\upsilon)}{E}{K_{III}}^2)\,\partial \mathrm{A} \tag{9}$$

$$\boldsymbol{K}_{flexibility}=\boldsymbol{C^{-1}} \tag{10}$$

From Equation 10, the introduced flexibility due to crack to the stiffness matrix can be calculated by the stress intensity factor of the crack tip.

In some of the studies, the stiffness of the cracked and intact beam were obtained from static solutions. Considering the force displacement graphs, the stiffness change can be observed. A representative force displacement graph of a cracked beam is

demonstrated in Figure 7. Dimarogonas and Papadopoulos (1983) considered the effect of crack closing and opening with local flexibility matrix calculated from LEFM, in particular, stress intensity factors and strain energy densities, on rotating machines.

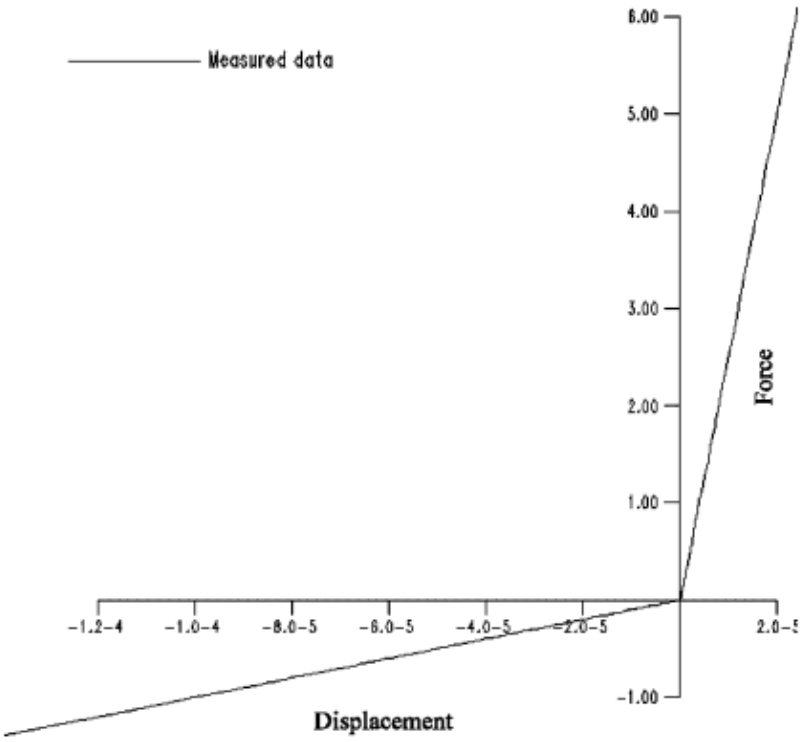

Figure 7: A force displacement graph (Worden, Farrar, Haywood and Todd, 2008)

Qian et al. (1990) published an article on the vibration of a beam having transverse edge crack. The authors introduced the bilinear behavior of the cracked beam by constructing two stiffness matrices for open and closed modes of the crack. The stress sign of the crack face stress was considered to determine the mode of the crack whether it is open or closed. Chati et al. (1997) investigated the vibration of the cracked beam by using bilinear models. The non-linearity due to presence of the crack is examined mathematically using equivalent one and two degree of freedom spring mass model. For extending the approach to infinite degree of freedom systems, a finite element

model was constructed in this article. In addition, the authors attempted to establish an effective natural frequency for the cracked beam by considering the natural frequencies of cracked and intact beam. The cracked beam and its simplified 1D spring mass model can be seen on Figure 8.

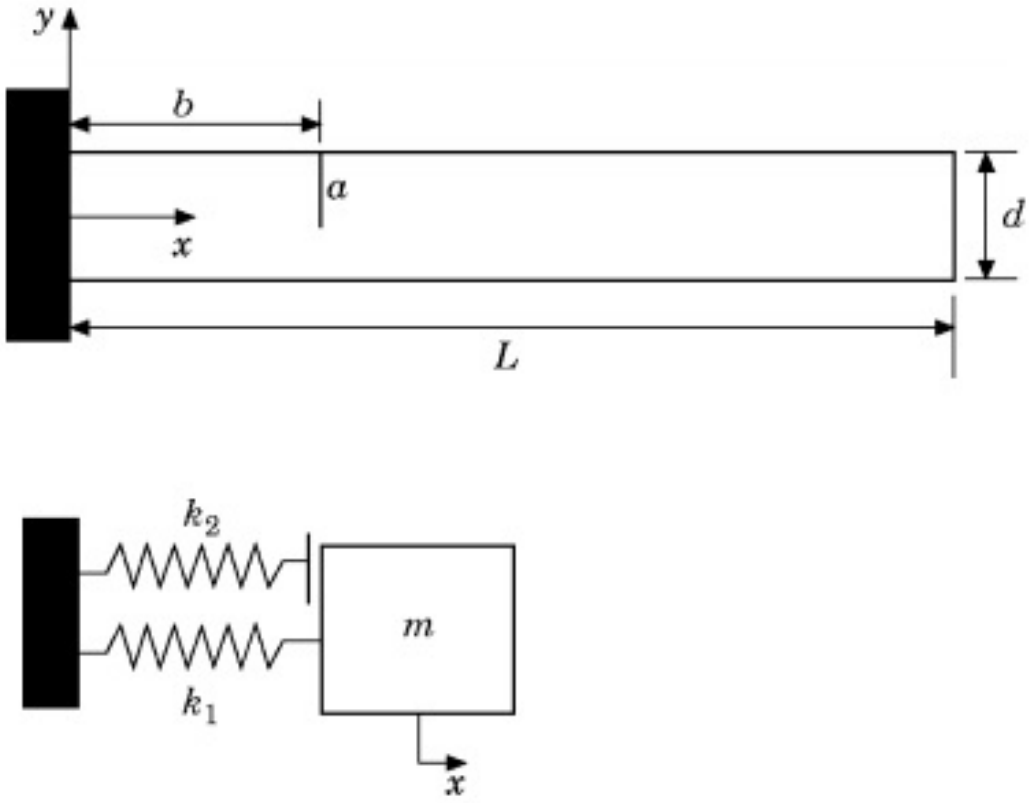

Figure 8: Beam model and spring mass model (Chati, Rand and Mukherjee, 1997).

The stiffness of the system is different when x is positive and negative. When x is positive, the crack is open. Otherwise, the crack is closed. The authors defined the natural frequency of this one dimensional nonlinear model as "bilinear frequency". It is formulated by Equation 11.

$$\omega_o = \frac{2\omega_1\omega_2}{\omega_1+\omega_2} \tag{11}$$

where,

$$\omega_1 = \sqrt{\frac{k_1}{m}}\ and\ \omega_2 = \sqrt{\frac{k_1+k_2}{m}} \quad (12)$$

Where, ω_1 and ω_2 are two linear natural frequencies of the one dimensional model when the x<0 and x>0, respectively. ω_o stands for the "bilinear natural frequency" of the system. This is a very basic but effective mathematical representation of natural frequency of a cracked beam. The authors compared their finite element results with bilinear frequency of their beam and correlate the results with small errors. In Figure 9, the finite element model of the authors is shown. Two models were constructed. One of them is constraint and other one is unconstraint model. The crack face penetration was not allowed in constraint model. The authors calculated the bilinear natural frequency by using the natural frequencies of these two FE models and try to extend their approaches to infinite degree of freedom systems. It was concluded that using bilinear frequency as an effective natural frequency was a good approximation for such cracked beams where eigenvalue solutions cannot be obtained due to nonlinearity caused by crack face interaction.

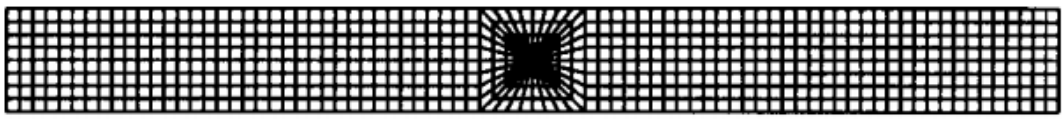

Figure 9: The undeformed mesh model (Chati, Rand and Mukherjee, 1997).

Saavedra and Cuitino (2001) investigated the vibration characteristics of free-free beam by using the same method. Stiffness matrix was defined by a piecewise continuous function which uses the relative rotation of the adjacent nodes as a center point. The authors observed the higher even harmonics due to crack induced nonlinear behavior. It was also reported that the forcing frequency should be the half of the

natural frequency to obtain high vibration amplitude at the specified location where the acceleration and displacement results were obtained. In the article of Chatterjee (2010) higher order FRFs were investigated by using a bilinear oscillator given in Figure 10. The generation of higher harmonics on the frequency response of cracked beam vibration were systematically explained by Volterra series response representations.

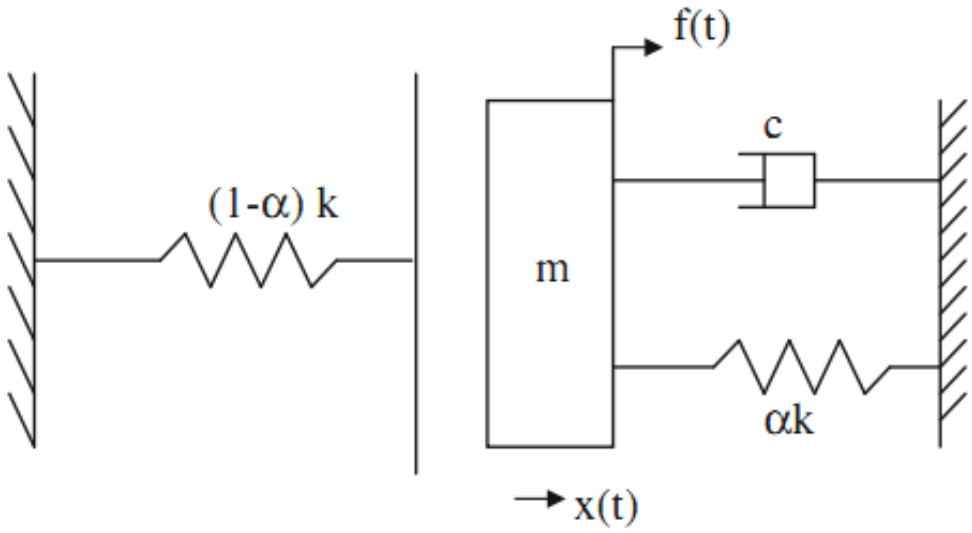

Figure 10: The bilinear oscillator (Chatterjee, 2010).

Giannini et al. (2013) demonstrated systematically the crack identification procedure by using bilinear finite element model. The breathing behavior of the cracked beam was given by piecewise continuous stiffness function as given in Equation 13.

$$K_d = K_{intact} - H(\theta_i - \theta_j)K_{cracked} : \begin{cases} H(\theta_i - \theta_j) = 1, \ \theta_i > \theta_j \\ H(\theta_i - \theta_j) = 1, \ \theta_i < \theta_j \end{cases} \quad (13)$$

Where K_d is the stiffness matrix for the element having breathing crack and θ_i stands for the rotation on the ith section. The value of the Heaviside function is determined by

the relative rotation of the i^{th} and j^{th} sections. $K_{cracked}$ is the stiffness of the cracked finite element which was determined by non-dimensional flexural damage parameter calculated by moments of inertia of cracked and intact beam. Important remarks were drawn by the author: examination of higher harmonics gave ability to detect cracks up to 5% depth when single mode techniques could detect cracks only larger than 15%. Batihan and Cigeroglu (2009) investigated the vibration characteristics of a beam with an breathing edge crack by a SDOF system with an bilinear stiffness using Galerkin's Method. Their model is presented in Figure 11. They solved the dynamic equations with harmonic balance method in order to interchange from nonlinear differential equations to nonlinear algebraic equations of motion. Further, the authors analyzed the effect of crack location and crack position. One of their important outcome is that the location is crack may be insignificant depending of the slope at the cracked section. For their clamped-clamped beam, the slope is zero at the mid-section at the fundamental frequency, thus the crack cannot be detected at this section. Also, it is observed by the authors that the crack depth has significant effect on the amplitudes of the harmonics. They also concluded that the crack parameters have more effects on the higher harmonics than on the first harmonic. This study seems to have similar purpose with this thesis. The crack depth and crack location are also parameters investigated in this thesis. The effect of crack location show similar pattern in both studied. The Table 18 shows the effect of crack depth on the crack detection parameter. The depth has significant effect on both studies. Further, the effect of crack location is concluded in both study such that it is significantly affected by the mode shape at the regarding frequency and crack location. In both study, it is stated that the crack location cannot be considered as an independent parameter for the crack detection since depending on the crack location its effect may be insignificant on the frequency response.

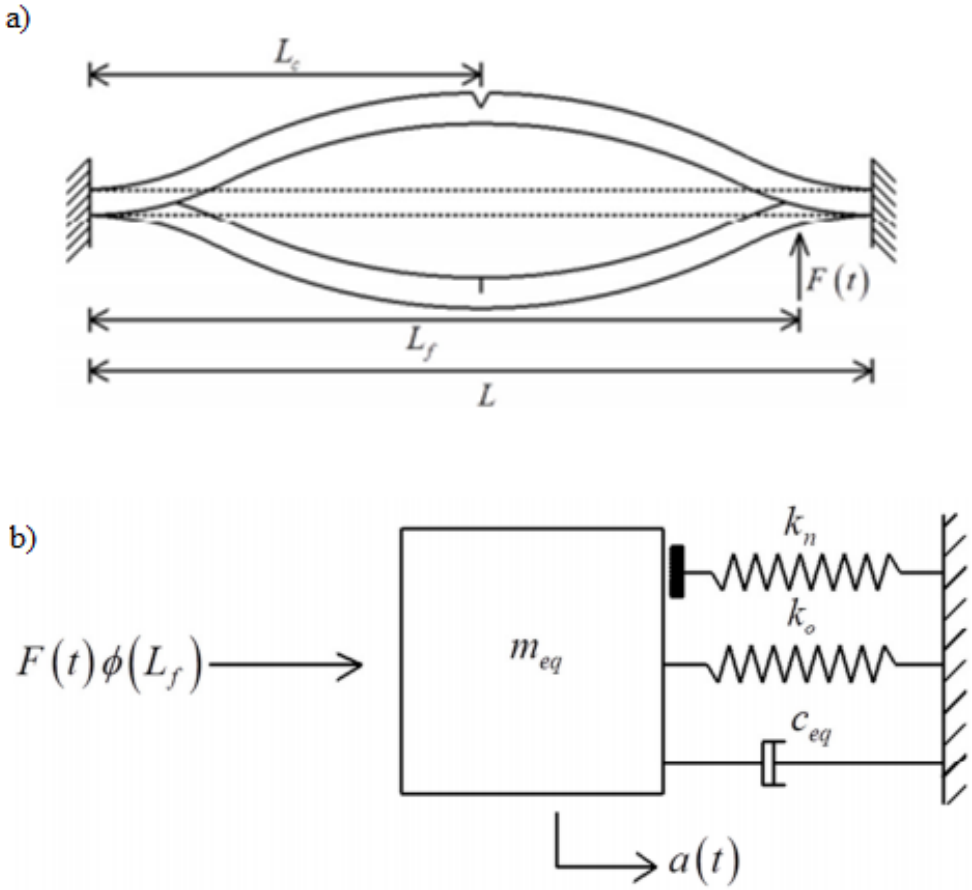

Figure 11: (a) The clamped-clamped beam with a crack at the mid-section (b) The SDOF model of beam by (Batihan and Cigeroglu, 2015)

The studies mentioned above assumed the crack either open or close. The change from closed configuration to open configuration occurs instantaneously. The typical load displacement curve for a cracked beam was given by Newman et al (1988) as in Figure 12. Clark et al. (1987) conducted several experiments to investigate this crack closure effect. In Figure 13, the resulting displacement force curve shape of the authors is presented.

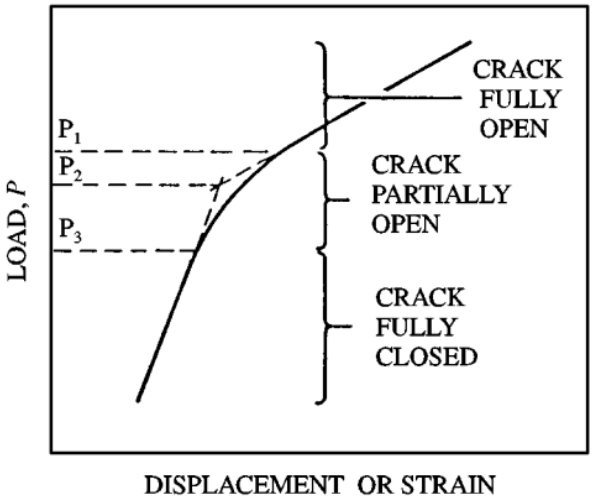

Figure 12: Typical load displacement curve (Newman Jr and Elber, 1988)

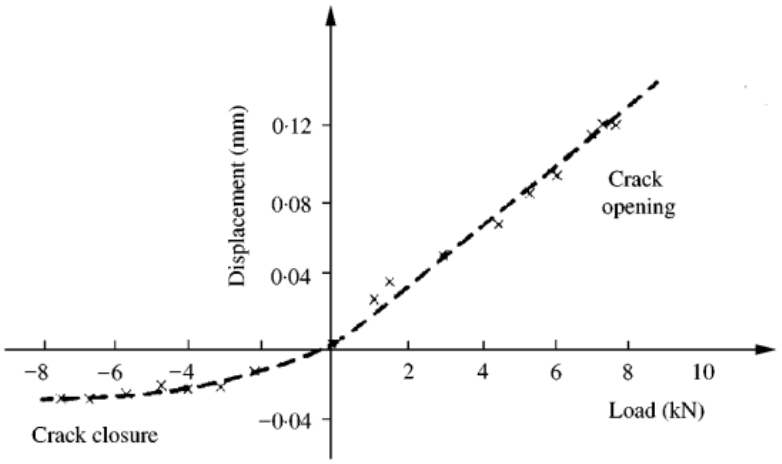

Figure 13: Force displacement graph from test (Clark, Dover and Bond, 1987).

Later, the researchers tried to simulate the vibration of the cracked beam more realistically. This approach started with some periodic functions of stiffness matrix and evolved to finite element simulation of cracked beam with incremental time steps. Cheng et al. (1999) investigated the vibration of the cracked beam by using a cosine function for stiffness matrix. Rather than using directly a constant flexibility matrix, the authors gave the stiffness matrix as shown in Equation 14.

$$K = K_{intact} + \Delta K(1 + \cos(wt)) \tag{14}$$

where,

$$\Delta K = \frac{1}{2}(K_{cracked} - K_{intact}) \tag{15}$$

The authors observed the generation of sub- and super-harmonics. Further, it was suggested to use non-linear vibration methods to detect the crack rather than to analyze the natural frequency shift. Pugno and Surace (2000) published an article on the vibration of cracked beam with several breathing cracks. The authors of this article pointed out the effect of crack closure. The ratio of instantaneous curvature of the beam to the maximum curvature was taken as a parameter by the authors to adjust the stiffness matrix such that transition from open crack mode to closed mode became smoother. Kisa and Brandon (2000) modified the stiffness matrix incrementally such that the transition of the stiffness matrix from open to closed crack phase occurs incrementally. In detail, the contact area of the crack was increased in each increment such that the interchange from open to closed crack did not happen instantaneously. The contact was formulated mathematically by two different springs by the author. One of them deal with the normal contact stiffness and other one stands for the stiffness in tangential direction. Carneiro and Riberio (2015) implemented p-version FEM to simulate the vibration of a cracked beam. Equations of motion was solved by Newmark's method in time domain. The authors employed the rigidity function proposed by Christides and Barr (1984) to introduce the flexibility of crack. It was assumed that the effect of crack was local and obeyed the principal of Saint Venant. The authors suggested that using velocities and accelerations gives more valuable information about the detection of cracks.

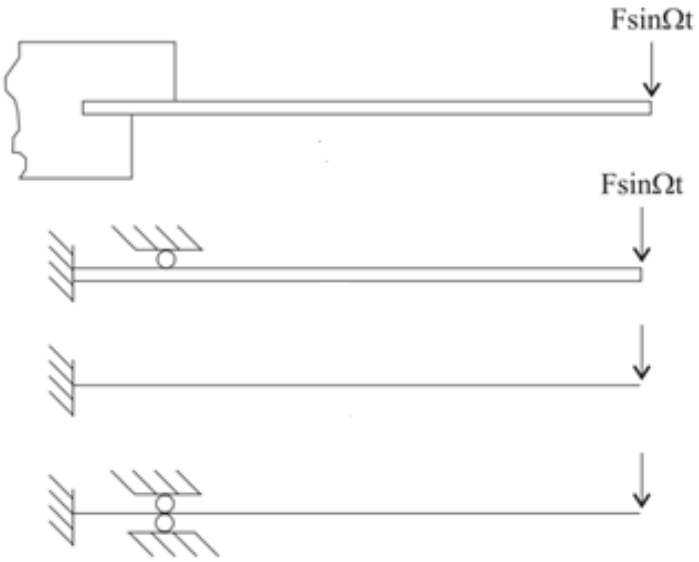

Figure 14: Excitation of a cantilever beam and representations of the clamping with three different models (Nandi and Neogy, 2002).

Development of technological facilities and advances in numerical methods allowed researchers to analyze the contacting conditions more precisely. Thus, the simulation of cracked beam developed, as well. In contrast to the previous studies which modeled the crack as either fully open or fully closed or having stiffness in between, the studies published in the last decade considered the instantaneous contact of the crack faces as a variable in the equation of motion. These studies were done by finite element method in general. Nandi and Neogy (2002) studied the breathing behavior of the transverse vibrating beams by introducing contact condition with small displacement approach. Contact was solved by virtual work method using two dimensional finite elements. The position and size of the crack was taken as a parameter. Further, the authors investigated the effect of the clamping by two heavy jaws. Different boundary conditions representing the imperfections in the clamping were presented by the authors as in Figure 14. The multiples of the excitation frequency was observed in the Fourier spectra by the authors. Also, the difference between the beams, hold perfectly and imperfectly, was stated. It was suggested to use half of the natural frequency of the cracked beam since the amplitude of the 2^{nd} harmonic was considerably amplified which was used as a damage indicator. Moreover, it was worth to note that the relative amplitude of the generated higher harmonics might be so small such that they cannot

be observed in a noisy data. Andreaus et al. (2007) modelled the vibration of the beam which has asymmetric edge crack under harmonic tip load. The beam was constructed with two dimensional elements as presented in Figure 15.

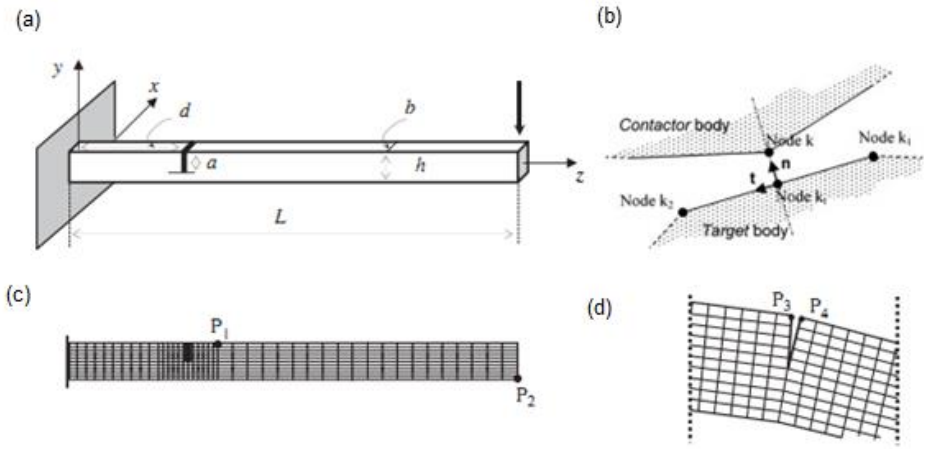

Figure 15: Finite element modelling of a cracked beam under contact condition (Andreaus, Ugo, Casini, Paolo, Vestroni and Fabrizio, 2007).

Frictionless contact was introduced by the authors between the crack faces. The constructed finite element model was compared with the bilinear oscillator results. The bilinear oscillator used for comparison with the constructed finite element model was shown in Figure 16.

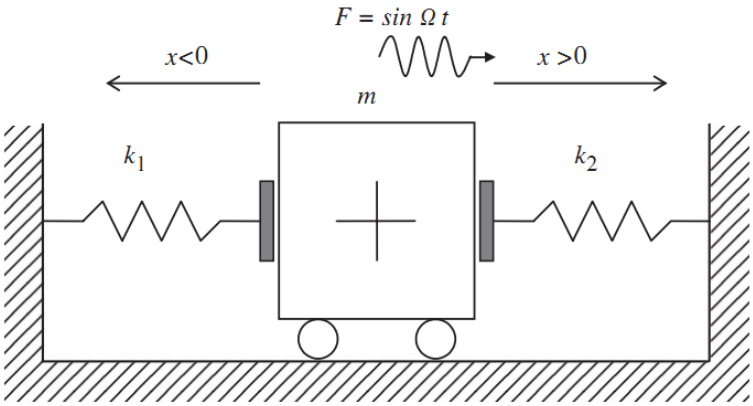

Figure 16: Bilinear oscillator representing the cracked beam vibration under forced vibration (Andreaus, Ugo, Casini, Paolo, Vestroni, Fabrizio and 2007).

The comparison was drawn such that bilinear oscillator results had good agreement with the finite element results. The authors suggested that for complex response of the

cracked beam, bilinear approach can give precise preliminary results especially about the best excitation frequency. Further, the authors indicated that exciting the cracked beam with (1/n) or n times the first natural frequency can give observable higher- or sub-harmonics at nth and (1/n)th harmonics. Orhan (2007) simulated the transversal vibration of cracked beam using three dimensional finite elements. Free and force vibration results of the cracked beam were compared in this study. Single and double crack configurations were modelled without any crack face interaction. The finite element model of the author presented in Figure 17. The author concluded that using free vibration results was more effective in detection of two crack configuration. Using force vibration results, however, the crack location and depth can be determined more precisely since their effect on natural frequency is very small.

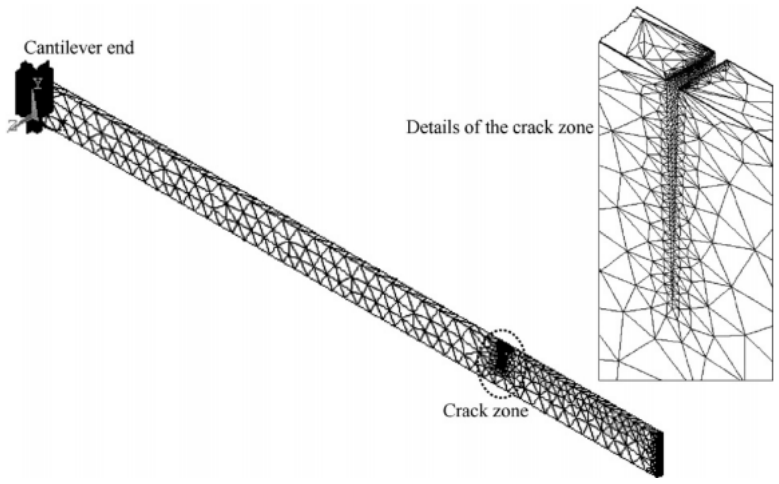

Figure 17: Three dimensional finite element model (Orhan, 2007).

Andreaus, Baragatti, & Vestroni (2011) compared three different numerical models for the vibration of the beam which has non-propagating transverse crack. The first model was one dimensional beam with a rotational spring at the crack location. The constant stiffness value of the spring was determined from LEFM. The second model of the authors was two dimensional finite element model. A contact algorithm was defined for the elements at the crack face such that penetration of the faces was prevented. The equation of motion for this model was solved with Newmark iteration.

The last model was a spring mass damper system. Authors compared three numerical model by examining the generation of sub- and super-harmonics in the Fourier spectra, the shape of the modal line and the deviations in phase portrait. The excitation frequency used in this article was one-third and one-half of the first natural frequency of the intact beam. Further, different crack sizes and locations were compared. Time history of the transversal acceleration of intact and cracked beams was presented in Figure 18 to show how the curve was deviated when a crack is introduced to the beam.

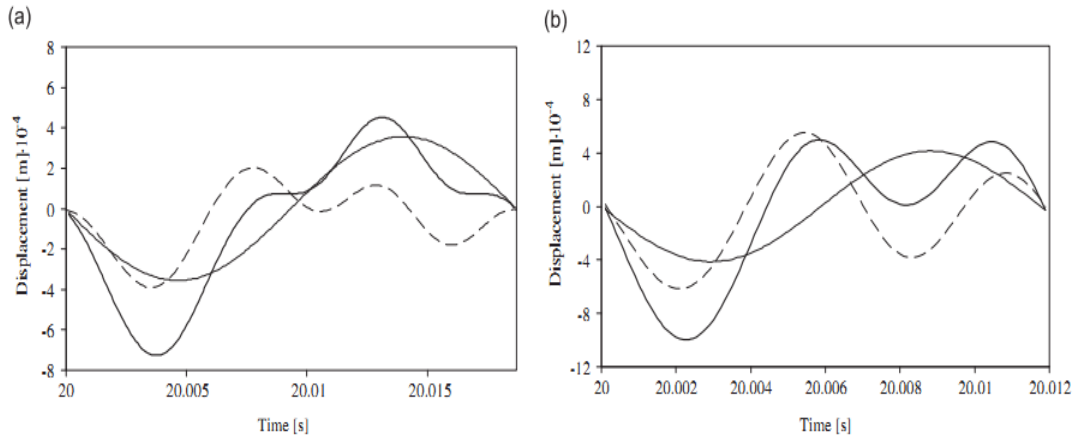

Figure 18: Typical displacement responses of a beam in time domain (Andreaus, Baragatti, & Vestroni, 2011)

The harmonic acceleration response deviated due to generation of sub- and higher-harmonics. The authors concluded that existence of a fatigue crack had considerable effect on the generation of harmonics which did not appear on the vibration of an intact beam. It was stated that second and third harmonic components were very sensitive to the existence of a crack. Moreover, the authors emphasized that the sub-multiples of natural frequency, i.e. 1/2 or 1/3 of the natural frequency, can be used as the excitation frequency to detect very small cracks. Bouboulas and Anifantis (2010) studied nonlinear behavior of a beam with nonpropagating edge crack using conventional two dimensional finite element method and compared their study with the former open crack methods and breathing crack methods in the literature. The authors employed the interaction between the crack lips by master-slave concept. In this concept, the penetration of the surface nodes through the counter surface nodes were prevented, and internal forces were raised after equilibrium conditions were satisfied. The

equation of motion of the cracked beam solved by iterative approach, particularly by modified Newton Rapson iteration method. The objectives of the authors were to investigate the effect of crack angle, depth and position into vibrational behavior or the beam. The discretized beam model in this article is presented in Figure 19. The FFT was applied to obtain the content of the response by the authors. Further, continuous wavelet transforms (CWT) was employed to account for the time varying changes from transient region to steady state region. The differences of the results with the previous authors were tabulated. There were slight deviations at the relative frequency of the harmonics from the compared finite element approaches published before.

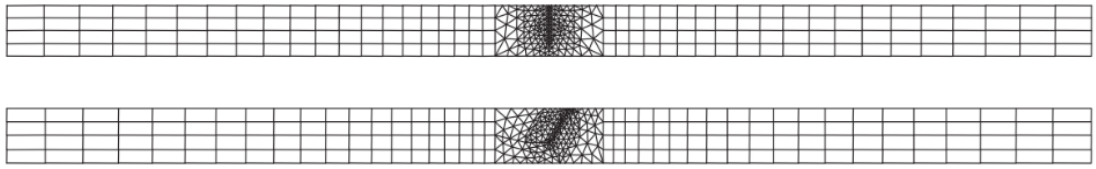

Figure 19: Finite element model (Bouboulas, A. S. and Anifantis, N. K., 2010).

Bouboulas and Anifantis (2013) extended their study to three dimensional finite elements method. Both torsional and axial modes of the beam were taken into account in the vibration of the cracked beam. Surface and edge crack configurations were analyzed and compared with open crack models. The finite element models of the cracked beam are illustrated in Figure 20. Full frictionless contact model was employed for the crack interaction. The authors investigated the effect crack angle, size and location on the response by considering axial and torsional modes of the beam and compared the results with the previous studies. Some differences was observed with the previous two dimensional methods especially in second bending natural frequency. Jyrki, Kari and Anthony (2013) investigated the minimum crack length that can be detected by vibrational methods on cantilevered beam with central crack. A structured sensor network and data interpretation methods were utilized in this article. Abaqus Explicit finite element code was employed to simulate the transversal vibration of the cracked beam under random excitation. The finite element model is shown on Figure 21. Two dimensional 4 node linear elements with reduced integration

were used. Rayleigh damping coefficients were introduced to damp the system. Further, the static deflection of the cracked beam was correlated with the analytical solution. It was indicated that there were some degree of noise on the acceleration response, which affect the smallest crack size that can be identified. The authors conclude that the minimum central crack size that can be identified on a cantilevered beam is 10% of the beam cross section. Also, authors suggested to put several sensors to both side of the crack to obtain valuable information.

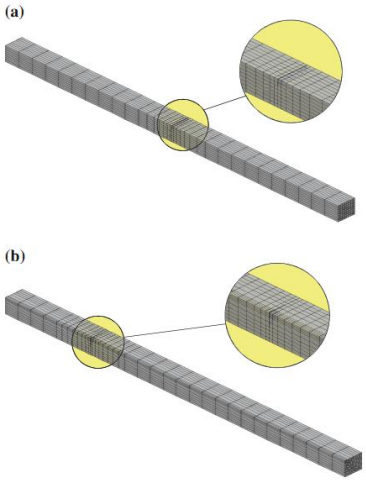

Figure 20: Three dimensional finite element model of a cracked beam (Bouboulas, A. S. and Anifantis, K. N., 2013)

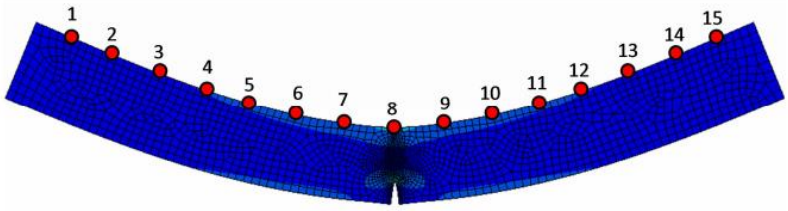

Figure 21: Two dimensional finite element model (Jyrki, Kari and Anthony, 2013)

Sinenko and Zinkovskii (2015) published an article about the effects of force application location on the frequency content of the response. Three dimensional finite element model was constructed for the cracked beam as shown in Figure 22. It was stated that using three dimensional finite element model allowed to consider all vibrational modes. The authors investigated the relative amplitudes of the sub- and

super-harmonics in the identification of the crack. The authors claimed that there are strong dependence of harmonics on the location of excitation point. Moreover, it was stated that there are some excitation point locations where no sub- and super-harmonics were generated in the response.

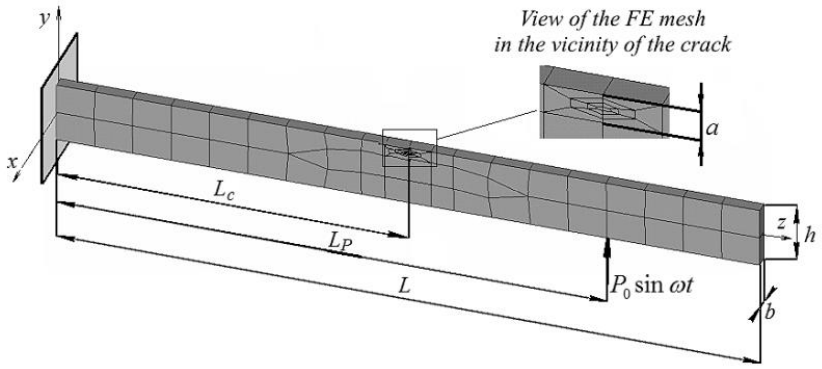

Figure 22: Three dimensional finite element model (Sinenko and Zinkovskii, 2015).

Broda et al. (2016) simulate the longitudinal vibration of a cracked cantilevered beam using two dimensional finite element method. The authors attempted to isolate the crack induced nonlinearities. It was claimed that the generated nonlinear features in the response could be because of boundary conditions or sensor network. The finite element model used in this article is presented in Figure 23.

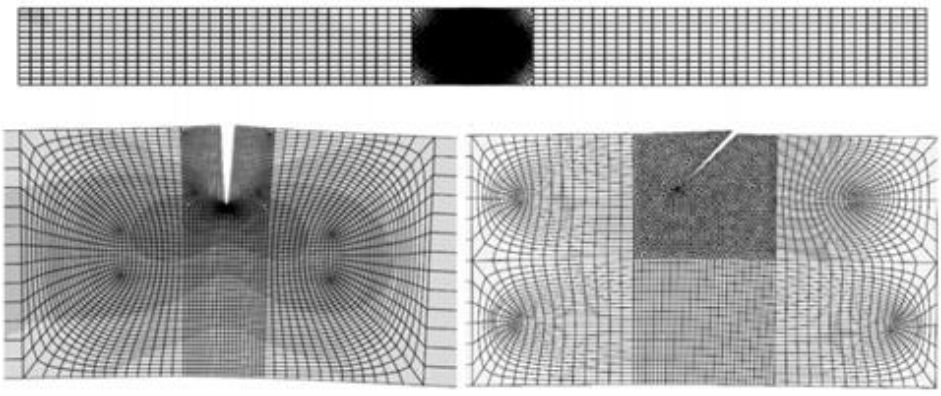

Figure 23: Two dimensional finite element model (Broda, Pieczonka, Hiwarkar, Staszewski , & Silberschmidt, 2016).

Several boundary conditions, such as fixed-free and free-free, were applied in order to comment on the effects of boundary conditions on the response. Orthogonal and slanted crack configurations were considered. The authors related the existence of crack on the beam to a parameter, called as "coefficient of nonlinearity" which was the ratio of higher-harmonics to the fundamental frequency. The results were compared with the fatigue cracked beams under forced longitudinal forced vibration. The authors concluded that fixed-free boundary condition and second harmonic gave the strongest crack localization effect. Further, the authors suggested that the excitation amplitude should be high enough such that it can open the crack. Even though the experimental results illustrated the localization of crack, the authors indicated that the indications were very weak and further information must be obtained for complex structures.

The following table summarizes the literature review in this study. The major considerations are the boundary conditions, excitation type and the crack modelling used. Also the availability of the experimental works are presented in the Table 1.

Considering the many articles addressed in this literature review one can draw the following conclusions;

- The cracked beam FE models are constructed by using rotational springs, stiffness matrix reduction or modification, cracked beam elements, 2D/3D solid elements.

- The presence of a sharp fatigue crack manifests itself as generation of sub-super harmonics in the response.

- Half or one third of the 1st natural frequency is found as the best excitation frequency in order to observe nonlinear effects in the response although there are some studies where the beam is excited with the 1st natural frequency.

- Smallest detectable crack size suggested as 10% of the cross section depth to observe the nonlinear effects on the frequency response

Table 1: List of references

REFERENCE	CRACK TYPE	BC	EXC	EXP.
Cawley and Ray (1988)	Slot, Fatigue	Fixed-Free	Modal	Yes
Nandwana and Maiti (1997)	Rotational Spring	Fixed-Free	Modal	Yes
Lele and Maiti (2002)	Rotational Spring	Fixed-Free	Modal	Yes
Aydın (2008)	Rotational Spring	Pinned, clamped, free	Modal	No
Zheng and Kessissoglou (2004)	Stiffness matrix	Fixed-Free	Modal	No
Saavedra and Cuitino (2001)	Stiffness matrix	Free-Free, Fixed-Free	Forced	Yes
Hjelmstad and Shin (1996)	Modulus	Fixed-Free	Forced	Yes
Chondros and Dimarogonas (1998)	Stiffness matrix	Fixed-Free	Forced	Yes
Clark et al. (1987)	Fatigue Cracked	4 point Bending	No	Yes
Dimarogonas et al. (1983)	Stiffness matrix	Rigid Body	Yes	No
Qian et al. (1990)	Stiffness matrix	Fixed-Free	Yes	Yes
Chati et al. (1997)	Stiffness matrix + FEM	Fixed-Free	Yes	No
Chatterjee (2010)	Stiffness matrix	Free-Free	Yes	No
Giannini et al. (2013)	Stiffness matrix	Fixed-Free	Yes	No
Cheng et al. (1999)	Stiffness matrix	Fixed-Free	Yes	No
Pugno and Surace (2000)	Stiffness matrix	Fixed-Free	Yes	No
Kisa and Brandon (2000)	Stiffness matrix	Fixed-Free	Modal	No
Carneiro and Riberio (2015)	Reduced Compliance	Fixed-Fixed	Forced	No
Nandi and Neogy (2001)	FEM Contact	Fixed-Free	Forced	No
Andreaus et al. (2007)	FEM Contact	Fixed-Free	Forced	No
Orhan (2007)	FEM	Fixed- Free	Forced	No
Andreaus and Baragatti (2009)	Fatigue Crack	Fixed- Free	Free	Yes
Andreaus et al.2011)	Spring + FEM	Fixed- Free	Forced	No

Bouboulas and Anifantis (2010)	FEM Contact	Fixed- Free	Forced	No
Bouboulas and Anifantis (2013)	FEM Contact	Fixed- Free	Forced	No
Jyrki, Kari and Anthony (2013)	FEM Contact	Fixed- Free	Forced	No
Sinenko and Zinkovskii (2015)	FEM Contact	Fixed- Free	Forced	No
Broda et al. (2016)	FEM Contact	Fixed- Free, Free-Free	Forced	Yes

1.2.Objective of this study

This study is a part of a research about the crack identification on a fatigue cracked cantilever beam by analytical, numerical and experimental methods. There are several researches on this subject, however there is still a need for more discussion about finite element method used for simulating the vibration of a beam due to limitations in number of iterations in numerical calculations. The current solutions seem to be unsatisfactory in the validation of numerical results with the experimental results. This study presents an alternative way to model the crack front and much more digitized time domain solutions than the previous works published on this subject. The main objective in this study is to point out the effectivity of numerical methods on the detection of crack induced nonlinear effects such as generation of sub- and higher-harmonics with an alternative mesh pattern and finer resolution in the vibration response. Further, the effect of the crack location, crack depth and excitation frequency on the characteristics of harmonics are investigated in this research.

CHAPTER 2

FINITE ELEMENT MODEL

The vibration analysis for the detection of cracks on the structures is conducted using an aluminum beam with a square cross section. The material properties of the material is given in the following sections. The numerical simulation of this beam is employed by two dimensional finite element method. Pre-processing is performed in ABAQUS^{TM} software and post-processing is performed in MATLAB^{TM}. Available crack models, i.e. seam, XFEM and slot type, are compared and the most functional one is selected for the analysis. The crack tip singularity is confirmed by NASGRO^{TM} software by conducting static analysis. Different boundary conditions are applied to the beam such as fixed-free and fixed-fixed. Forced vibration response of the beam at the specified locations are obtained under harmonic and impulse loading.

2.1. Specimen Dimension

A square cross sectional beam is modelled with the dimensions given in Figure 24. The free length of the beam is 500 mm for all the cases. The length of the model is adjusted according to the boundary condition. The length of the cantilevered part is taken as 40 mm for each case. For example, fixed-free model is 540 mm as given in Figure 25.

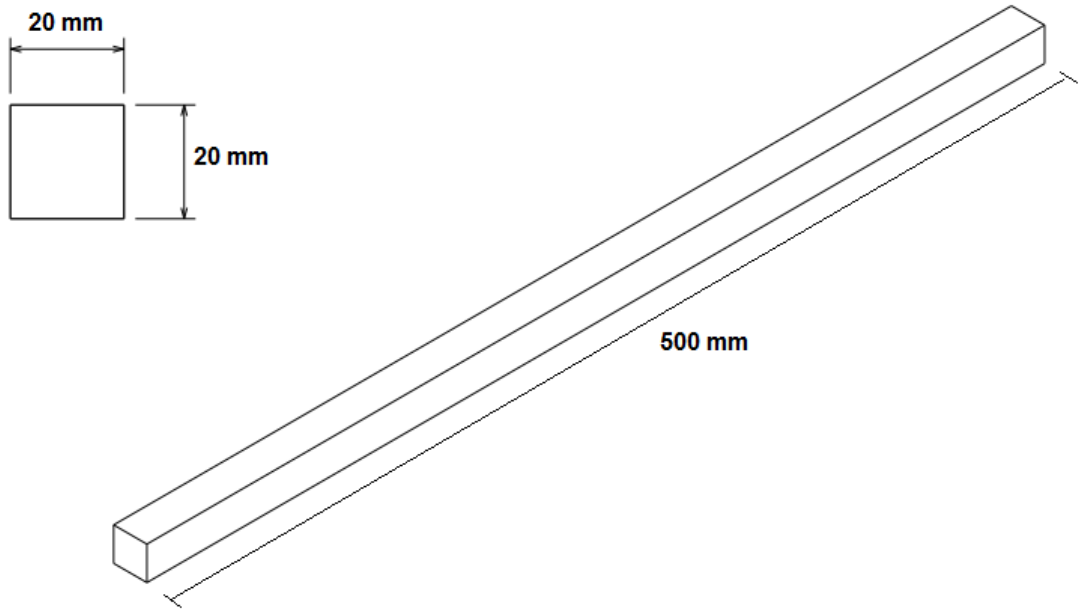

Figure 24: Dimensions of the modelled beam.

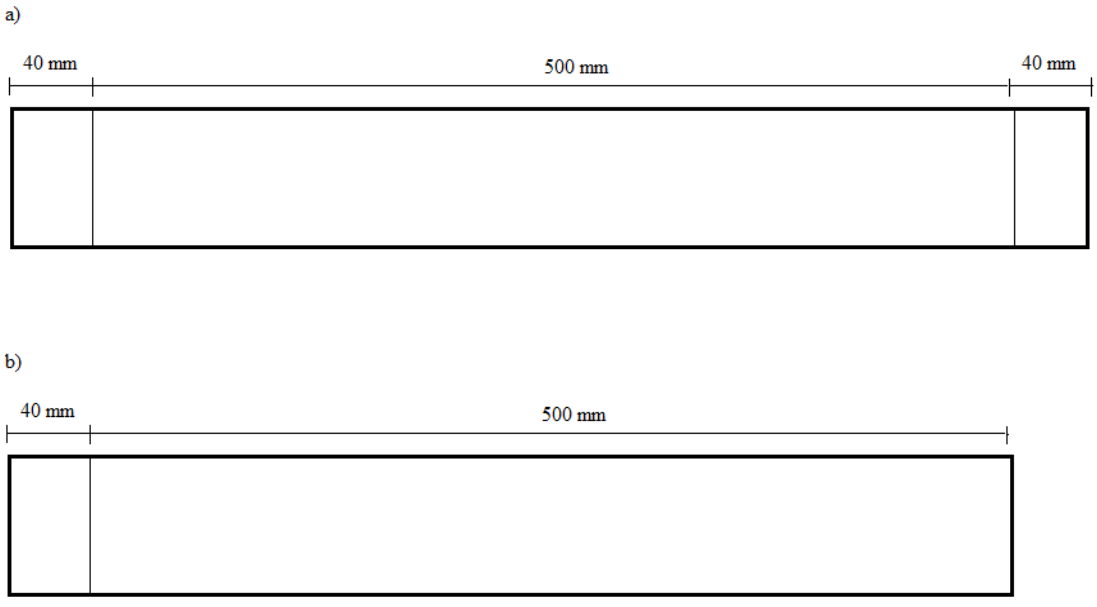

Figure 25: The model dimensions for a) fixed-free b) fixed-fixed beam

2.2. Geometrical Parameters

The parameters are the position and depth of crack, load location and amplitude, free length of the beam and the location of sensors. The representation of the parameters are given in Figure 26.

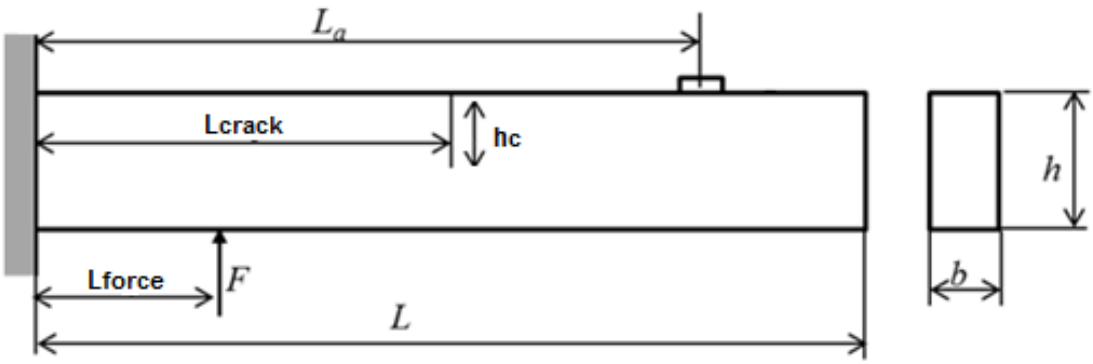

Figure 26: Geometrical parameters of the beam.

The description of the geometrical parameters are given in Table 2. These parameters are adjusted for different case studies in order to observe their effects on the frequency response of the cracked beam. The sensor location is not unique for this study. There are 5 sensors on the beam with a distance of 100 mm from each other. Also, the force amplitude is not fixed. The excitation amplitude effect is examined in the following case studies in the numerical results part. The cross section of the beam is square, thus the value of b and h are the same.

Table 2: Geometrical parameters

L	Free length of the beam
L_{crack}	Crack Location
L_{force}	Force location
La	Accelerometer location
h_c	Crack Depth

2.3. Discritication and element properties

2.3.1.Intact beam

The global element size is selected as the same with the cracked beam such that no stiffness variation is encountered in the analysis due to number of degrees of freedom.

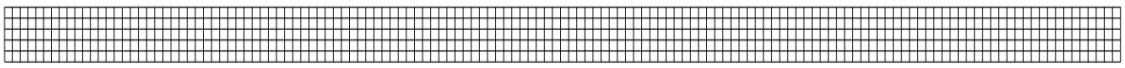

Figure 27: Finite element discretization of the intact beam.

Plane stress finite elements are used by assuming the distribution of the strain through the thickness is negligible. Also, the element type is selected as explicit, which is compatible with the solution method.

Table 3: Element properties of the intact beam

Parameters	Values & Types
Global edge length	4 mm
Number of elements	690
Number of nodes	834
Element type	CPS4R (Plane stress, 4 Node, Reduced Integration)

The quadratic type elements would give better accuracy but the computational time increases with higher order element types. Thus, linear elements are used in this analysis. The global element length is selected such that the height of the beam is represented with enough number of elements with good aspect ratio.

2.3.2.Cracked beam

The homogeneous distribution of the element shape and size cannot be employed for the cracked beams because of the crack tip singularity. The elements should be arranged such that the stress distribution around the crack tip correctly represented. Triangular elements are used around the crack tip is in this analysis. There should be sufficient number of elements around the crack tip. It is set to 12 element in this case. There are five types of crack configuration in this study. The length and position of the cracks are changed to decide on their effects. Thus, there are six finite element models for these configurations. Crack length is the depth of the crack from the free surface and the crack position is the distance between the crack and cantilevered end.

Configuration 1

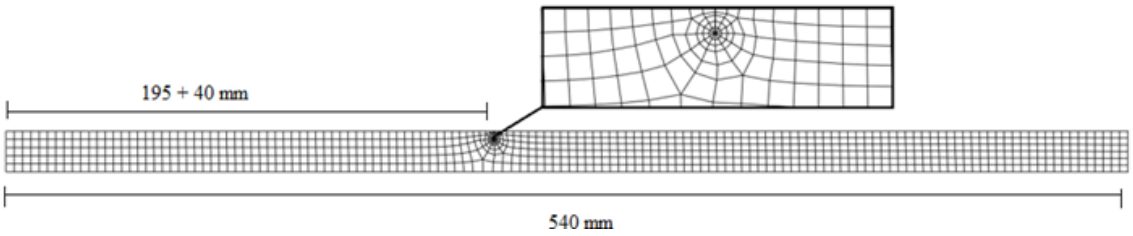

Figure 28: Finite element model for 1st configuration cracked beam.

Table 4: Finite element properties for 1st configuration cracked beam

Parameters	Values & Types
Global edge length	4 mm
Crack depth	4 mm
Crack location	195 mm from the fixed end
Minimum edge length	0.52 mm (at the crack tip)
Number of elements	816
Number of nodes	960
Element type	CPS4R + CPS3 (Plane Stress, 3 Node)

Linear tri and quadrilateral elements are used in this model. Tri elements are located at the crack tip and aligned around the crack tip by using mesh seed method. There are some distortions at the elements around the crack tip because of the transition from quad to tri type elements. Their effects on the stiffness matrix of the beam are assumed be negligible. The minimum edge length is important since it affects the stable time increment. Smaller the minimum edge length in the model, smaller the time increment and longer the computational time of the solution. Thus, a balance must be attained

between the minimum element size and the computational time. The time increment is also affected by the modulus and density of the smallest element.

Configuration 2

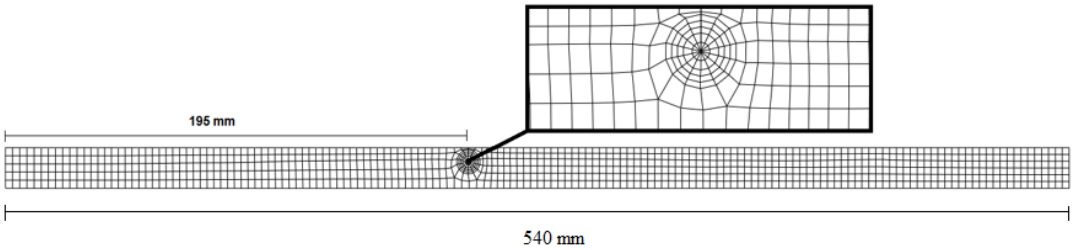

Figure 29: Finite element model for 2nd configuration cracked beam.

Table 5: Finite element properties for 2nd configuration cracked beam

Parameters	Values & Types
Global edge length	4 mm
Crack depth	7 mm
Crack location	195 mm from the fixed end
Minimum edge length	0.67 mm (at the crack tip)
Number of elements	932
Number of nodes	1093
Element type	CPS4R + CPS3 (Plane Stress, 3 Node)

Configuration 3

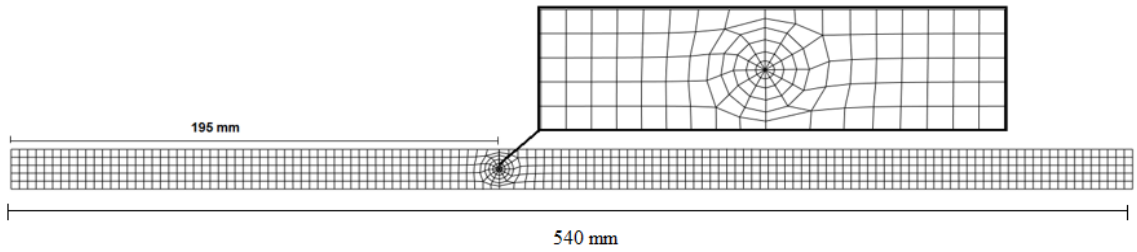

Figure 30: Finite element model for 3rd configuration cracked beam.

Table 6: Finite element properties for 3rd configuration cracked beam

Parameters	Values & Types
Global edge length	4 mm
Crack depth	10 mm
Crack location	195 mm from the fixed end
Minimum edge length	0.76 mm (at the crack tip)
Number of elements	721
Number of nodes	861
Element type	CPS4R + CPS3 (Plane Stress, 3 Node)

Configuration 4

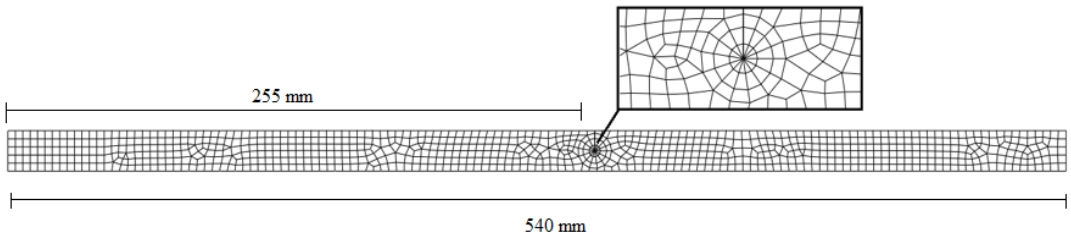

Figure 31: Finite element model for 4th configuration cracked beam.

Table 7: Finite element properties for 4th configuration cracked beam

Parameters	Values & Types
Global edge length	4 mm
Crack depth	10 mm
Crack location	255 mm from the fixed end
Minimum edge length	1.14 mm (at the crack tip)
Number of elements	979
Number of nodes	843
Element type	CPS4R + CPS3 (Plane Stress, 3 Node)

Configuration 5

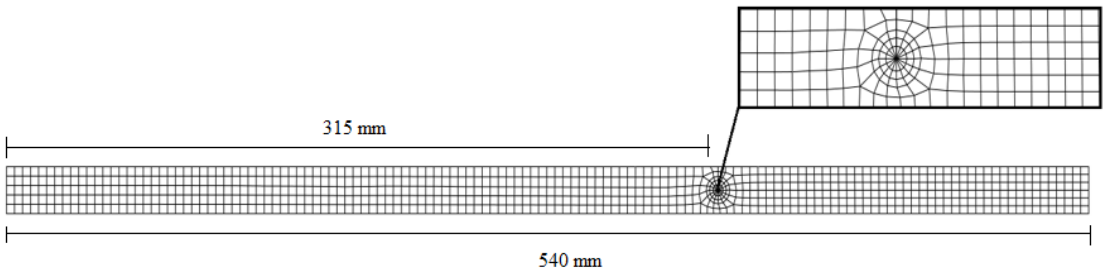

Figure 32: Finite element model for 5th configuration cracked beam.

Table 8: Finite element properties for 5th configuration cracked beam

Parameters	Values & Types
Global edge length	4 mm
Crack depth	10 mm
Crack location	315 mm from the fixed end
Minimum edge length	1.14 mm (at the crack tip)
Number of elements	979
Number of nodes	843
Element type	CPS4R + CPS3 (Plane Stress, 3 Node)

Configuration 6

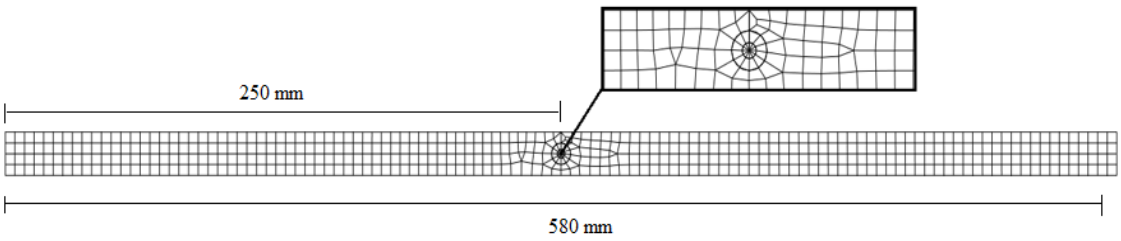

Figure 33: Finite element model for 6th configuration cracked beam.

Table 9: Finite element properties for 6th configuration cracked beam

Parameters	Values & Types
Global edge length	4 mm
Crack depth	10 mm
Crack location	250 mm from the fixed end
Minimum edge length	1.14 mm (at the crack tip)
Number of elements	979
Number of nodes	843
Element type	CPS4R + CPS3 (Plane Stress, 3 Node)

2.4. Loads and boundary conditions

Two different boundary conditions are compared in this study, which are fixed-free and fixed-fixed. The total length of beam is adjusted such that the free length of the beam is 500 mm for each configuration. For the fixed regions 40 mm of the beam is given zero displacements in every direction. Configurations 1,2,3,4 and 5 are given in Figure 34. The left side is the fixed part and load is applied 125 mm from the fixed end.

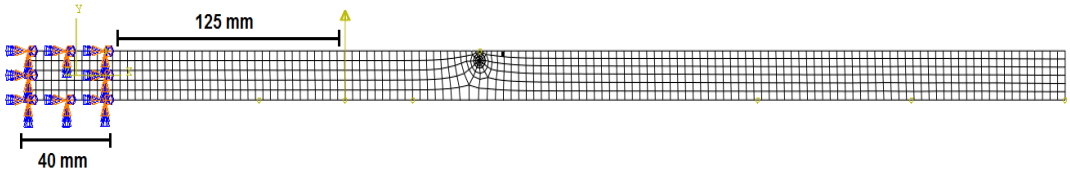

Figure 34: Boundary conditions and external load for the configurations 1,2,3,4,5.

Configurations 6 is given the fixed-fixed boundary conditions in Figure 35. And the load is applied from the same location.

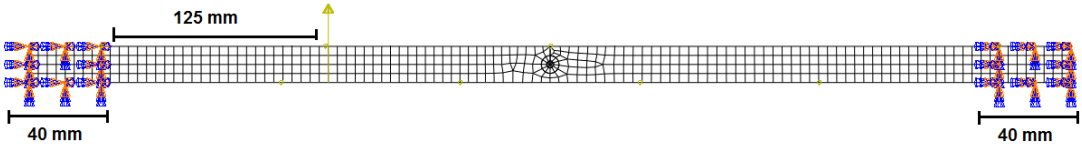

Figure 35: The boundary conditions and external load for the configurations 6.

2.5. Material definitions

The material properties which are used through the numerical simulations of the intact and cracked beam are summarized in Table 10.

Table 10: Material properties of the FE model

Parameters	Values & Types
Material	Aluminum
Density	2700 kg/m^3
Elastic Modulus	70000 MPa
Poisson's Ratio	0.3

2.6. Crack modelling

The crack models available in the Abaqus software are examined with static analysis. The selected crack models must be compatible with the solution method. Dynamic explicit solver is used throughout the simulations. The compatible crack models are slot type, Abaqus extended FEM (XFEM) and seam crack. Slot type cracks can be utilized by opening a slight gap between the elements at the crack location. A representative slot type crack can be seen in Figure 36. This type of crack does not come up with true stress profile at the crack tip. Crack tip singularity cannot be represented with this model. Comparison is made between other models.

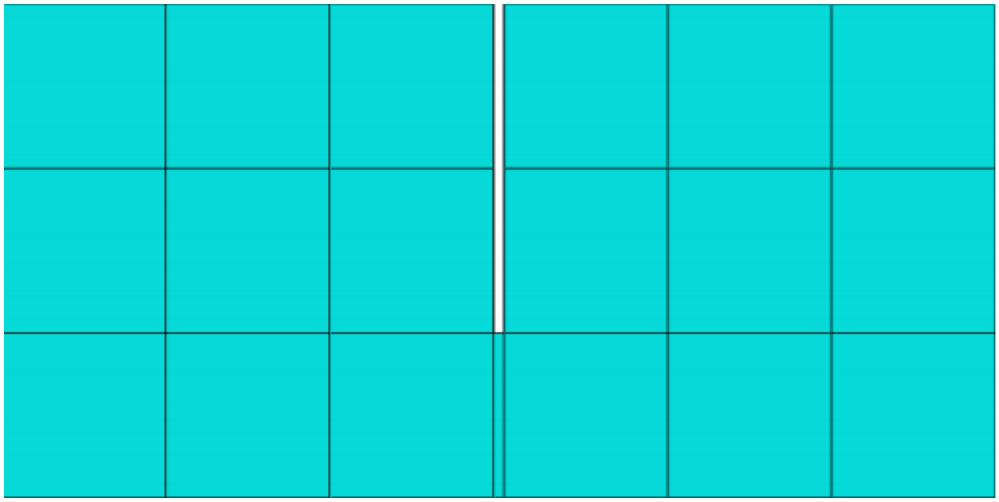

Figure 36: Slot type crack.

XFEM crack modelling tool of Abaqus is very effective. There is no need to adjust the mesh with the crack position. A two dimensional face is modelled and located at the crack section to represent the crack face as presented in Figure 37.

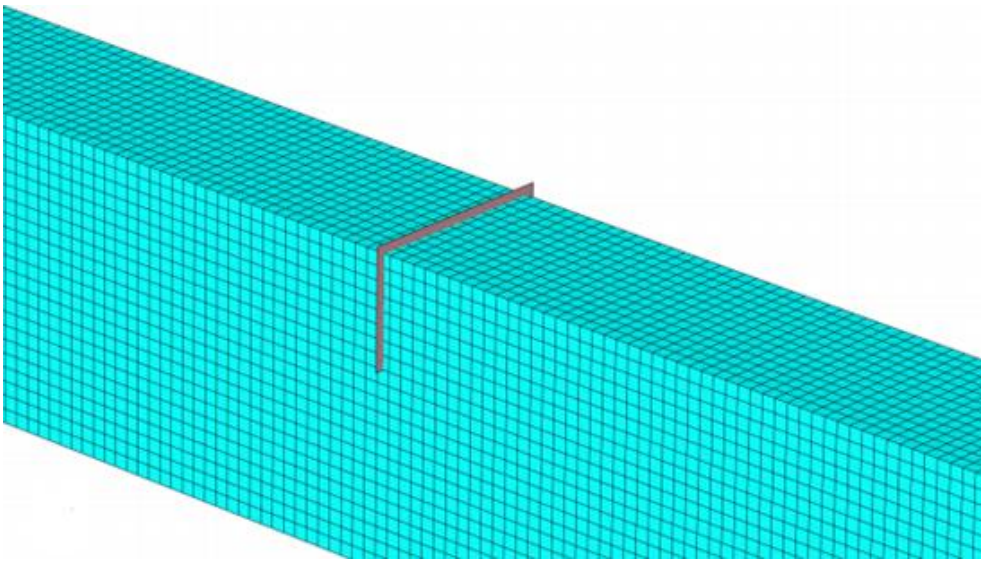

Figure 37: XFEM crack model.

Abaqus automatically calculate the stress intensity factor with the specified mathematical theorie. The accuracy of the stress profile can be attained with the number of stress contours selected from the Abaqus user interface. The problem with this crack type is that XFEM is not compatible with the dynamic explicit solvers and

two dimensional elements. Thus, XFEM crack model is not used in this analysis. The seam crack model seems to be best choice due its compatibility with the explicit solver and plane stress elements.

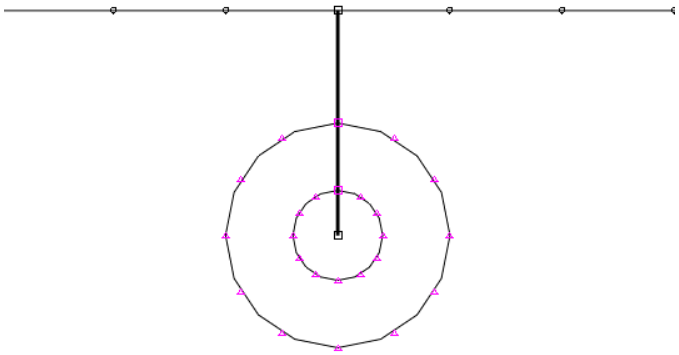

Figure 38: Seam crack model.

A representative seam crack can be seen in Figure 38. The figure shows the upper face of the beam at the crack section. The bold line show the seam crack face. Namely, there are duplicate nodes at the bold line, which separates the elements at the both sides of the crack line. After introducing contact condition to the both sides of the face, opening and closing crack behavior can be attained. Since stress gradient at the crack front is too high, the mesh geometry and shape is important. The meshes must be refined at this location. Figure 39 shows the crack tip meshing approach in this study. Two dimensional beam is partitioned with three circles. The mesh type at this location is set to sweep with quad dominated element shape from Abaqus mesh control tool. Other parts of the beam has quad form elements. Further, the crack edges are seeded in order to have uniform and enough number of elements at the crack faces.

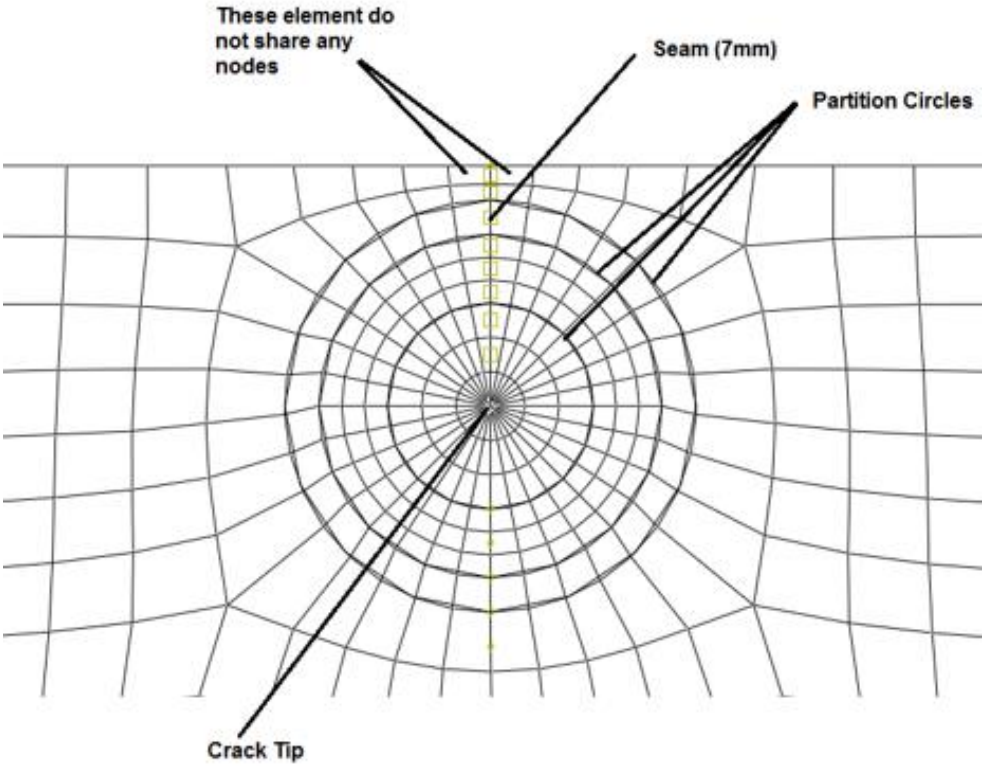

Figure 39: Crack tip meshing.

As indicated before, the elements on the seam line do not share any nodes. Thus, they can be separated from each other. Transition elements from fine to course mesh has irregular form but it has negligible effects on the overall vibration behavior of the beam. The mesh size changes for each configuration. The minimum edge length is arranged such that the time step is not too small. For the perfect representation of the crack tip singularity, mid side node method could be used. This kind high degree elements, however, needs implicit solvers and long computational time.

The mid side method is summarized in Figure 40. There are nodes at the one fourth of the element edges. These quadratic degree elements gives more realistic stress distribution at the crack tip. The stress is decaying with the inverse of the square root of the radius from the crack front. This profile can be attained by mid side node method. In this study, linear elements are used since the overall stiffness of the beam is not effected drastically by the crack tip stress profile.

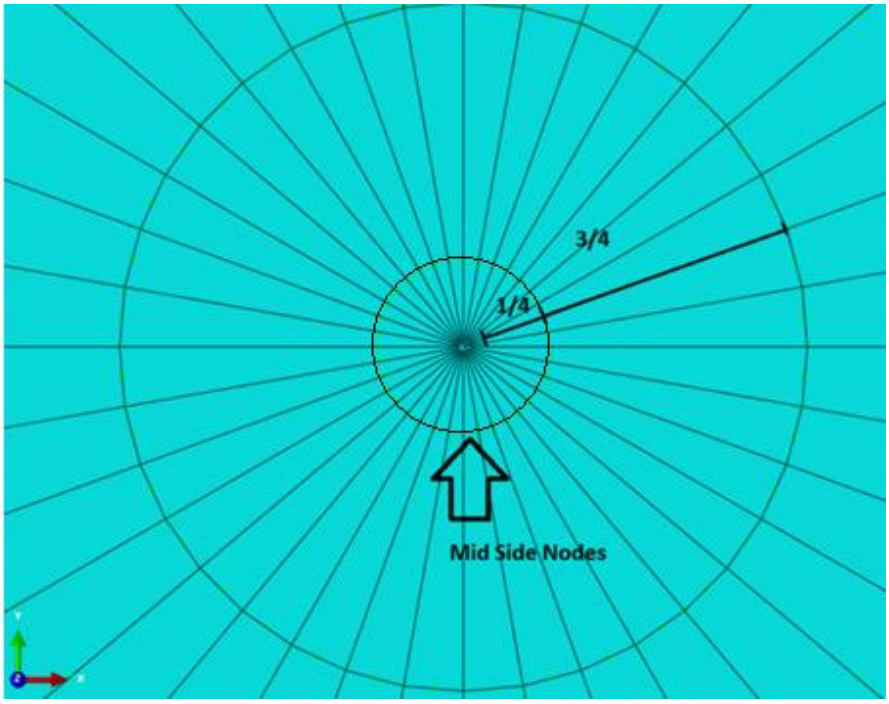

Figure 40: Mid side node method.

2.7. Contact definition

Abaqus explicit surface to surface contact method is used. The crack face friction is considered to be negligible. Thus, the normal contact is defined as “Hard contact” from pressure over-closure part. Also, there is no prevention to the separation of the surfaces after contact. Tangential property of the contact is “frictionless”. Introducing contact condition through the crack face utilizes partial contact condition in the simulation.

2.8. Sensor network

The acceleration and displacement responses are collected from 5 different locations in each configuration from root to the free end with a constant spacing. The free length

of the beam is taken as 500 mm in each configuration in this study. Thus, the spacing is taken as 100 mm. The representative sensor network is given in Figure 41.

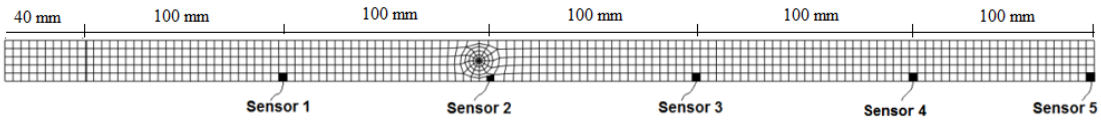

Figure 41: Sensor network on the beam.

For configuration 6, the sensor 5 is not located since the beam is fixed at that location. There is no displacement or acceleration at this location.

2.9. Damping

For the dissipation of the energy on the vibrating beam, some damping is introduced to the model. The explicit solver of the Abaqus software has bulk viscosity constants in the step definition in order to damp the high frequency numerical vibration content. This damping, however, is not enough to damp the vibration in the interested frequency range. Thus, additional damping definitions, called "Rayleigh damping" are introduced to the model. The Rayleigh damping has two coefficients; "alpha" and "beta". Alpha is available mass proportional damping coefficient to damp the lower frequency range. Beta is a stiffness proportional coefficient, which stands in order to damp high frequency vibration. The calculation of the Rayleigh damping coefficients, the following procedure is followed.

Let ξ_i is the damping coefficient at the specified frequency.

$$\xi_i = 0.05$$

Calculation of Rayleigh coefficients given in Abaqus manual 6.14 as follows,

$$\xi_i = \frac{\alpha}{2w_i} + \frac{\beta w_i}{2}$$

Stiffness proportional damping coefficient “Beta” reduces the stable time increment in explicit analysis. Thus, beta is not used for this analysis. Then,

$$\alpha = 2\xi_i w_i$$

For the fundamental frequency of $w_1 = 64\ Hz$. The Rayleigh coefficients used for configuration 1 to 5 are as follows,

$$\alpha = 6.4$$

$$\beta = 0$$

For the configuration 6, the fundamental natural frequency is $w_1 = 403\ Hz$. Then,

$$\alpha = 40.3$$

$$\beta = 0$$

CHAPTER 3

NUMERICAL CALCULATIONS

Finite element model of the intact and damaged beams are constructed. There are six different FE models for different crack depth, position and boundary conditions. The initial conditions are not specified, they are taken as zero by default. The time domain response of the model to the applied load is recorded from different sensor locations and evaluated.

3.1. Solution method

The vibration of the beam is governed by the dynamic equation of motions. For complicated structures and boundary conditions, the analytical solution would be difficult or impossible. These kind of differential equations must be solved by discretization of the domain into small steps and solving each step separately. There are some methods to solve steady state response of the structure, but they are compatible only with linear systems, in which the stiffness matrix does not change with time. Methods based on Eigen modes of the structure are cost-effective in accordance to the direct integration methods. Thus, linear systems are generally solved by these methods. For the vibration of a cracked beam, which is a nonlinear system, there are two methods for the solution of time domain transient and steady state response. They are implicit and explicit solvers. The common purpose of these methods is to find the parameter such as displacement, at a later time by knowing the variable at the current time. Each method has its own advantages and disadvantages.

3.1.1.Dynamic implicit solver

Implicit solvers use not only the current dynamic variables, but also the same quantities at the later time to solve the quantities at the later time. There is theoretically no limit for the time step size in implicit solvers. For the response to be realistic, the time step should not be too high, i.e. not more than two orders or magnitude larger than stability limit. Thus, the given time step affect the quality of the response. As a rule of thumb, the time step must not be larger than one tenth of the system vibration period in order to ensure that the solution is converges and unrealistic results are avoided. There is a limit which defines this stability. Thus, the stability limit and period of vibration provides a clue for the selection of the solver type by considering the computational time and quality of the results. The most crucial characteristics of the implicit method is that the equilibrium must be attained at each time step with the internal, external and inertial forces on the body. The equilibrium equations are solved iteratively. To attain the equilibrium at each time step is not cos-effective for this study. The computational time doubled and sometimes tripled in the simulations of this study when dynamic implicit solver is used. Thus, dynamic explicit solver seems to be better choice for the simulations of the cracked beam. A comparison between the explicit and implicit dynamic analysis results are presented in the following sections.

3.1.2.Dynamic explicit solver

Explicit solver use central difference method to estimate the later time. The mathematical procedure for the calculation of the displacements is summarized in the Equations 16-19.

$$\dot{\boldsymbol{u}}^{(i+\frac{1}{2})} = \dot{\boldsymbol{u}}^{(i-\frac{1}{2})} + \frac{\Delta t^{(i+1)}+\Delta t^{(i)}}{2}\ddot{\boldsymbol{u}}^{(i)} \tag{16}$$

$$\boldsymbol{u}^{(i+1)} = \boldsymbol{u}^{(i)} + \Delta t^{(i+1)}\dot{\boldsymbol{u}}^{(i+\frac{1}{2})} \tag{17}$$

Where, $\dot{\boldsymbol{u}}$ is the velocity and $\ddot{\mathbf{u}}$ is the displacement. The superscript (i) stands for the increment number. Using these equations, the later state of the system can be calculated by knowing the mid increment values at the $(i-\frac{1}{2})$ and (i) The explicit solver uses diagonal element mass matrices, which make this method cost-effective. The acceleration at the current state can be calculated using diagonal mass matrix as given in Equation 18.

$$\ddot{\mathbf{u}}^{(\mathrm{i})} = \mathbf{M}^{-1} * (\mathbf{F}^{(\mathrm{i})} - \mathbf{I}^{(\mathrm{i})}) \tag{18}$$

Where M is the diagonal lumped mass matrix, F is the externally applied load and I is the inertial force vector. Since the calculation of the acceleration at the current state is governed by Equation 18, no iterations are needed. For the initial step, the mid increments calculated from the initial conditions for the velocity and acceleration.

$$\dot{\mathbf{u}}^{(\mathrm{i}-\frac{1}{2})} = \dot{\mathbf{u}}^{(0)} - \frac{\Delta \mathbf{t}^{(0)}}{2} \ddot{\mathbf{u}}^{(0)} \tag{19}$$

There is a stability limit for the time increment in explicit analysis since the central difference method is conditionally stable. The stability can be attained by setting the time increment according to the following inequality.

$$\Delta t \leq \frac{2}{\omega_{max}} = \frac{l}{C} = l\sqrt{\frac{\rho}{E}} \tag{20}$$

Where, ω max is the highest Eigen value, "l" is the minimum edge length and "c" is the speed of sound in the system and "E" is the modulus of the corresponding element. Namely, the time step is governed by the speed of sound, minimum edge length and the smallest element in the model. If the damping of the system is considered, the stability condition becomes smaller. The calculated time step is multiplied by a factor calculated with the critical damping coefficient at the highest mode as given in Equation 21.

$$\Delta t \leq \frac{2}{\omega_{max}}(\sqrt{1+\xi^2}-\xi) \tag{21}$$

Where, ξ stands for the critical damping coefficient at ω_{max} and ξ is the critical damping coefficient. Thus, the damping should be selected carefully if the computational time is considered. There is a default damping parameter, called "bulk viscosity" in Abaqus for the unsteady response features due to numerical calculations. For the damping of the structure's vibration, however, an additional damping parameter such as Rayleigh damping parameters, should be introduced by considering the drop in the time step. The Rayleigh damping coefficients given in the analysis are alpha and beta. Alpha damp the system by modifying the mass matrix and beta damp the system by modifying the stiffness matrix. Determination of these constant is important since any unrealistic coefficient value may drastically increase the computational time. Also the size of the minimum element and the modulus of this element are important parameters for the computational time. That's why, the meshes at the crack front is selected such that the time step is acceptable. The analysis and simulations in this study are done by dynamic explicit method which is computationally more effective. The comparison between a dynamic explicit and implicit acceleration FFT results given in Figure 42-43. There is no much difference in the amplitudes and frequencies of the harmonics but with the same time increment,

the explicit analysis has computationally effectiveness with little loss of accuracy at the amplitudes at the sub and super harmonics.

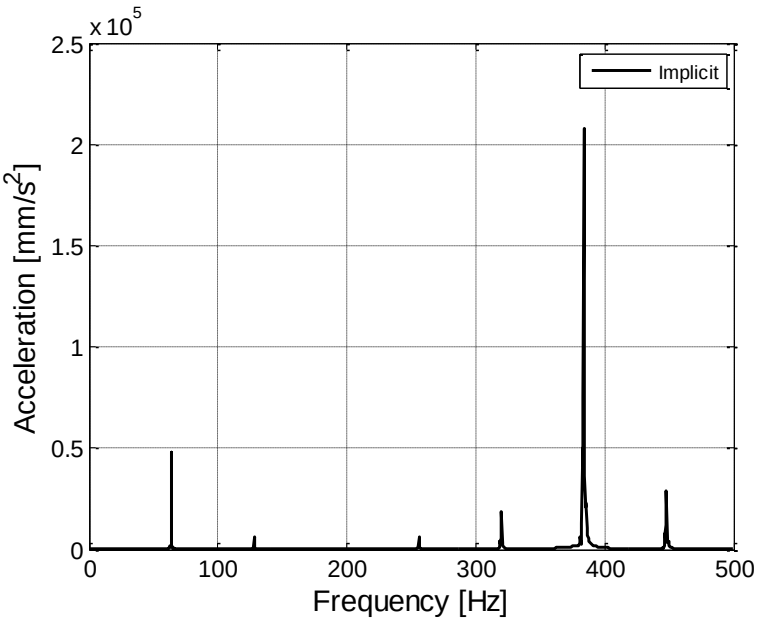

Figure 42: FFT of the acceleration responses at sensor 1 of configurations 3 with w_c=1.00, L_f = 0.25, L_c = 0.39 and excitation amplitude of 100 N in linear scale with dynamic implicit solver

3.2. Signal processing

For the static evaluations, compliance and force-displacement curves are obtained directly from static solvers and post-processing tools of Abaqus. For dynamic evaluations, it is not as straight forward as in the case of static analysis. The output is in time domain. The data is crowded and non-linear effects are not visible. Without having frequency content of the response, crack identification is almost impossible. Thus, a procedure is devised to elicit a clear frequency spectra from time domain response. The procedure is presented in Figure 44.

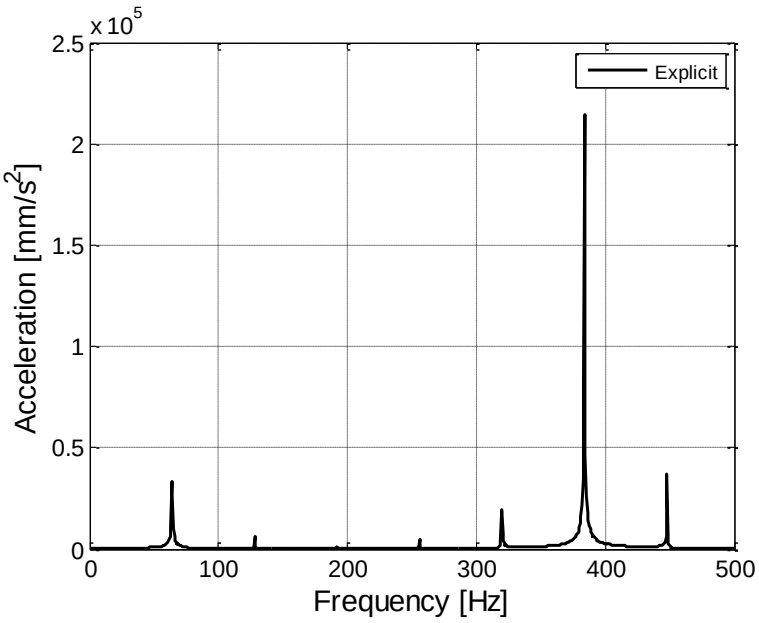

Figure 43: FFT of the acceleration responses at sensor 1 of configurations 3 with w_c=1.00, L_f = 0.25, L_c = 0.39 and excitation amplitude of 100 N in linear scale with dynamic explicit solver

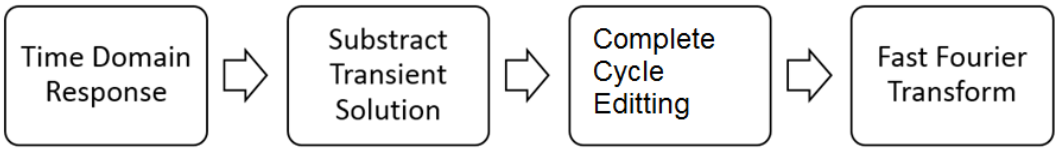

Figure 44: Post processing procedure.

The transient solution (first 2 seconds) subtracted from overall solution of 5 seconds in order to obtain the steady state solution at the end. Than the data is edited such that the fundamental frequency has a complete harmonic cycle in the time domain response. Otherwise, FFT results have high amount of leakage. This process is done with the following formula. The total sampling time for steady state response is 3s. Thus, integer number of complete cycles at the fundamental frequency must be found.

$$integer\ number\ of\ complete\ cycles = \frac{sampling\ time}{\frac{1}{fundamental\ frequency}} \quad (22)$$

The integer part of the calculated real number from Equation 22 is taken and multiplied with the fundamental excitation frequency in order to find the exact sampling time having complete harmonic cycle at the fundamental frequency. There is still some kind of leakage due to discrete time response but it is in the acceptable level for this analysis. Further, FFT of the acceleration results by using flat top filter in Matlab are also given in Appendix in order not to have any doubt about the amplitudes at the frequency response.

There is no aliasing problem for the response, since the resolution of the data is too high than the resolution required to obtain the required frequency band. There are 10^7 points in 1 second solution. The total solution time is 5 seconds for each case in dynamic evaluations. Last 3 second of the response is taken as steady state response for all cases. Thus there are $3*10^7$ data point in each solution. This number of data points is far enough to catch the frequencies in the interested band of 0-500 Hz without aliasing problem. Thus, no additional anti-aliasing filter is applied to time domain response. Figure 45 shows raw and post-processed data step by step. The steady state response is checked by taking FFT of different sampling times. For the same analysis, last 4s, 3s and 2s responses are presented in Figure 46, 47, and 48.

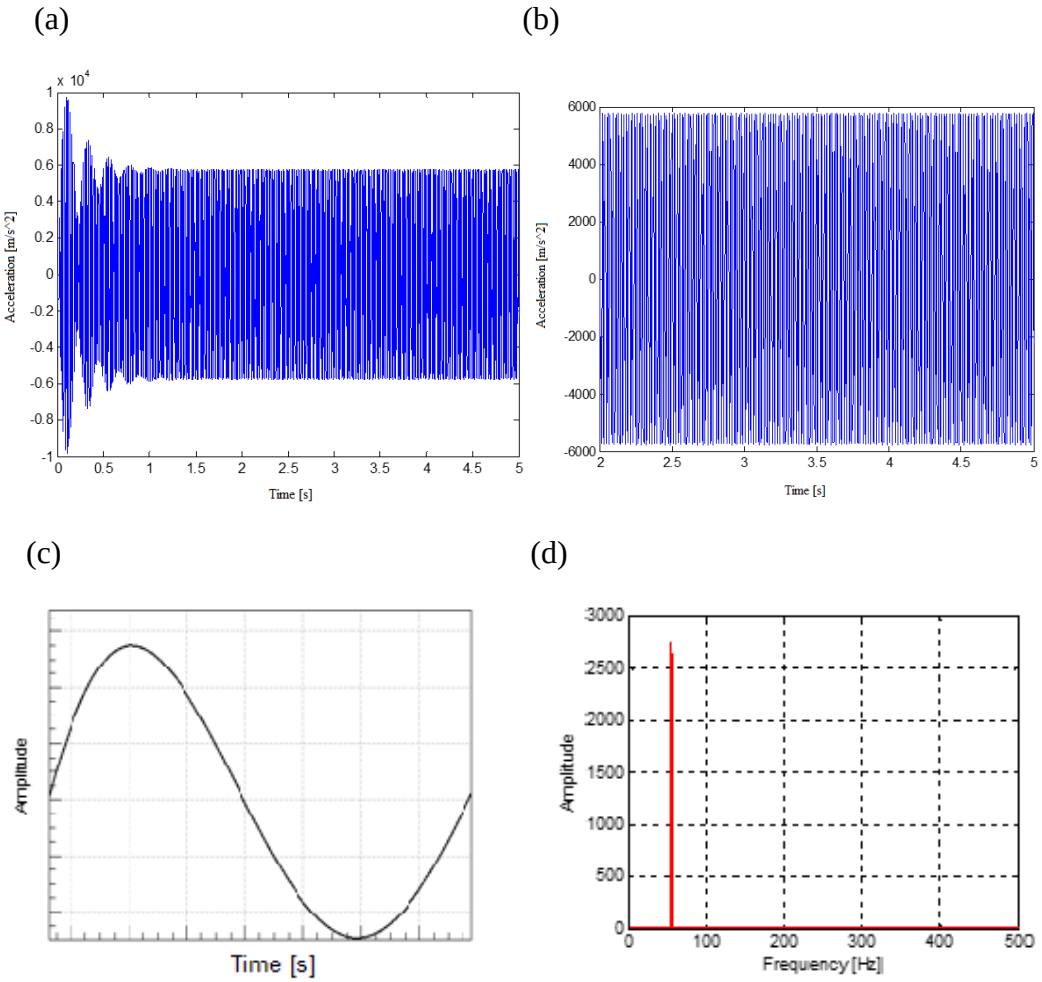

Figure 45: Post processing of time domain response (a) raw data (b) steady state response (c) (representative) complete cycle editing (d) FFT response

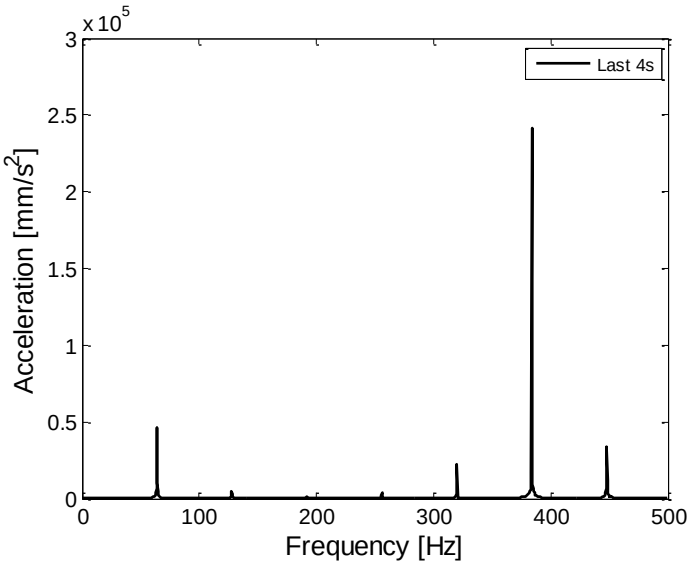

Figure 46: The last 4 s of acceleration responses at sensor 1 of configurations 3 with w_c=1.00, L_f = 0.25, L_c = 0.39 and excitation amplitude of 100 N.

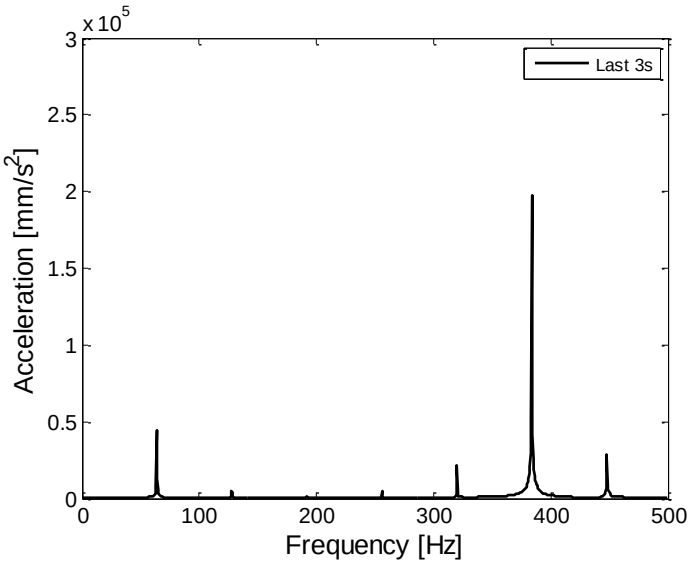

Figure 47: The last 3 s of acceleration responses at sensor 1 of configurations 3 with w_c=1.00, L_f = 0.25, L_c = 0.39 and excitation amplitude of 100 N.

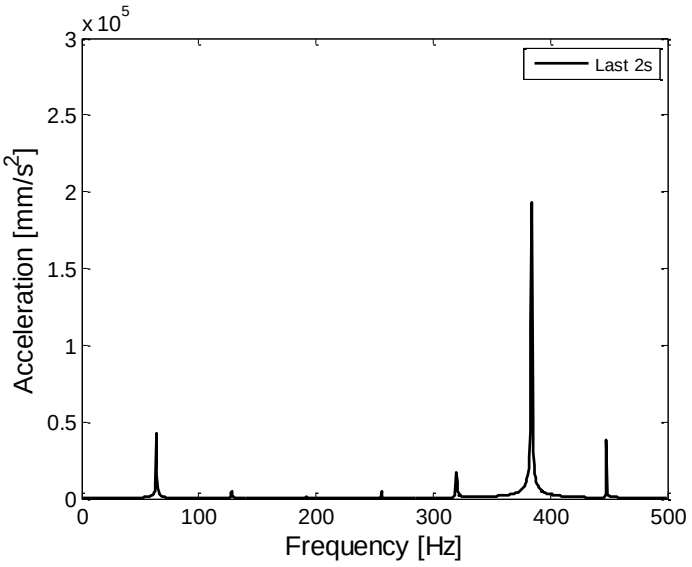

Figure 48: The last 2 s of acceleration responses at sensor 1 of configurations 3 with w_c=1.00, L_f = 0.25, L_c = 0.39 and excitation amplitude of 100 N.

Table 11: The acceleration amplitude at different sampling time

	$A_{max,i}$	**Difference %**	$w_{max,i}$	**Difference %**
Last 4 s	2.418E5	-	384	%0
Last 3.5 s	1.971E5	%18	384	%0
Last 3 s	1.929E5	%2	384	%0

The amplitudes of the maximum harmonic and its frequency is given in Table 11. The transient response has not been damped between last 4 and 3.5 s. The difference between this 0.5 s at the amplitude of the maximum harmonic is 18%. The steady state response almost reached between the last 3.5 and 3s. The difference at the amplitude of the maximum harmonic is only 2%. Also, 3s sampling time is good enough for the resolution at the frequency spectra. The frequency of the maximum harmonic is constant for last 4, 3.5 and 3s. Thus, the analysis is done at last 3s for the case studies.

3.3. Discerete fourier transform

For the evaluatıon of crack existence on the structure by using vibration response, the frequency content of the time signal should be obtained. The discrete time signal is transformed into frequency spectra with discrete Fourier transform and with signal processing methods. In this section, the analytical background of discrete Fourier transform is discussed.

A cyclic continuous signal can be represented with Fourier series as follows,

$$x(t) = c_0 + c_1 e^{\frac{i2\pi t}{T}} + c_2 e^{\frac{i4\pi t}{T}} + \cdots = \sum_{n=0}^{\infty} C_n e^{i\frac{2\pi nt}{T}} \quad (23)$$

A discrete signal can be represented with the vector in Equation 24.

$$x[n] = [x_1, x_2, x_3, \ldots., x_N] \quad (24)$$

Finally, the Fourier transform of a discrete signal is represented with Equation 25.

$$X[k] = \sum_{n=0}^{N-1} x[n] e^{i\frac{2\pi kn}{N}} \quad (25)$$

Where,

“X” is the signal “x” in frequency domain, “k” represent the number of frequency component, “N” stands for the number of samples in the signal, “x” is the time signal, “n” is the nth sample and “j” is the imaginary unit.

If data points are limited there should be aliasing problem when using the DFT algorithm. Namely, if the number of data points are not enough, the maximum frequency content should be lower than the half Nyquist frequency which is twice the maximum frequency occurring in the signal. From the equation, the maximum frequency content which can be calculated is limited to (N-1)/T when the data points are limited. For the simulation in this study, the number of points are enough to have true frequency content from DFT algorithm. If the number of points were less, than zero padding which is the generation of imaginary zero amplitude points in the signal, could be used to increase the number of data point that can be used with discrete Fourier transform. As an important reminder, the signal should have frequency content with a constant period. Thus, the DFT algorithm is used for steady state solution, which is found after subtracting first 2 seconds of the solution from the whole 5 seconds solution in this study.

CHAPTER 4

NUMERICAL RESULTS

4.1. Statical analysis results

The cracked and intact beams are investigated under static load as a first step in order to obtain the displacement at a given load level and to observe the stiffness change in the open and closed crack phases. Further SIF is obtained to ensure the quality of the FEA.

4.1.2.Force displacement graph

An incremental loading is applied to the cracked and intact beam. Force is applied into upward and downward directions in order to check the closed and open crack phase stiffness. The force-displacement curve is given in Figure 50. Configuration 3 is used in this analysis.

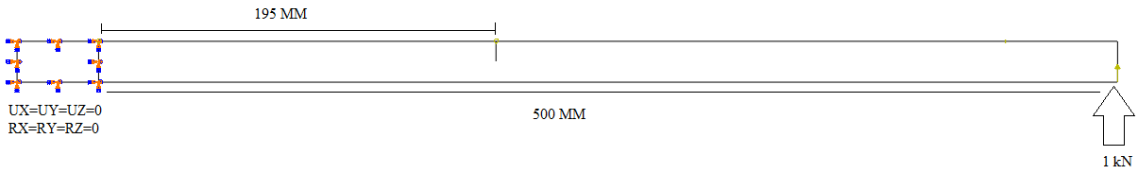

Figure 49: Static analysis model

It can be seen that the closed crack stiffness and intact beam stiffness are very similar. The open crack phase of the cracked beam, however has lower stiffness and higher

displacement. The stiffness change from open to close form does not happen instantaneously in the lateral vibration of the beam but this gives an idea about how much nonlinearity is given to the system with a crack having a depth of 10 mm.

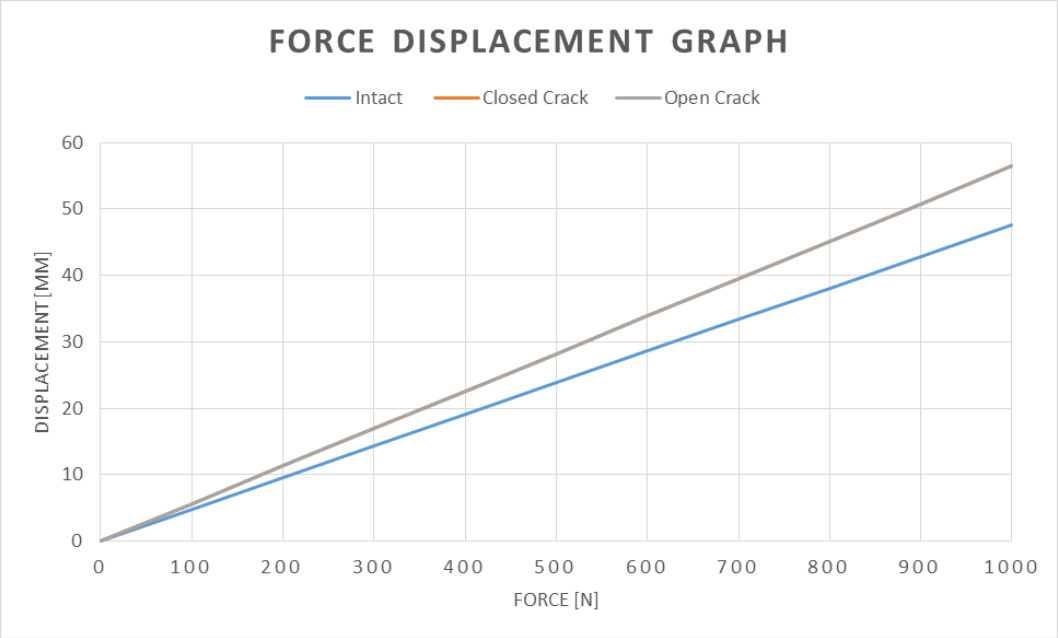

Figure 50: Force displacement curve.

4.2. Dynamic analysis results

4.2.1.Linear normal mode analysis

The linear normal mode analysis is applicable for linear structures. The crack face interaction in this study makes the system nonlinear. Thus, the natural frequencies of the cracked beam cannot be found by Eigen value problems. There is an approach in the literature for bilinear systems. The cracked beams are also kind of bilinear systems. There are two stiffness matrices. One for the crack open case and the other for the crack closed case. Then, the cracked beam natural frequency can be estimated by Equation 26 (Chati, Rand, & Mukherjee, 1997).

$$f_{bilinear} = \frac{2f_{cracked}f_{intact}}{(f_{cracked}+f_{intact})} \quad (26)$$

The following table shows the bilinear natural frequencies of the configurations used in this study. The natural frequencies of the cracked beams are used to excite them at their natural frequencies.

Table 12: Table of configurations

Model	Crack Position	Crack Depth	BC
Configuration 1	195 mm	4 mm	Fixed-Free
Configuration 2	195 mm	7 mm	Fixed-Free
Configuration 3	195 mm	10 mm	Fixed-Free
Configuration 4	255 mm	10 mm	Fixed-Free
Configuration 5	315 mm	10 mm	Fixed-Free
Configuration 6	250 mm	10 mm	Fixed-Fixed

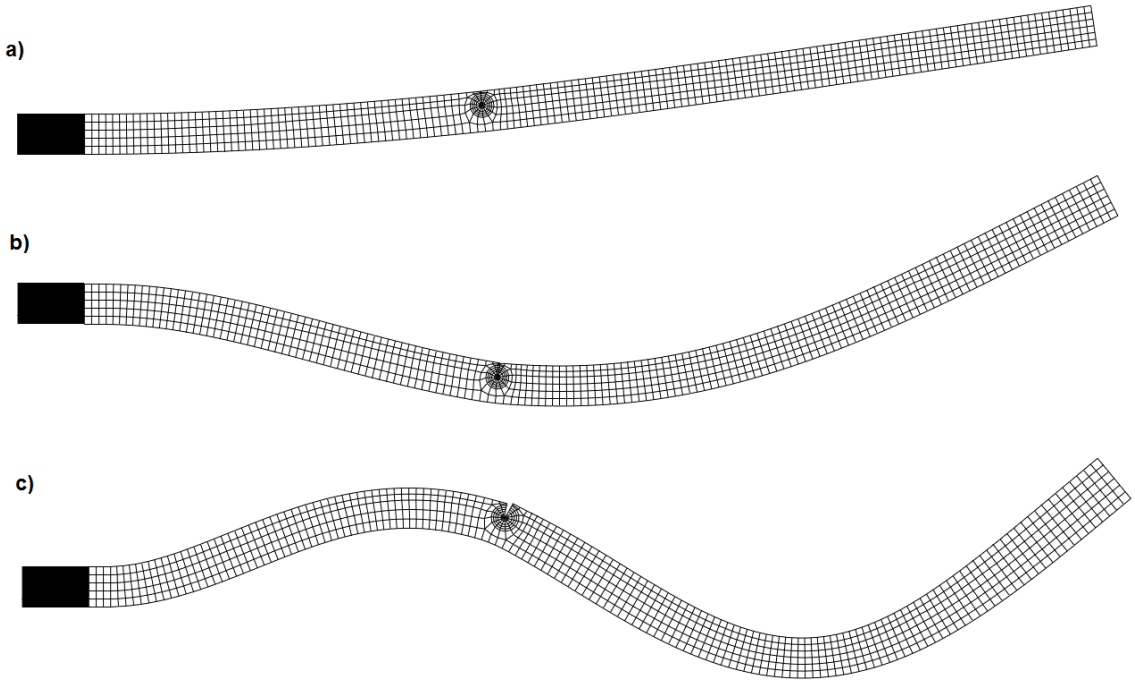

Figure 51: Linear mode shapes of the cracked beam configuration 2. (a) 1st mode shape (b) 2nd mode shape (c) 3rd mode shape

Table 13: Linear normal mode results

Models	1st Mode	2nd Mode	3rd Mode
Configuration 1	64.07 Hz	398.82 Hz	1106.1 Hz
Configuration 2	62.65 Hz	388.00 Hz	1081.9 Hz
Configuration 3	60.86 Hz	373.14 Hz	1052.5 Hz
Configuration 4	62.94 Hz	363.32 Hz	1107.5 Hz
Configuration 5	63.84 Hz	367.65 Hz	1036.1 Hz
Configuration 6	384.8 Hz	1120.5 Hz	1990.8 Hz

Table 14: Bilinear natural frequencies

Models	f_{intact}	$f_{cracked}$	$f_{bilinear}$
Configuration 1	64.42 Hz	64.07 Hz	64.24 Hz
Configuration 2	64.42 Hz	62.65 Hz	63.52 Hz
Configuration 3	64.42 Hz	60.86 Hz	62.58 Hz
Configuration 4	64.42 Hz	62.94 Hz	63.67 Hz
Configuration 5	64.42 Hz	63.84 Hz	64.12 Hz
Configuration 6	403.5 Hz	384.8 Hz	393.9 Hz

The natural frequency is lower for the beam having crack with higher depth and small distance to the fixed end. The excitation frequency for the configurations 1-5 is taken as 63.6 Hz which is the average of the natural frequencies at these configurations. It is just an approach for this study. The bilinear natural frequencies for the cracked beam is an estimation since the there is also transition phase from closed to open crack mode. Thus, having average as an excitation frequency seems to be a good approach. The configuration 6 is excited with its bilinear natural frequency which is indicated in the table.

4.2.2.Free vibration results

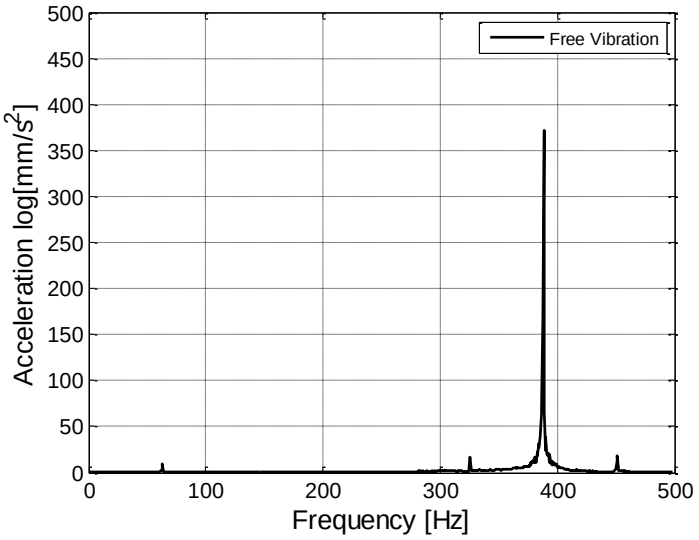

Figure 52: FFT of acceleration response of free vibration of configuration 3 after initial velocity condition of 100 mm/2 from the crack tip

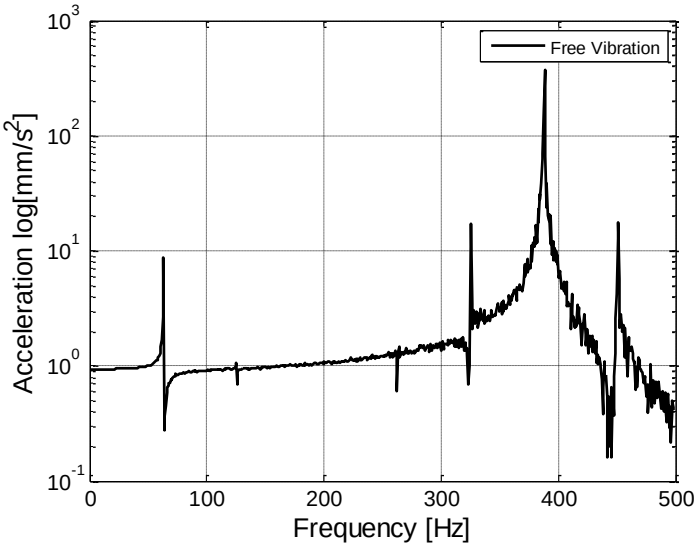

Figure 53: FFT of displacement response of free vibration of configuration 3 after initial velocity condition of 100 mm/2 from the crack tip

4.2.3.Frequency response analysis

The forced vibration characteristics of the cracked and intact beams are analyzed in this section. Different configurations with different crack sizes, depths and boundary conditions are compared step by step. The aim of this study is to show the capability of the finite element method in detection of crack induced harmonics in the Frequency spectra. For this purpose, a damage indicator is defined with the Equation 27 as defined in (Broda, Pieczonka, Hiwarkar, Staszewski , & Silberschmidt, 2016).

$$D_{c,i} = \frac{A_{max,i}}{A_e} \tag{27}$$

Where, $D_{c,i}$ is the damage indicator due to crack at the ith sensor location, $A_{max,i}$ stands for the maximum of the amplitudes at the harmonics except the fundamental frequency and A_e is the amplitude of the fundamental harmonic at the selected sensor location. The damage indicators are calculated in each case study in order to determine how the parameters, such as excitation frequency and sensor location, affect the damage indications. Displacement and acceleration responses are obtained in each case studies. The parameters in the dynamic analysis are given in Equation 28. The case studies in which the effect of the parameters are examined are summarized in the Table 15.

$$L_C = \frac{L_{crack}}{L}, w_C = \frac{w}{w_n}, L_F = \frac{L_{force}}{L}, d_C = \frac{h_{crack}}{h} \tag{28}$$

Table 15: Summary of case studies

	Case Study 1	Case Study 2	Case Study 3	Case Study 4	Case Study 5	Case Study 6
Configurations	3,4,5	1,2,3	3	3	6	3
Boundary Condition	Fixed-Free	Fixed-Free	Fixed-Free	Fixed-Free	Fixed-Fixed	Fixed-Free
L_C	3 types	0.39	0.39	0.39	0.50	0.39
w_C	1.00	1.00	3 types	0.50	0.50	1.00
L_F	0.25	0.25	0.25	0.25	0.25	2 types
d_C	0.50	3 types	0.50	0.50	0.50	0.50
Force, "A"	100 N	100 N	100 N	3 types	100 N	100 N

* Force is applied Asin (wt)

4.2.3.1.Sensor selection

For the case studies in the following sub sections, a single sensor location is selected such that the harmonics are clear in the frequency response. For this purpose, the sensor locations for a type of crack and excitation frequency range are compared with each other to find the best sensor location that shows the highest damage indication as given by Equation 27. The response in Figure 54 shows the acceleration response at the intact beam. The acceleration is purely harmonic for the intact beam. The acceleration response at the cracked beam, however, shows deviations from the harmonic behavior as in Figure 55. The amplitudes of the harmonics can be seen in frequency spectra presented in Figure 56. The damage parameters are shown in the last column of the Table 16. Sensor 1 (at 100 mm from the support) shows the damage better than all the sensors even if the amplitudes are smaller than other sensors.. This is the sensor closest the fixed end of the beam. From now on, the case studies are evaluated with the data obtained from sensor 1.

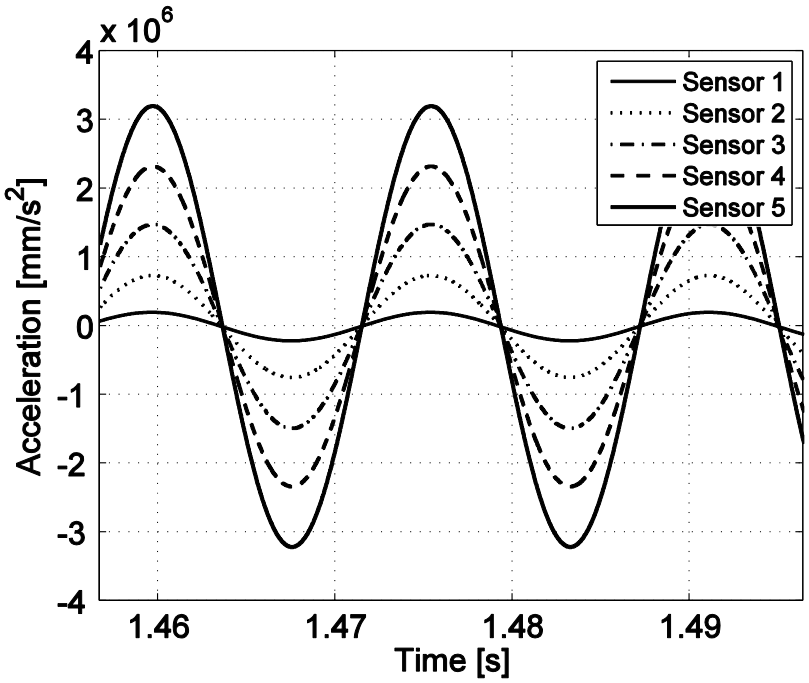

Figure 54: The acceleration time responses at all sensor locations for configuration 2 excited at $L_f = 0.25$ with 100 N. The curves are from 5 to 1 in top to bottom order.

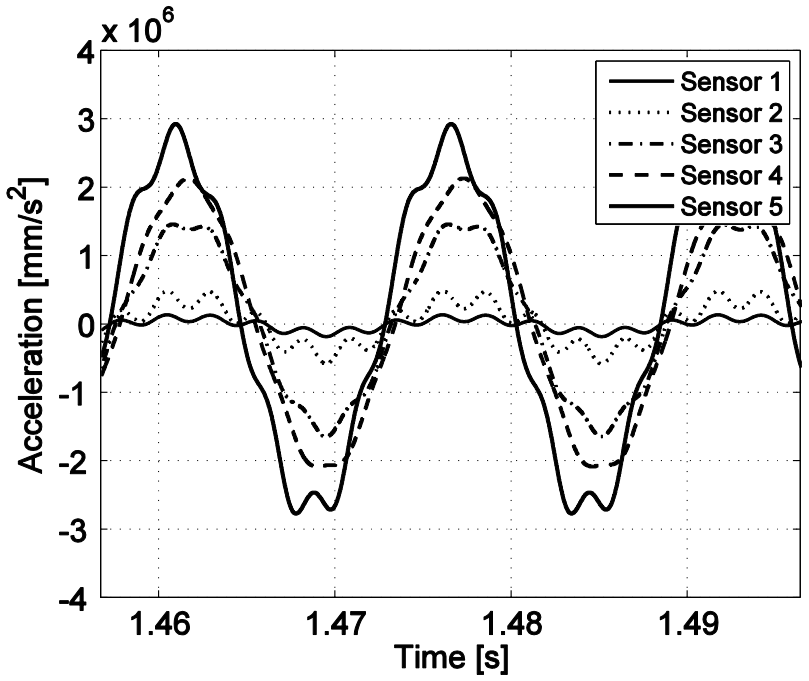

Figure 55: The acceleration time responses at all sensor locations for configuration 2 excited at $L_f = 0.25$ with 100 N. The curves are from 5 to 1 in top to bottom order.

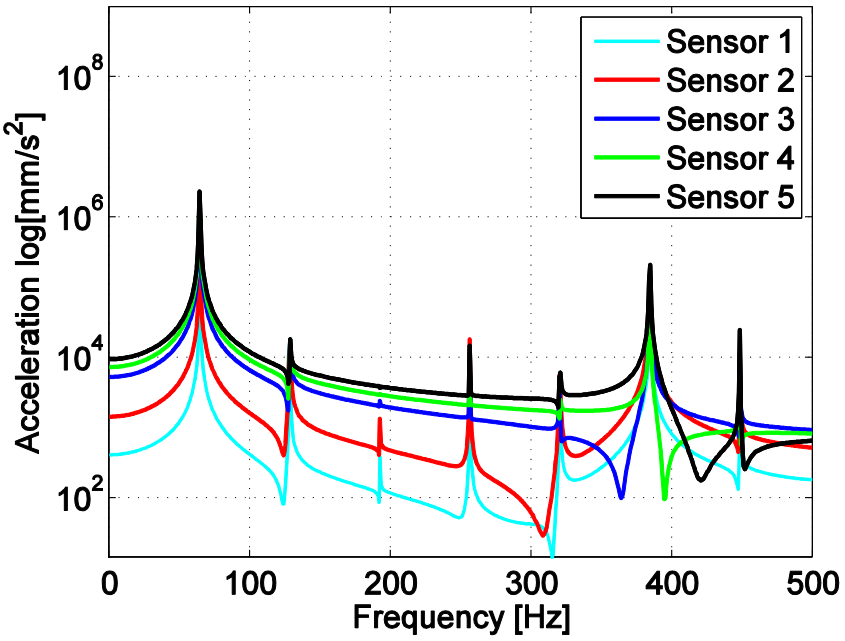

Figure 56: FFT of the acceleration responses at all sensor locations for configuration 2 excited at $L_f = 0.25$ with 100 N. The curves are from 5 to 1 in top to bottom order.

Table 16: Damage indicator parameter at each sensor location

	$A_{max,i}$ [mm/s^2]	n*	A_e [mm/s^2]	$D_{c,i}$
Sensor 1	9.517E4	6th	4.866E4	0.511
Sensor 2	3.532E5	6th	1.333E5	0.377
Sensor 3	1.333E6	6th	8.533E4	0.063
Sensor 4	1.856E6	6th	5.198E4	0.028
Sensor 5	2.389E6	6th	2.147E5	0.008

*The nth harmonic which has the maximum amplitude.

4.2.3.2.Case study 1 – Effect of crack location

For this case study, the crack is located at three different locations on the cantilever beam. The crack depth is kept constant at half of the beam height in each analysis. The displacement of the beam is expected to be higher at the cracked beam than intact beam.

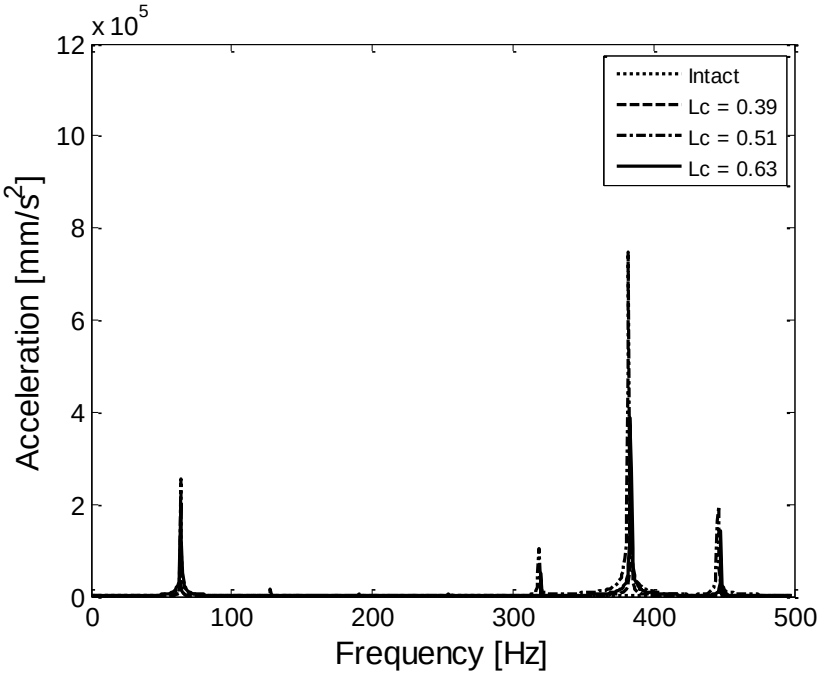

Figure 57: FFT of the acceleration responses at sensor 1 of configurations 3, 4 and 5 with w_c=1.00, L_f = 0.25,d_c = 0.5 and excitation amplitude of 100 N in linear scale.

Table 17: Damage indication parameter at sensor location 1

	$A_{max,1}$	A_e	$D_{c,1}$
Intact	~0	2.085E5	0.00
L_c = 0.39	1.929E5	4.279E4	4.50
L_c = 0.51	8.954E5	2.395E5	3.74
L_c = 0.63	4.189E5	2.358E5	1.77

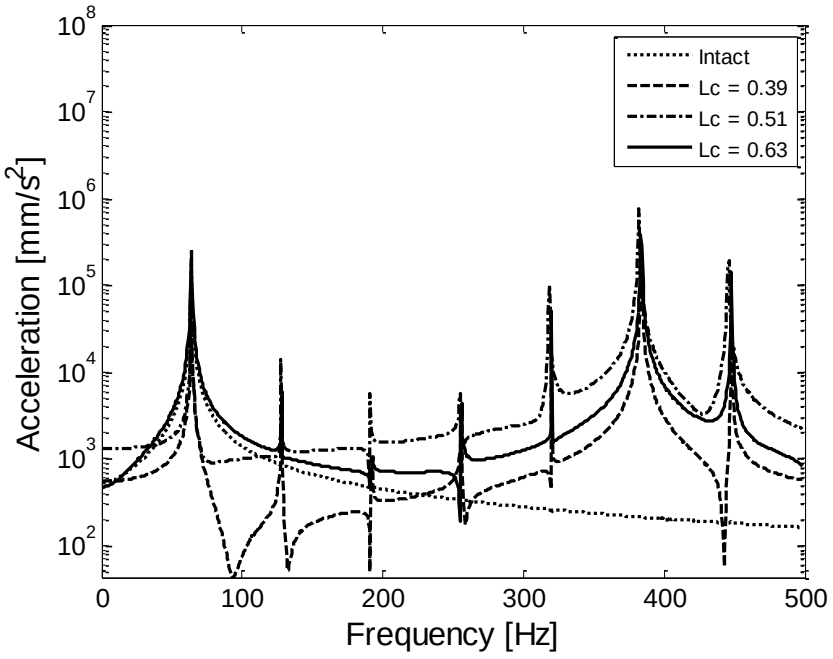

Figure 58: FFT of the acceleration responses at sensor 1 of configurations 3, 4 and 5 with w_c=1.00, L_f = 0.25,d_c = 0.5 and excitation amplitude of 100 N in logarithmic scale.

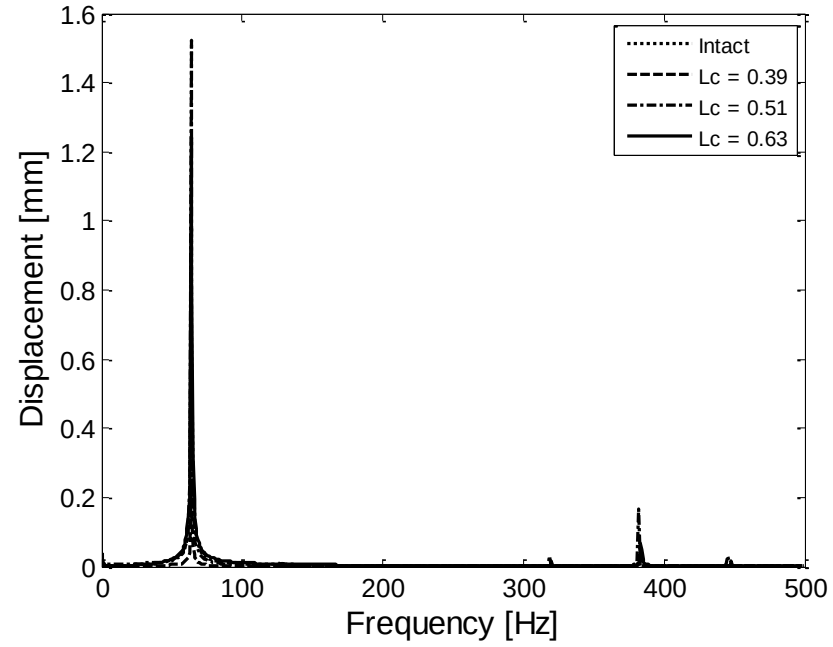

Figure 59: FFT of the displacement responses at sensor 1 of configurations 3, 4 and 5 with w_c=1.00, L_f = 0.25, d_c = 0.5 and excitation amplitude of 100 N in linear scale.

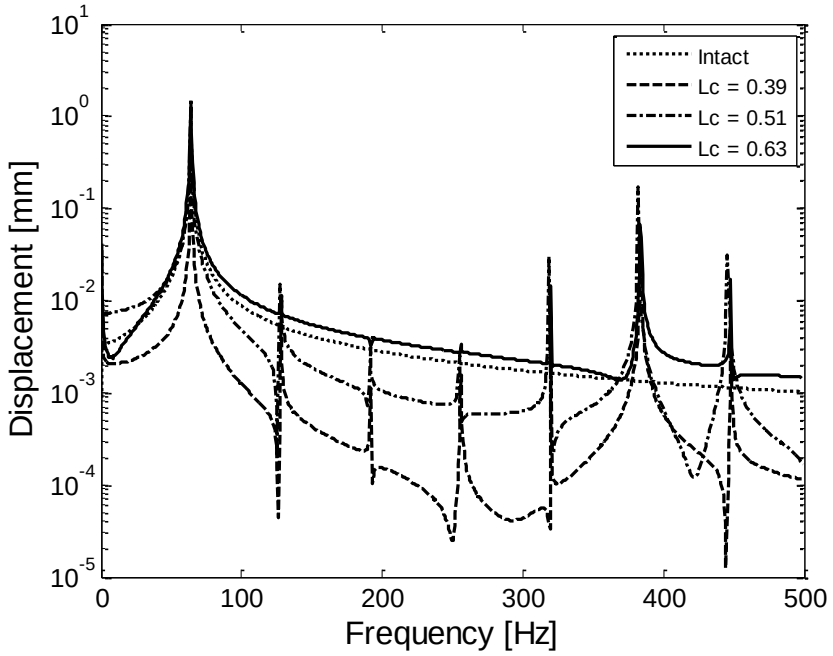

Figure 60: FFT of the displacement responses at sensor 1 of configurations 3, 4 and 5 with w_c=1.00, L_f = 0.25, d_c = 0.5 and excitation amplitude of 100 N in logarithmic scale.

The results show an interesting pattern as a result of the simulation. The amplitude of the acceleration is the highest when the crack is located near to the middle sections of the beam. Also, the maximum amplitude (6^{th}) of the harmonics is very high when the crack is at the 0.51 of the beam length. This can be explained with the second mode of the beam. The second natural frequency for the fixed free beam configurations are at about 390 Hz. The 6^{th} harmonic in the frequency response coincident with the 10% band of the second natural frequency of the cantilevered beam.

First two mode shapes of the cracked beam given in Figure 61. The mode shape of the second natural frequency is mostly affected by the cracks at the mid-section of the beam since the curvature is high at the cracked section in second mode shape. As a result, the crack location can be selected after a preliminary study on the structure's modal characteristic, the excitation frequency and amplitude.

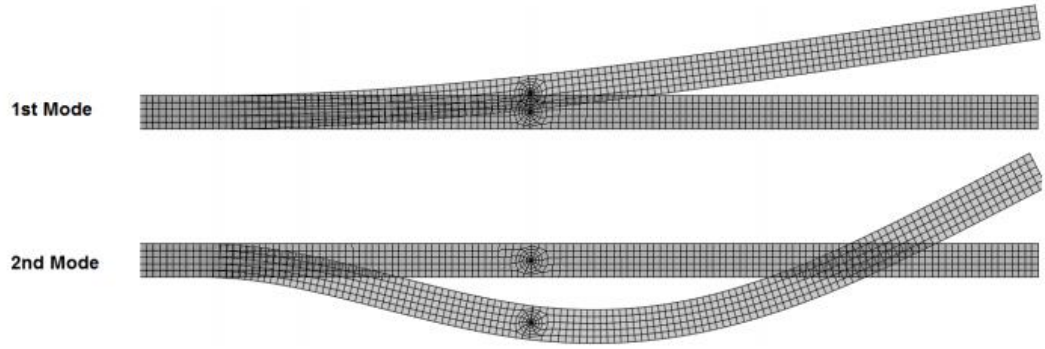

Figure 61: The first two mode shapes of the beam

The location of the crack cannot be taken as an independent parameter in the crack detection analysis. On the other hand, the damage parameter is the highest when the crack is closest to the cantilever end of the beam. Even though the amplitudes of the harmonics (Ae and $A_{max,\,i}$) are is not the highest ones among the others, the damage parameter is the highest for the crack location of 0.39 of the free length of the beam. The displacement responses can also be seen on Figure 59-60. One can observe that cracked beam response converges to that of the intact beam when the crack approaches to the free end of the beam.

4.2.3.3.Case study 2 – Effect of crack depth

In this case study, the crack location is taken as constant. The depth of the crack is changed from 20% of the cross section to the 50% percent of the cross section to observe the changes in the damage indicator parameter and the generation of the harmonics. Nonlinearity is expected to be lower for the smallest cracks and that the response approaches to the intact beam behavior when the crack gets smaller. Figures 62-63 and 64-65 show the acceleration and displacement response of the beam when it is excited with the first natural frequency of the beam. Since the highest amplitude harmonics are clearly observed, the excitation amplitude is taken as 100N for this study. The effect of the excitation is examined at the following sections, as well. Force location is 125 mm from the fixed end throughout this case study. The amplitudes of the harmonics and damage indicators can be seen in Table 18. The damage indicator

is too small for the smallest crack depth as expected since the stiffness of the open and close crack phases of the beam become very close when the crack depth gets smaller. As a result, the amplitude of the harmonics get smaller. It is hard to detect cracks with depth of %20 or smaller of the cross section. The damage indicator does not increase linearly as in the Table 18.

Table 18: Damage indication parameter at sensor location 1

	$A_{max,1}$	A_e	$D_{c,1}$
Intact	~0	2.085E5	0.00
$d_c = 0.20$	1.139E4	1.293E5	0.08
$d_c = 0.35$	4.866E4	9.517E4	0.51
$d_c = 0.50$	1.929E5	4.279E4	4.50

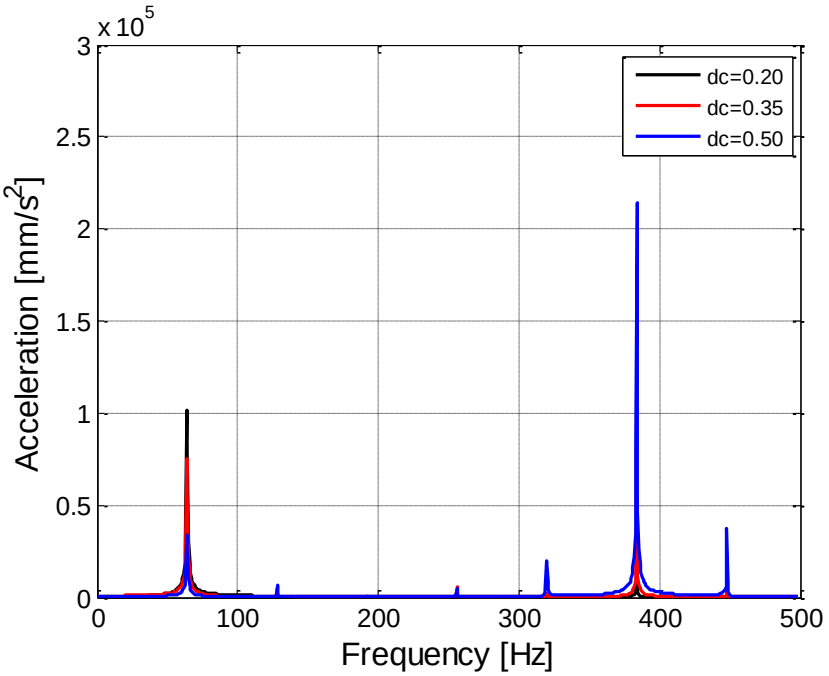

Figure 62: FFT of the acceleration responses at sensor 1 of configurations 1, 2 and 3 with w_c=1.00, L_f = 0.25, L_c = 0.39 and excitation amplitude of 100 N in linear scale.

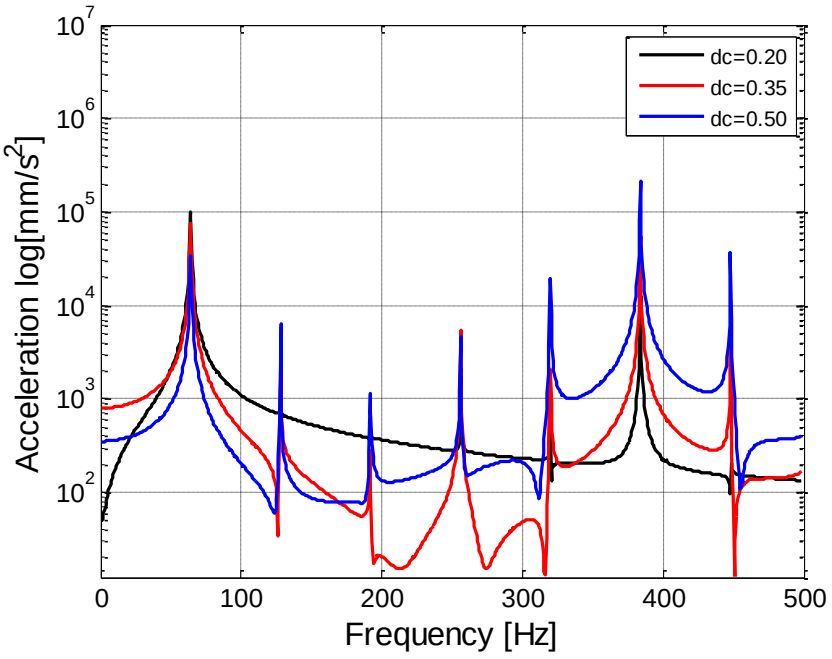

Figure 63: FFT of the acceleration responses at sensor 1 of configurations 1, 2 and 3 with w_c=1.00, L_f = 0.25, L_c = 0.39 and excitation amplitude of 100 N in log scale.

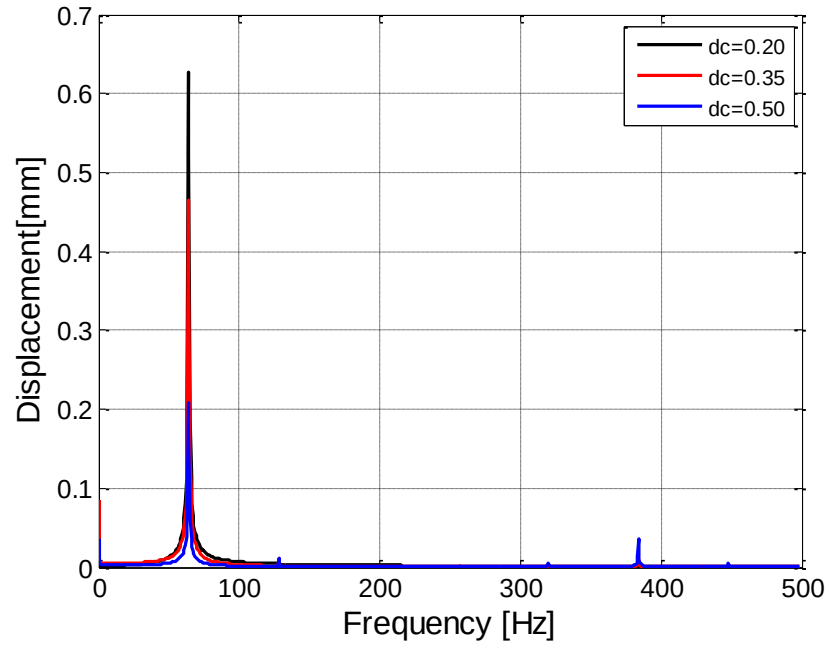

Figure 64: FFT of the displacement responses at sensor 1 of configurations 1, 2 and 3 with w_c =1.00, L_f = 0.25, L_c = 0.39 and excitation amplitude of 100 N in linear scale.

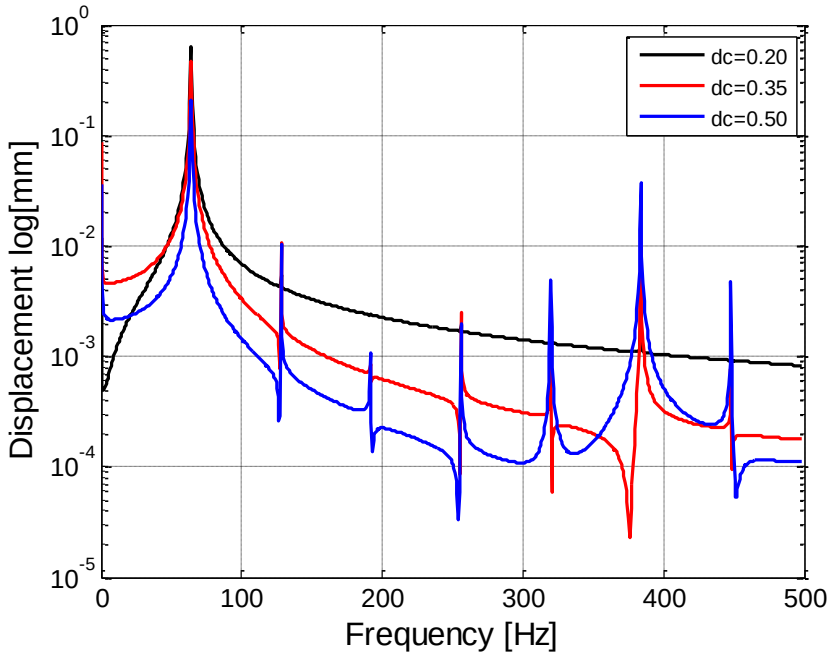

Figure 65: FFT of the displacement responses at sensor 1 of configurations 1, 2 and 3 with w_c =1.00, L_f = 0.25, L_c = 0.39 and excitation amplitude of 100 N in log scale.

The damage parameter increases rapidly after a certain depth of crack. The change of damage indicator from %20 depth to %35 depth is much smaller than from %35 to %50 depth. As a result, the amplitudes of the harmonics increase rapidly after a certain crack depth. The amplitude of the acceleration at the excitation frequency converges to the intact beam when the crack depth gets smaller.

4.2.3.4.Case study 3 – Effect of excitation frequency

The excitation frequency is one of the parameters that affects the crack detection capability. The excitation frequencies coincident with one of the natural frequencies of the structure amplify the structure's displacement and acceleration response. The amplitudes of the harmonics are amplified, as well. The responses are presented in Figure 66-69 for this case study. The half natural frequency is selected as a first one since the second harmonic is coincide with the 1st natural frequency of the structure.

The w_c of 2.45 is selected because none of the harmonics is coincide with any of the natural frequencies.

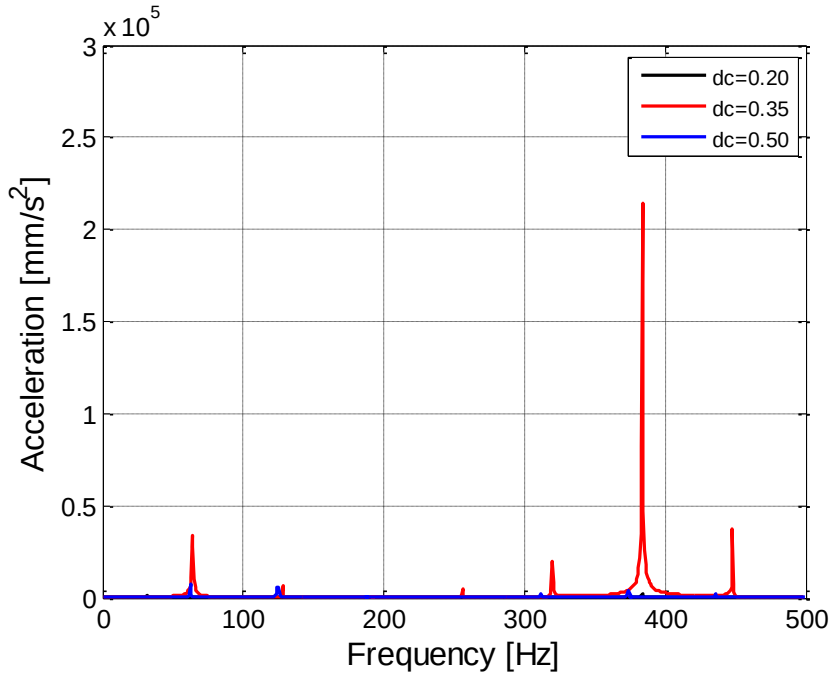

Figure 66: FFT of the acceleration responses at sensor 1 of configuration 3 with d_c = 0.50, L_f=0.25, L_c = 0.39 and excitation amplitude of 100 N in linear scale.

Table 19: Damage indication parameter at sensor 1

	$A_{max,i}$	n*	A_e	$D_{c,1}$
w_c = 0.50	2.239E3	12th	1.646E3	1.36
w_c = 1.00	1.929E5	6th	4.279E4	4.50
w_c = 2.00	7.725E3	½th	5.804E3	1.33

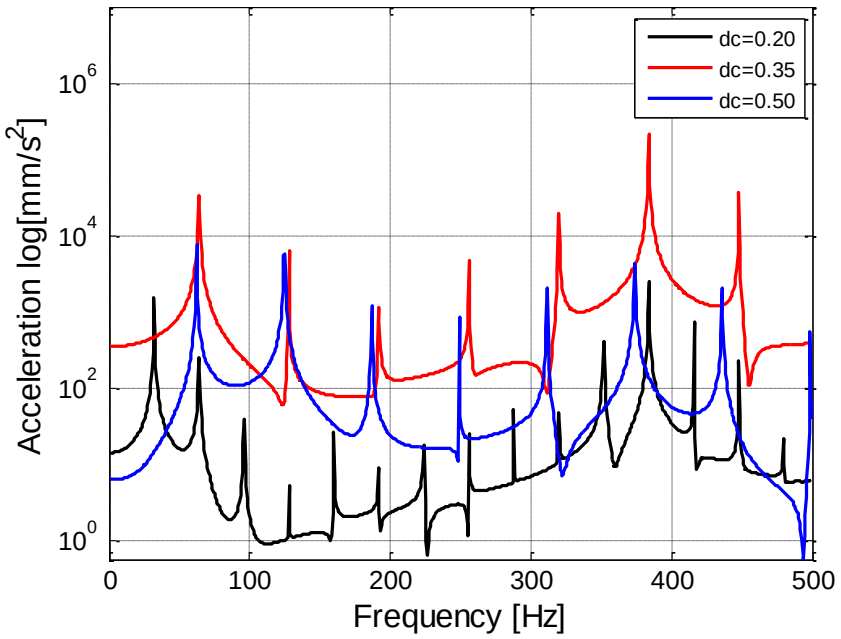

Figure 67: FFT of the acceleration responses at sensor 1 of configuration 3 with d_c = 0.50, L_f=0.25, L_c = 0.39 and excitation amplitude of 100 N in log scale.

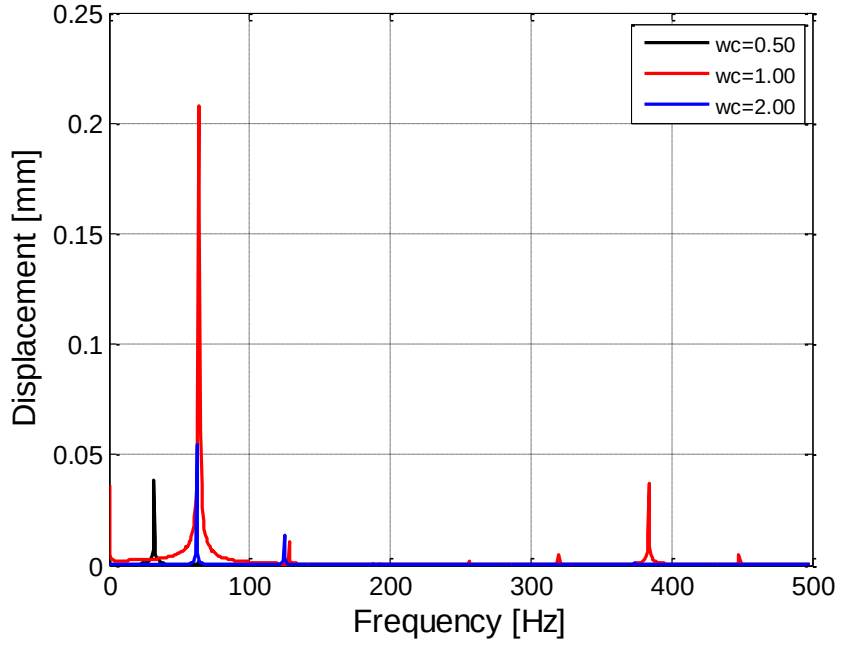

Figure 68: FFT of the displacement responses at sensor 1 of configuration 3 with d_c = 0.50, L_f=0.25, L_c = 0.39 and excitation amplitude of 100 N in linear scale.

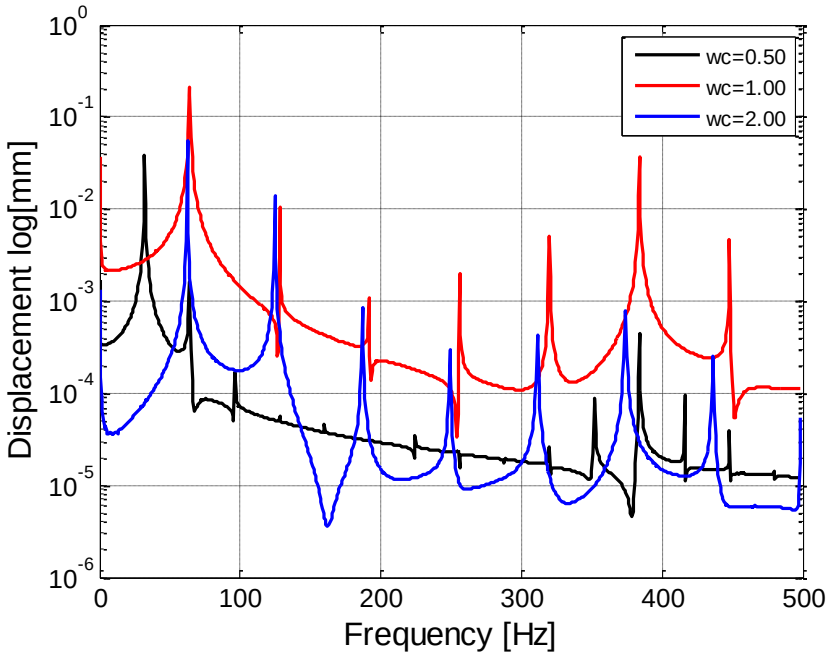

Figure 69: FFT of the displacement responses at sensor 1 of configuration 3 with d_c = 0.50, L_f=0.25, L_c = 0.39 and excitation amplitude of 100 N in log scale.

The damage indicator has the highest value when the beam is excited with the first natural frequency as expected. When the frequency of the vibration is higher than the natural frequency, the amplitudes of the harmonics becomes smaller. For the excitation at 153 Hz, none of the natural frequencies are excited since none of the harmonics is coincident with it. Thus, the damage indicator for w_c = 2.45 has the smallest value. Excitation with the half natural frequency excites the first and second natural frequencies, thus it makes the crack more detectable at the vibration response. The displacement response of the beam shows similar pattern with the acceleration response. Most of the work in the literature conduct the analysis with the half natural frequency in order to make the second harmonic, which is actually the first natural frequency, more detectable since it is amplified at natural frequency. Also, exciting the beam with the first natural frequency, amplify the displacement and acceleration and make the system more nonlinear. A real crack may not open when the force at this section is not high enough to overcome crack closure effects. As a result, the excitation frequency selection seems to be a system dependent parameter.

4.2.3.5. Case study 4 – Effect of excitation amplitude

The amplitude of the vibration is an important parameter for this study since the nonlinearity in the system is not too high and system may behave like linear when the amplitude is small. The following figures show the frequency response under different excitation amplitudes.

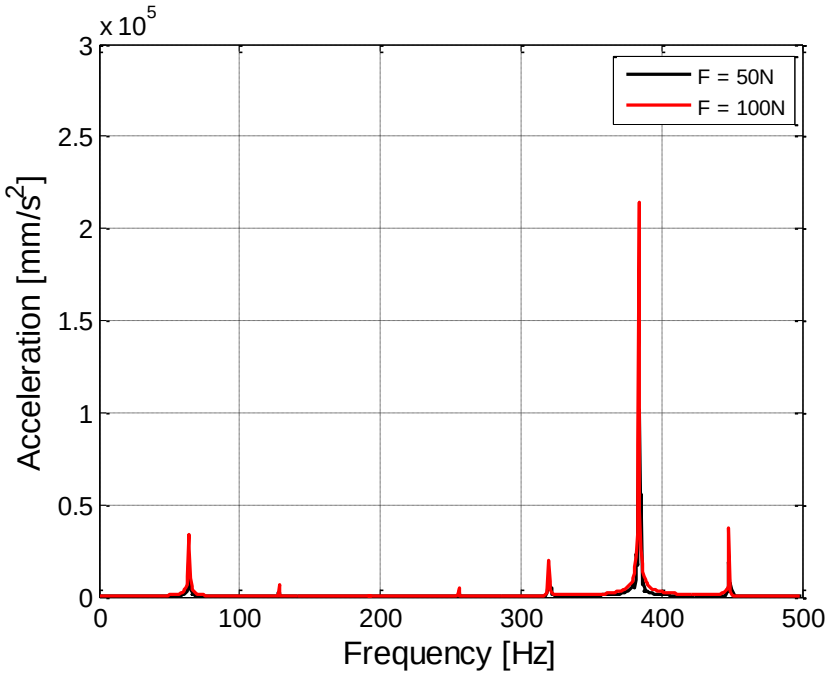

Figure 70: FFT of the acceleration responses at sensor 1 of configuration 3 with d_c = 0.50, L_f=0.25, w_c = 1.00 and L_c = 0.39 in linear scale.

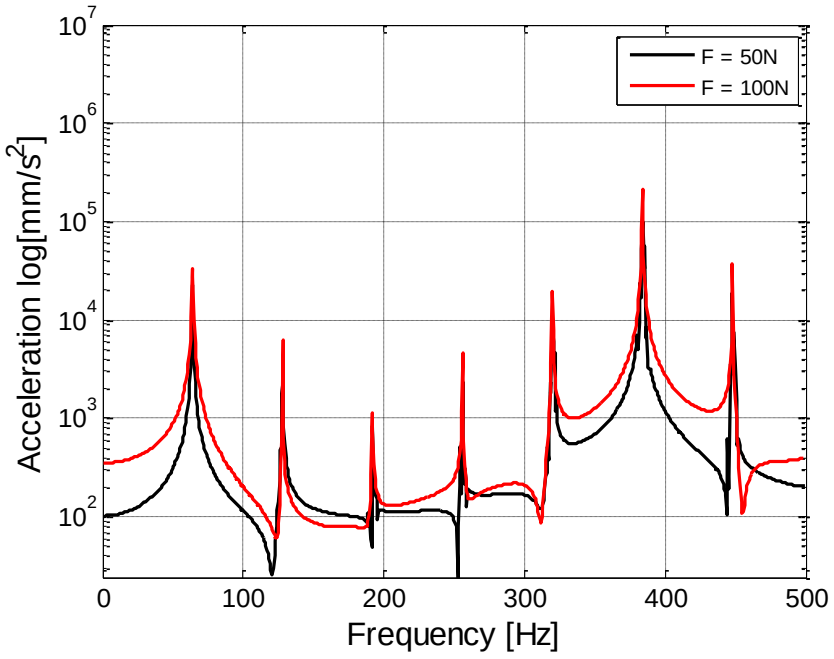

Figure 71: FFT of the acceleration responses at sensor 1 of configuration 3 with d_c = 0.50, L_f=0.25, w_c = 1.00 and L_c = 0.39 in logarithmic scale.

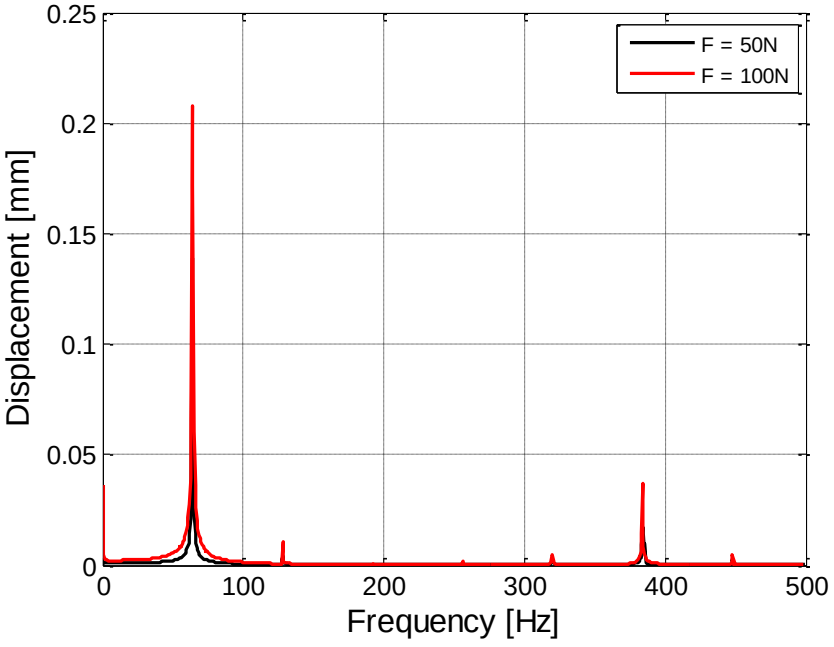

Figure 72: FFT of the displacement responses at sensor 1 of configuration 3 with d_c = 0.50, L_f=0.25, w_c = 1.00 and L_c = 0.39 in linear scale.

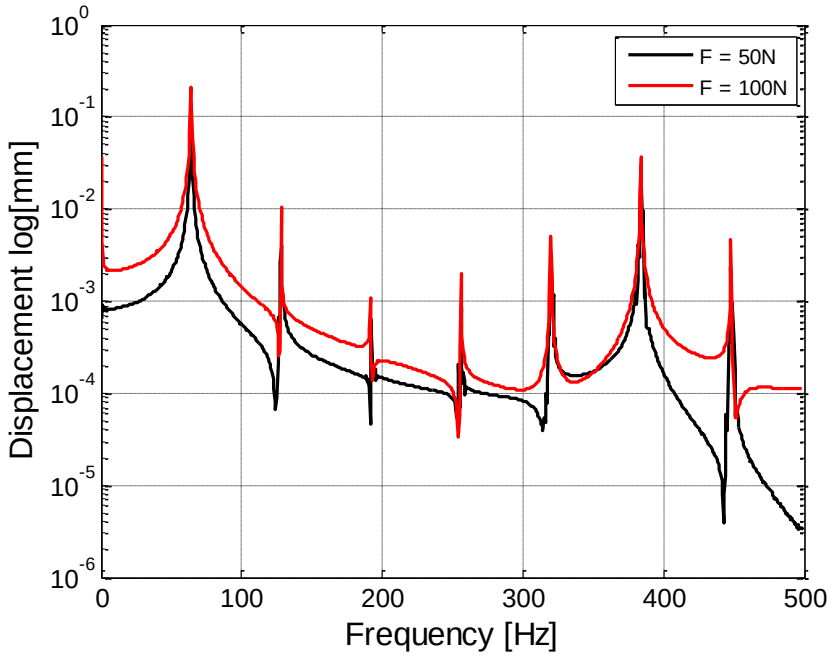

Figure 73 : FFT of the displacement responses at sensor 1 of configuration 3 with d_c = 0.50, L_f=0.25, w_c = 1.00 and L_c = 0.39 in logarithmic scale.

The excitation with 5 N seems to have noisy content. No additional filter is applied intentionally to show the difference when the force is too small. One of the reason of the noise is that the time domain response does not reach to steady state because of the amplitude of the excitation. The amplitude of the transient part in the exact solution of an underdamped system is a function of the amplitude of vibration. Smaller the excitation amplitude, higher the amplitude of the transient component. Moreover, one cannot see the crack closure effects from the finite element results in this study since there is no residual stresses due to crack opening in FE model. In a real structure, one may not detect any nonlinear characteristic in the structure even if it exists when the load is too small. Further, the damage indication parameter is not good for any of the amplitude in this case study. Thus, when the amplitude of the excitation is low and excitation frequency is the half of the 1st natural frequency, the damage indication parameter is very small even if the second harmonic excites the first natural frequency.

Table 20: Damage indication parameter at sensor 1

	$A_{max,i}$	n*	A_e	$D_{c,1}$
F = 50 N	4.672E4	6th	9.740E3	4.79
F = 100 N	2.143E5	6th	3.366E4	6.36

*The nth harmonic which has the maximum amplitude.

4.2.3.6.Case study 5 – Effect of boundary condition

The beam is constraint from both sides and one side in this case study. The first and second natural frequency of the beam having 500 mm free length and constraint from both sides are 384 Hz and 1120 Hz, respectively. The beam constraint from one side has its first two natural frequencies at 63.6 Hz and 385 Hz. The beams are excited with their half natural frequency of 192.5 Hz and 31.8 Hz. The results of the acceleration and displacement are presented in Figure 74 to 77. The harmonic content is clear both in acceleration and displacement results. Considering Table 21, the beam having fixed-fixed boundary condition has much higher amplitudes of acceleration and damage indicator parameter than the beam having fixed-free boundary condition. Both beams are excited at half of their first natural frequencies and have the highest harmonics at their first natural frequencies. The boundary condition seems to have great effect on the crack detection capability. For the fixed-fixed boundary condition, the crack is at exactly the maximum displacement point which is the midpoint of the beam. This makes the harmonics more detectable in the frequency spectra. Thus, boundary conditions should be applied by considering the mode shapes of the structure and location of the crack. Higher crack opening during vibration makes the system more nonlinear. The second natural frequency of the fixed-fixed beam is outside of the frequency of interest but a harmonic at the first natural frequency is enough to comment on the damage indication characteristics of the structure. The harmonic content is visible at the displacement frequency response, as well.

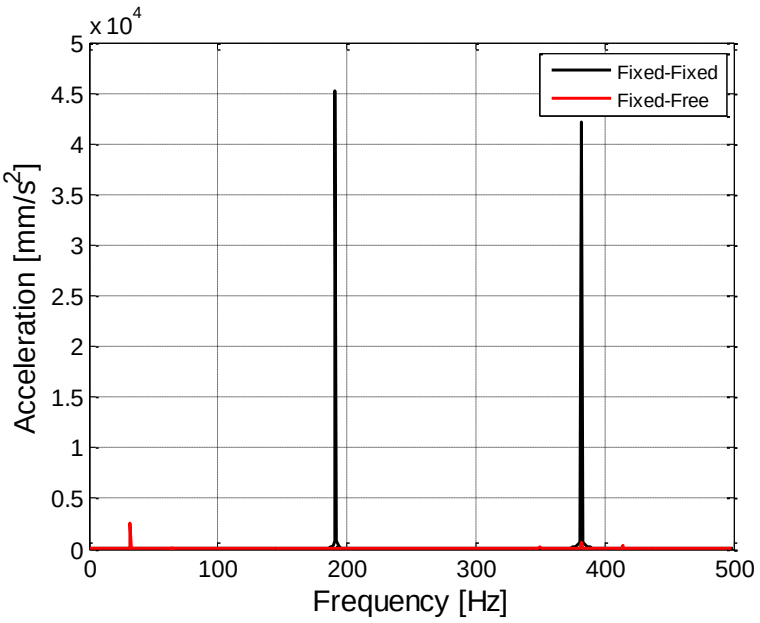

Figure 74: FFT of the acceleration responses at sensor 1 of configuration 6 with d_c = 0.50, L_f=0.25, w_c = 0.50, L_c = 0.50 and excitation amplitude of 100 N in linear scale.

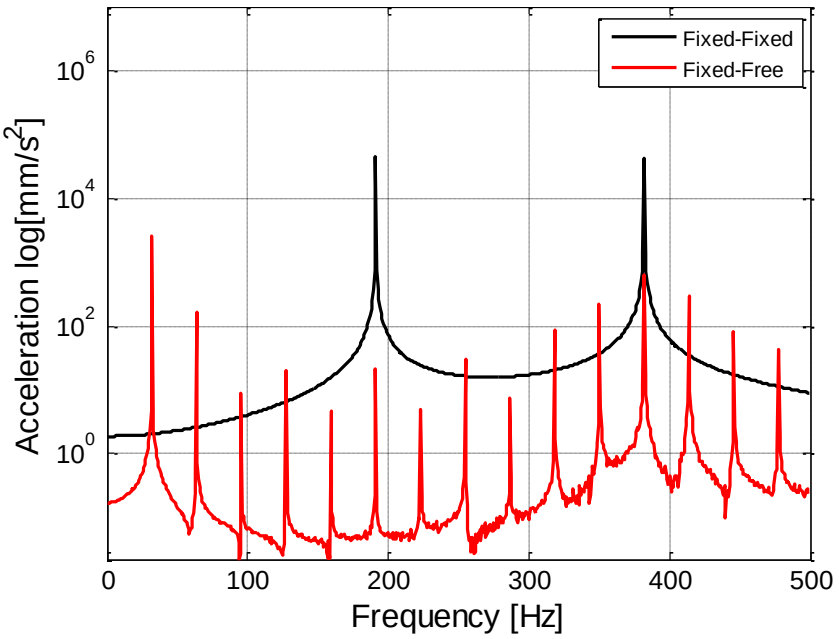

Figure 75: FFT of the acceleration responses at sensor 1 of configuration 6 with d_c = 0.50, L_f=0.25, w_c = 0.50, L_c = 0.50 and excitation amplitude of 100 N in log scale.

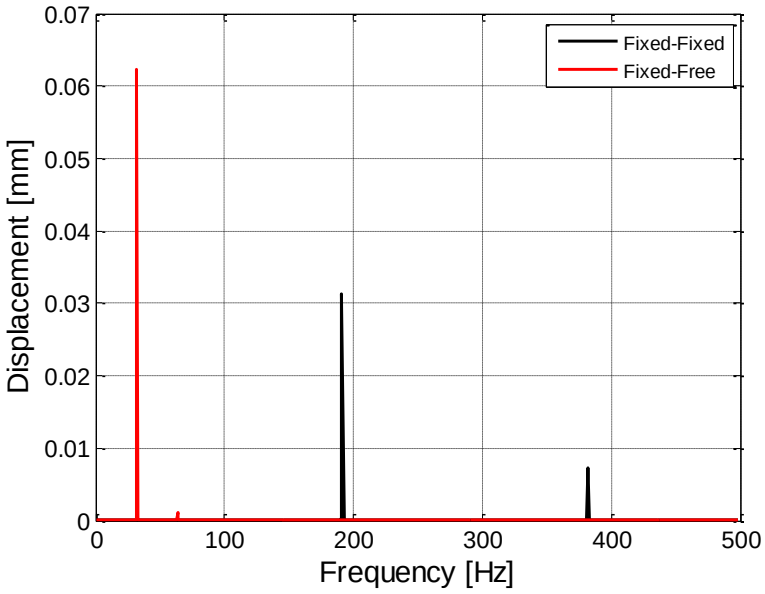

Figure 76: FFT of the displacement responses at sensor 1 of configuration 6 with d_c = 0.50, L_f=0.25, w_c = 0.50, L_c = 0.50 and excitation amplitude of 100 N in linear scale.

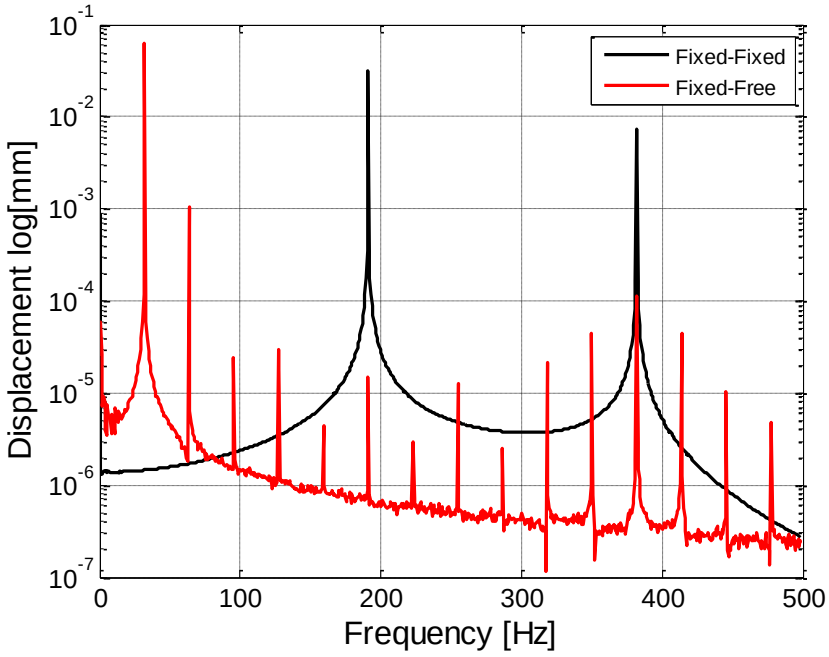

Figure 77: FFT of the displacement responses at sensor 1 of configuration 6 with d_c = 0.50, L_f=0.25, w_c = 0.50, L_c = 0.50 and excitation amplitude of 100 N in log scale.

Table 21: Damage indication parameter at sensor 1

	$A_{max,i}$	A_e	$D_{c,1}$
Fixed - Fixed	7.701E4	2.968E4	2.59
Fixed – Free	2.239E3	1.646E3	1.36

4.2.3.7.Case study 6 – Effect of force location

In this case study, the location of the force is changed. The locations are 125 mm far from the fixed end and 125 mm from the free end. Configuration 3 finite element model is used for this analysis, since it has the highest crack depth and highest nonlinearity on the structure. The acceleration and displacement frequency spectra are given in Figure 78 to 81. It can be seen that the amplitudes are higher in the beam which is excited from the point that is closer to the fixed end, as expected. Highest amplitude of the harmonics is observed in second natural frequency of the structure in the acceleration graph for both beam. The amplitudes of the highest and fundamental harmonics and damage indication parameter are summarized in Table 22. The amplitude of the highest harmonic is at the fundamental or excitation frequency in the acceleration response. The damage indication parameter is higher in the beam which is excited from the point which is closer to the fixed end even if the amplitude is higher in its counterpart. The difference is not too much. Thus, the excitation of the structure might be selected by considering other constraints such as force actuator configuration, the support structure configuration since the amplitude of the vibration will be higher at the regions which is close to the free and of the beam.

Table 22: Damage indication parameter at sensor 1

	$A_{max,i}$	A_e	$D_{c,1}$
Lf = 0.25	1.929E5	4.279E4	4.50
Lf = 0.75	1.338E6	3.341E5	4.00

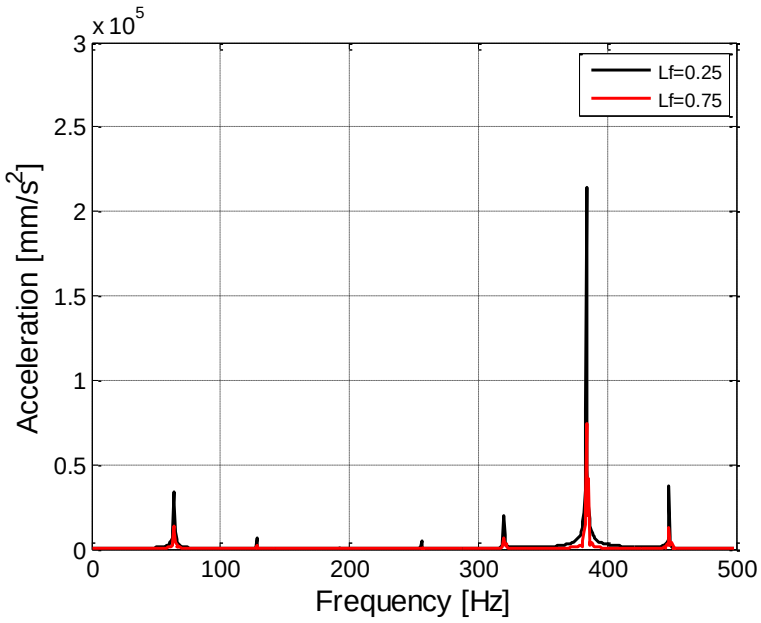

Figure 78: FFT of the acceleration responses at sensor 1 of configuration 3 with d_c = 0.50, L_c=0.39, w_c = 1.00 and excitation amplitude of 100 N in linear scale.

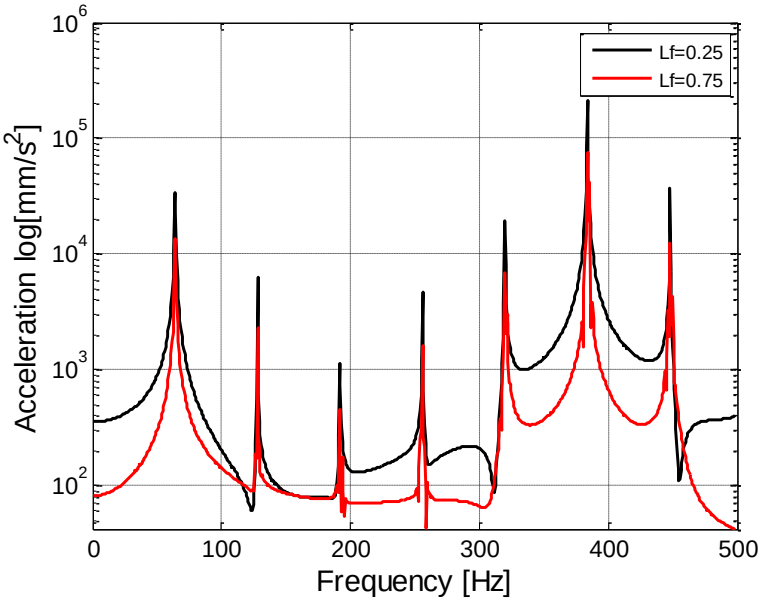

Figure 79: FFT of the acceleration responses at sensor 1 of configuration 3 with d_c = 0.50, L_c=0.39, w_c = 1.00 and excitation amplitude of 100 N in logarithmic scale.

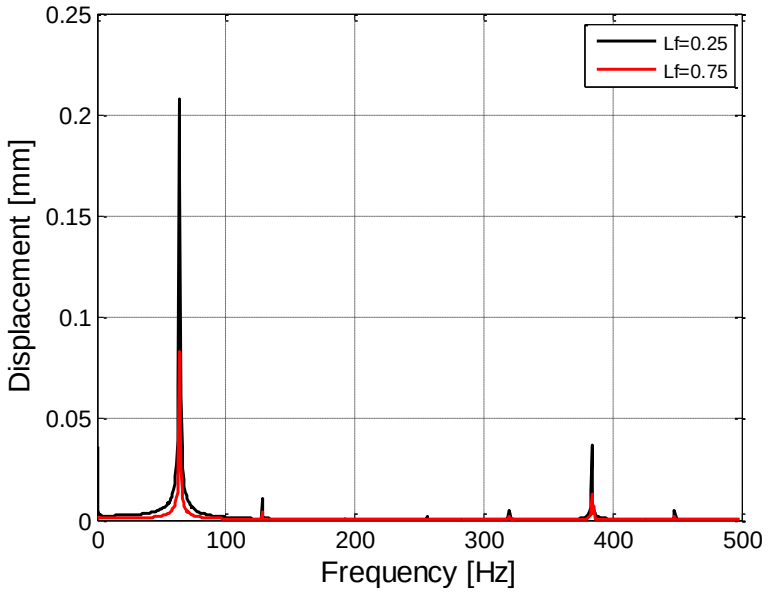

Figure 80: FFT of the displacement responses at sensor 1 of configuration 3 with d_c = 0.50, L_c=0.39, w_c = 1.00 and excitation amplitude of 100 N in linear scale.

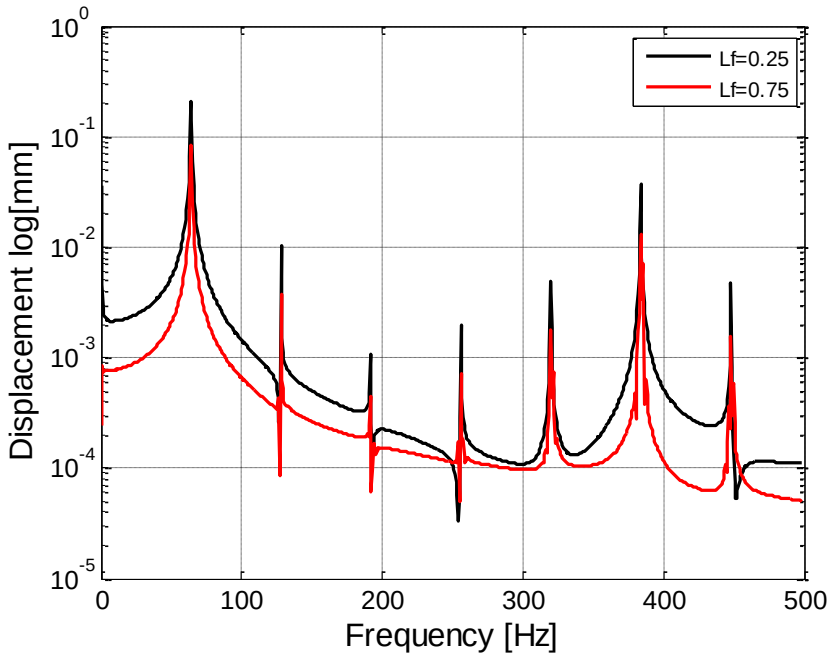

Figure 81: FFT of the displacement responses at sensor 1 of configuration 3 with d_c = 0.50, L_c=0.39, w_c = 1.00 and excitation amplitude of 100 N in logarithmic scale.

CHAPTER 5

DISCUSSION & CONCLUSION

Structural health monitoring has become an increasingly demanding subject in the industry because it decreases the service and maintenance costs. Further, the safety of the structures is crucial in the aerospace industry. As a result of these demands, monitoring of the structures during their service life becomes a requirement. Structural monitoring can detect the upcoming failure in advance and warn the operator about the failure. The number of academic studies on this subject is also increasing day by day in the literature. One of the most demanding methods in structural health monitoring is the one which use the vibration responses and the modal characteristics of the structure. In this study, the vibration based structural health monitoring method was studied using finite element analysis on a cracked cantilever beam under forced vibration. To objectives of the study is to show the ability of finite element method in the detection of cracks on the structure using vibration responses and to examine the effects of different structural parameters such crack depth, crack location, excitation frequency and amplitude and boundary condition on the crack indications. For this purpose, six different square cross sectional cracked beams are modelled using finite element method with two dimensional plane stress elements. Seam crack method is conducted to employ the crack on the structure. Frictionless contact condition is assumed for the interaction of the crack faces. The cracked and intact beams are excited with a harmonic load. Five different sensor locations are selected to observe the vibration of the beam. The one closest to the fixed end of the beam is selected to process the vibration data since it is showed that this sensor demonstrate the damage

very clearly on the frequency spectra of the acceleration and displacement through a proposed damage indicator. The crack detection capability is set to a parameter, called "damage parameter" in the case studies. It is the ratio of highest amplitude of the harmonics to the fundamental harmonic at the excitation frequency. The results show that the crack depth has drastic effects on the damage parameter. The damage parameter increases with the crack depth. It increases exponentially with the crack depth. Also, there is a limit to detect the cracks on the structure. Very small cracks are hard to detect since the structure behaves like linear. The location of the crack affect the damage parameter such that the ones closer to the fixed end of the beam gives higher damage parameter. When the crack become closer to the free end, the beam behaves like an intact beam. The excitation frequency is important to detect the cracks. The highest damage indicator is seen when the crack is excited with the first natural frequency. There are studies on the literature which suggest to use half natural frequency in excitation but the results of this study demonstrate that exciting the beam with the first natural frequency shows higher damage indicator than the ones excited with the half natural frequency. There might be other problems in the real structures or test setups when the beam is excited with the first natural frequency due to high level of vibration. The amplitude of excitation is another parameter in this study. It is observed that the higher the amplitude, higher the damage parameter. The change is not too much from 5 N to 50 N. When the amplitude is too low, the data becomes noisier. Two types of boundary conditions are applied to the beam, which are fixed-fixed and fixed-free. The free length of the beam is kept constant. Both beams are excited at their first natural frequencies. The results show that fixed-fixed boundary condition amplify the damage indicator. This increase in the damage indicator cannot be explained just by the boundary condition since the mode shape of the beam is different for both configurations. Thus, the location of the crack can affect the results. Lastly, a beam is excited from different locations of the beam to observe the effect of the force location under constant force. Not much difference is observed from the results. The beam excited from the point which is closer to the fixed end of the beam has slightly higher damage indictor parameter value.

To sum up, the aim of this study is to prove the capability of the finite element method on the structural health monitoring using vibration response of the structure. This objective is done clearly. Using this finite element method, the effects of different parameters on the damage indication is investigated. There are still more subject that can be examined in this subject such as the crack closure effects, test validation and contact friction. The author leaves these subjects as a future work on this subject.

REFERENCES

Abraham, O. N., and Brandon, J. A. (1995). The Modelling of the Opening and Closure of a Crack. *ASME,* 370-377.

Andreaus , U. and Baragatti, P. (2009). Fatigue crack growth, free vibrations, and breathing crack detection of aluminium alloy and steel beams. *J. Strain Analysis*, 595-608.

Andreaus, U., and Baragatti, P. (2012). Experimental damage detection of cracked beams by using nonlinear characteristics of forced response. *Mechanical Systems and Signal Processing*, 382-404.

Andreaus, U., Baragatti, P., and Vestroni, F. (2011). Cracked beam identification by numerically analysing the nonlinear behavio ur of the harmonically forced response. *Journal of Sound and Vibration*, 721-742.

Andreaus, Ugo, Casini, Paolo, Vestroni and Fabrizio. (2007). Non-linear dynamics of a cracked cantilever beam under harmonic excitation. *International journal of non-linear mechanics*, 566-575.

Batihan, A. C., and Cigeroglu, E. (2015). Nonlinear Vibration of a Beam with a Breathing Edge Crack. *IMAC XXXIII: Conference & Exposition on Structural Dynamics.* Florida.

Bouboulas, A. S., Georgantzinos, S. K., and Anifantis, N. K. (2012). Vibration Analysis of Cracked Beams Using the Finite. *INTECH*, 181-204.

Bouboulas, A. S. and Anifantis, K. N. (2013). Three-dimensional finite element modeling of a vibrating beam with a breathing crack. *Arch Appl Mech*, 207-223.

Bouboulas, A. S. and Anifantis, N. K. (2010). Finite element modeling of a vibrating beam with a breathing crack observations on crack detection. *Structural Health Monitoring*, 131-145.

Broda, D., Pieczonka, L., Hiwarkar, V., Staszewski , W. J., and Silberschmidt, V. V. (2016). Generation of high er harmonics in longitudinal vib ration of beam s with breathing crack s. *Journal of Sound and Vibration*, 206-219.

Buezas, F. S., Rosales, M. B., and Filipich, C. P. (2011). Damage detection with genetic algorithms taking into account a crack model. *Engineering Fracture Mechanics*, 695-712.

Carneiro, G. N., and Ribeiro, P. (2016). Vibrations of beams with a breathing crack and large amplitude displacements. *Journal of mechanical engineering science*, 34-54.

Carr, G. E., Jaureguizahar, L. F., and Chapetti, M. D. (2013). Analysis of Breathing Cracks Using Vibrations. *Society for Experimental Mechanics*, 32-40.

Cawley, P., and Ray, R. (1988). A Comparison of the Natural Frequency Changes Produced by Cracks and Slots. *ASME*, 366-370.

Chati, M., Rand, R., & Mukherjee, S. (1997). Modal analysis of a cracked beam. *Journal of Sound and Vibration*, 249-270.

Chatterjee, A. (2010). Structura l damage assessment in a cantile ver beam with a breathing crack using higher order frequ ency response functions. *Journal of Sound and Vibration*, 3325-3334.

Cheng, S. M., Wu, X. J., and Wallace, W. (1999). Vibrational response of a beam with a breathing crack. *Journal of Sound and <ibration*, 201-208.

Chondros , T. G., and Dimarogonas , A. D. (1998). Vibration of a Cracked Cantilever Beam. *ASME*, 742-746.

Clark, R., Dover, W. D., and Bond, L. J. (1987). The effect of crack closure on the reliability of NDT predictions of crack size. *NDT International*, 269-275.

Dimargonas, A. D., and Papadopoulos, C. A. (1983). Vibration of cracked shafts in bending. *Journal of sound and vibration*, 583-593.

Giannini, O., Casini, P., and Vestroni, F. (2013). Nonlinear harmonic identification of breathing cracks in beams. *Computers and Structures*, 168-177.

Gudmundson, P. (1983). The dynamic behaviour of slender structures with cross-sectional cracks. *J. Mech. Phys. Solids*, 329-345.

Hjelmstad, K. D., and Shin, S. (1996). Crack identification in a cantilever beam from response. *Journal of Sound and Vibration*, 527-545.

Jyrki, K., Kari, S., and Anthony, E. (2013). Vibration-Based Structural Health Monitoring of a Simulated Beam with a Breathing Crack. *Key Engineering Materials*, 1093-1100.

Kisa, M., and Brandon, J. (2000). The effects of closure of cracks on the dynamics of a cracked cantilevered beam. *Journal of Sound and <ibration*, 1-18.

Krawczuk, M., Palacz, M., and Ostachowicz, W. (2003). The dynamic analysis of a cracked Timoshenko beam by the spectral element method. *Journal of Sound and Vibration*, 1139-1153.

Lele, S. P., and Maiti, S. K. (2002). Modelling of transverse vibration of short beams for crack detection and measurement of crack extension. *Journal of Sound and <ibration*, 559-583.

Loya, J. A., Rubio, L., and Saez, J. F. (2006). Natural frequencies for bending vibration of timonshenko cracked beams. *Journal of sound and vibration*, 640-653.

Mazanoglu, K., Yesilyurt, I., and Sabuncu, M. (2009). Vibration analysis of multiple-cracked non-uniform beams. *Journal of Sound and Vibration*, 977-989.

Nandi, A., and Neogy, S. (2002). Modelling of a beam with a breathing edge crack and some observations for crack detection. *Journal of vibration and control*, 673-693.

Nandwana, B. P., & Maiti, S. K. (1997). Detection of the location and size of a crack in stepped cantilever beam based on measurements of natural frequencies. *Journal of sound and vibration*, 435-446.

Newman Jr, J. C., & Elber, W. (1988). A comparison of measurement methods and numerical procedures for the experimental characterization of fatigue crack closure. *Mechanics of Fatigue Crack Closure*, 171-185.

Orhan, S. (2007). Analysis of free and forced vibration of a cracked. *NDT&E International*, 443-450.

Pugno, N., and Surace, C. (2000). Evaluation of the non-linear dynamic response to harmonic excitation of a beam with several breathing cracks. *Journal of sound and vibration*, 749-762.

Qian, G. L., Gu, S. N., and Jiang, J. S. (1989). The dynamic behaviour and crack detection of a beam with a crack. *Journal of sound and vibration*, 233-243.

Saavedra, P. N., and Cuitino, L. A. (2001). Crack detection and vibration behaviour of cracked beams. *Computers and Structures*, 1451-1459.

Sinenko, E. A., and Zinkovskii, A. P. (2015). Influence of the exciting force application point on the amplitude spectrum of flexural vibrations in a beam with a "breathing crack". *Strength of Materials*, 51-60.

Stojanovic, V., Ribeiro, P., and Stoykov, S. (2013). Non-linear vibration of Timoshenko damaged beams by a new p -version finite element method. *Computers and Structures*, 107-119.

Tlaisi, A., Swamidas, S. J., Haddara, M. R., and Akınturk, A. (2012). Modelling and calibration for crack detection in circular shafts supported on bearings using lateral and torsional vibration measurements. *Advances in mechanical engineering*.

Tsai, T. C., and Wang, Y. Z.;. (1996). Vibration analysis and diagnosis of a cracked shaft. *Journal of sound and vibration*, 607-620.

Worden, K., Farrar, C. R., Haywood, J., and Todd, M. (2008). A review of nonlinear dynamics applications to structural health monitoring. *Structural control and health monitoring*, 540-567.

Xu, H., Su, Z., Cheng, L., and Guyader, J.-L. (2015). A " Pseudo-excitation " approach for structural damage identificatio n: From " Strong" to " Weak " modality. *Journ al of Sound and Vibration*, 181-198.

Zheng, D. Y., and Kessissoglou, N. J. (2004). Free vibration analysis of a cracked beam by finite element method. *Journal of Sound and Vibration*, 457-475.

APPENDIX

DYNAMIC ANALYSIS RESULTS WITH FLAT TOP FILTER

CASE STUDY 1 – EFFECT OF CRACK LOCATION

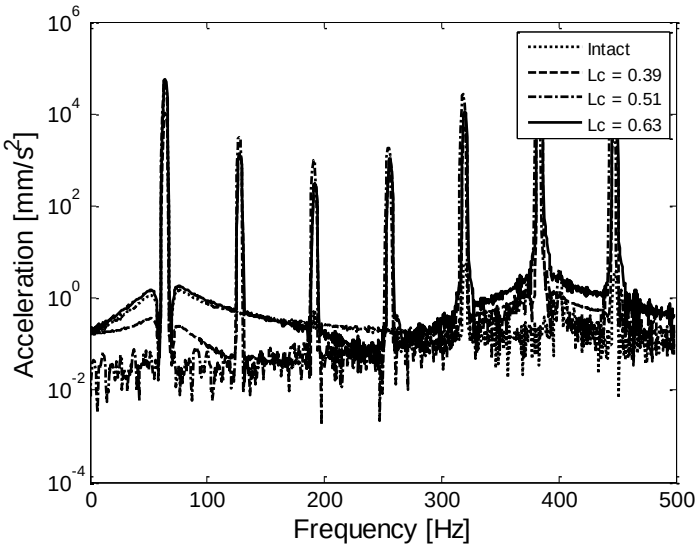

Figure 82: FFT of the acceleration responses at sensor 1 of configurations 3, 4 and 5 with w_c=1.00, L_f = 0.25,d_c = 0.5 and excitation amplitude of 100 N in logarithmic scale with flat top filter.

CASE STUDY 2 – EFFECT OF CRACK DEPTH

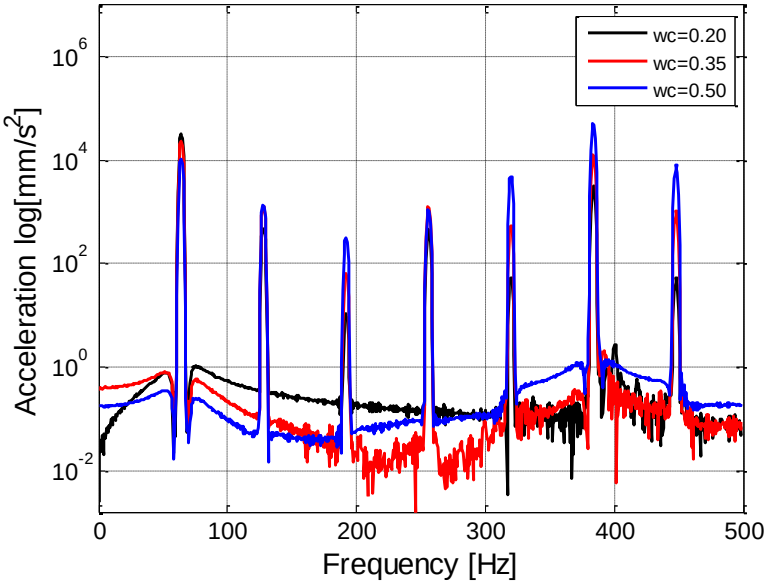

Figure 83: FFT of the acceleration responses at sensor 1 of configurations 1, 2 and 3 with w_c=1.00, L_f = 0.25, L_c = 0.39 and excitation amplitude of 100 N in log scale with flat top filter.

CASE STUDY 3 – EFFECT OF EXCITATION FREQUENCY

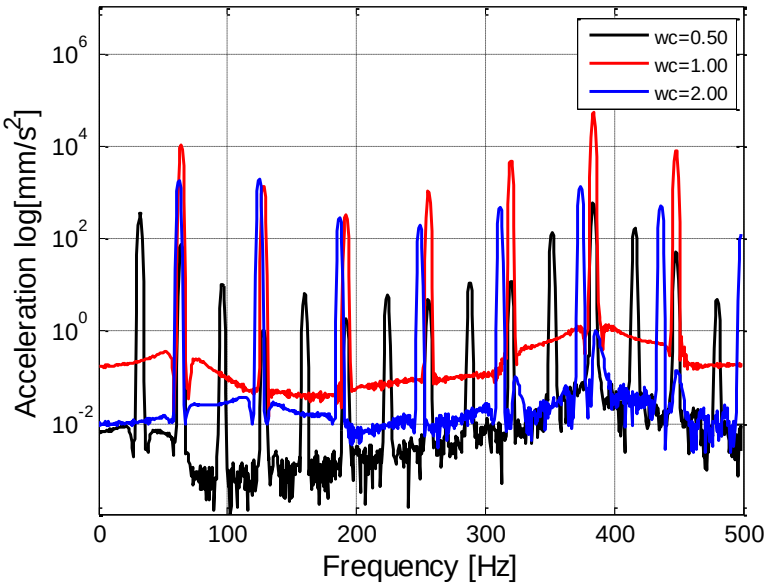

Figure 84: FFT of the acceleration responses at sensor 1 of configuration 3 with d_c = 0.50, L_f=0.25, L_c = 0.39 and excitation amplitude of 100 N in log scale with flat top.

CASE STUDY 4 – EFFECT OF EXCITATION AMPLITUDE

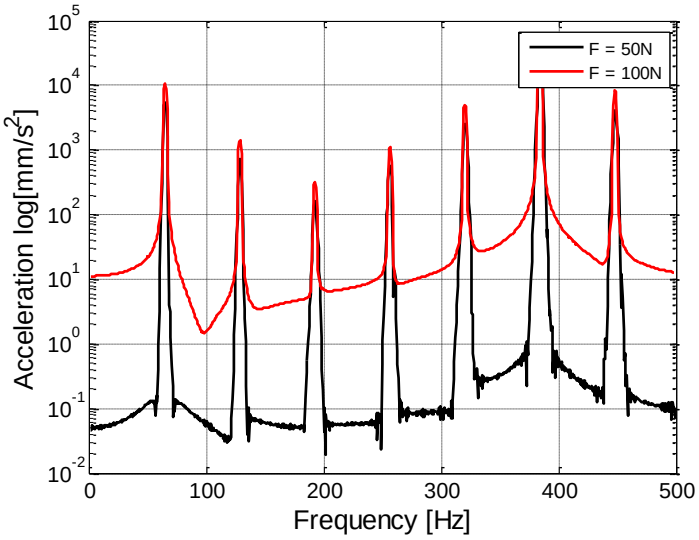

Figure 85: FFT of the displacement responses at sensor 1 of configuration 3 with d_c = 0.50, L_f=0.25, w_c = 1.00 and L_c = 0.39 in logarithmic scale with flat top filter.

CASE STUDY 5 – EFFECT OF BOUNDARY CONDITION

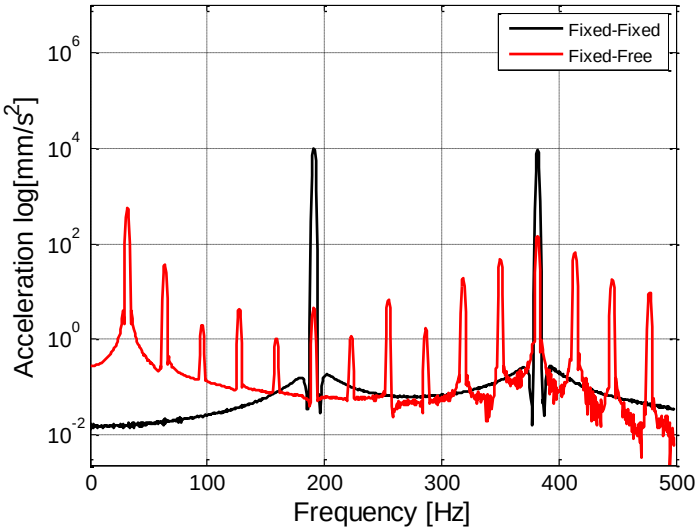

Figure 86: FFT of the acceleration responses at sensor 1 of configuration 6 with d_c = 0.50, L_f=0.25, w_c = 0.50, L_c = 0.50 and excitation amplitude of 100 N in log scale with flat top filter.

CASE STUDY 6 – EFFECT OF EXCITATION LOCATION

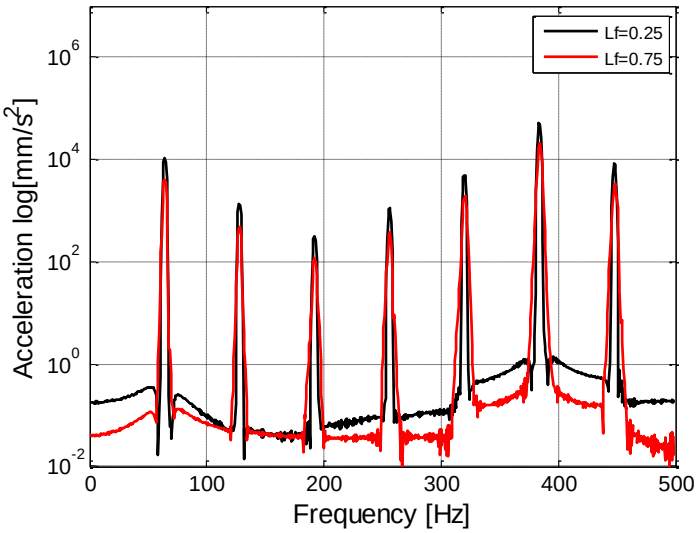

Figure 87: FFT of the acceleration responses at sensor 1 of configuration 3 with d_c = 0.50, L_c=0.39, w_c = 1.00 and excitation amplitude of 100 N in logarithmic scale with flat top filter.